NEW MEXICO BUREAU OF GEOLOGY AND MINERAL RESOURCES

Hydrogeology and Geochemistry of the Animas River Alluvial Aquifer after the Gold King Mine Spill, San Juan County, New Mexico

B. Talon Newton
Ethan Mamer
Stacy Timmons

AQUIFER MAPPING PROGRAM

Open File Report 592
October 2017

New Mexico Bureau of Geology and Mineral Resources

A division of New Mexico Institute of Mining and Technology

Socorro, NM 87801
(575) 835 5490
Fax (575) 835 6333
www.geoinfo.nmt.edu

Hydrogeology and Geochemistry of the Animas River Alluvial Aquifer after the Gold King Mine Spill, San Juan County, New Mexico

B. Talon Newton
Ethan Mamer
Stacy Timmons

Open File Report 592
October 2017

AQUIFER MAPPING PROGRAM

New Mexico Bureau of Geology and Mineral Resources

PROJECT FUNDING

Funded by the U.S. Environmental Protection Agency Clean Water Act, Section 106 through the New Mexico Environment Department under MOU 16-667-2000-0004.

The views and conclusions are those of the authors, and should not be interpreted as necessarily representing the official policies, either expressed or implied, of the State of New Mexico.

Left cover image:
This is the Interim Water Treatment Plant, which is treating the Gold King Mine water along Cement Creek, near Silverton, Colorado. Photo by Stacy Timmons, NM Bureau of Geology and Mineral Resources.

Right cover image:
Animas River, near Aztec, New Mexico, stage elevation measurement in January 2017. Photo by Talon Newton, NM Bureau of Geology and Mineral Resources.

CONTENTS

Executive Summary 1

I. Introduction 5
- The Gold King Mine spill and response 5
- Geologic background 6
- The Animas River 8

II. Data and Methods 9
- Sample site inventory 9
- Timing of water level measurements and sample collection 9
- Continuous data recorders 14
- Water sampling 14

III. Results and Interpretations 17
- Water level measurements 17
  - Well network description 17
  - Water table analysis 18
  - Hydrograph trends 19
- Groundwater chemistry 22
  - Field parameters 22
  - Water quality 28
  - General water chemistry 30
  - Trace metals and redox reactions 42
  - Stable isotopes of hydrogen and oxygen 46
  - Groundwater age 47

IV. Discussion 51
- Hydrogeologic conceptual model 51
  - Recharge 51
  - Groundwater flow directions 53
  - Groundwater/surface water interactions 55
- Potential groundwater contamination 56

V. Conclusions 59

VI. Future Work 61

Acknowledgments 63

References 64

Figures

1. Study area 5
2. Location of the San Juan Basin and geologic cross-section 6
3. Simplified geologic map and geologic cross-section from Durango to Farmington 7
4. Median Animas River discharge 8
5. Locations of groundwater level measurement sites 10
6. Well water sample sites 11
7. Surface water sample sites 12
8. Timing of sampling events 15
9. Map showing annual fluctuation in the water level for each well in 2016 17
10. Water table map based on water level measurements during March 2016 18
11. Water table maps delineated for March 2016 and October 2016 19
12. Locations of different hydrograph type wells 20
13. Example of a river-stage-controlled-groundwater hydrograph 21
14. Example of an irrigation-controlled hydrograph 21
15. Example of a winter-recharge/summer-evapotranspiration hydrograph 22
16. River and ditch sample locations 23
17. The range of dissolved oxygen concentrations as a function of the maximum dissolved oxygen value for each well with 2 or more measurements at different times 24
18. Locations of wells categorized by observed maximum dissolved oxygen concentration and temporal variability of dissolved oxygen concentrations 25
19. Continuous water level and specific conductance data for AR-0075, which is located less than ten feet from the Animas River 26
20. Continuous water level and specific conductance data in four wells and an irrigation ditch 27
21. Continuous water temperature data for AR-0028 and monthly average air temperatures at the Farmington Four Corners Regional Airport 28

22. Continuous water level and temperature data for AR-0181 ... 28
23. Redox ladder shows important redox pairs for different Eh values ... 28
24. Location of wells that produced water exceeding EPA SMCLS for total dissolved solids, sulfate, iron, manganese, and aluminum ... 30
25. Trends of total dissolved solids and sulfate ... 31
26. Spatial variability observed for strontium, barium, and chloride ... 31
27. Linear regressions for total dissolved solids as a function of dissolved oxygen ... 35
28. Time series graphs for wells that show a linear relationship between total dissolved solids and dissolved oxygen ... 36
29. Time series graphs for wells that do not show a linear relationship between total dissolved solids and dissolved oxygen ... 36
30. Analysis of the direction of change in dissolved oxygen and total dissolved solids between sample events ... 37
31. Piper diagram showing relative cation and anion concentrations for water samples ... 37
32. Location of wells, which are identified by their water type as defined by relative cation and anion concentrations ... 38
33. Graph of bicarbonate and sulfate vs. calcium and magnesium ... 38
34. Graphs of major ions to assess water-mineral interactions ... 39
35. Dissolved oxygen concentrations plotted as a function of relative sulfate concentrations ... 40
36. Modeled mixing curve ... 41
37. Barium as a function of relative sulfate concentrations ... 41
38. Strontium as a function of relative sulfate concentrations ... 42
39. Chloride concentrations plotted as a function of relative sulfate concentrations ... 43
40. Total iron plotted as a function of dissolved iron ... 43
41. Dissolved iron plotted as a function of Eh ... 44
42. Eh-pH diagram for Fe-O-H_2O system with data plotted on the diagram ... 44
43. Total manganese as a function of dissolved manganese ... 45
44. Eh-pH diagram for Mn-O-H_2O system ... 45
45. Dissolved manganese as a function of Eh ... 45
46. Stable isotopic compositions of river samples ... 46
47. The average stable isotopic compositions of most groundwater plots along or near the river evaporation line ... 47
48. δD values for groundwater as a function of relative sulfate concentration ... 47
49. Groundwater age maps ... 48
50. Piper diagram shows chemistry data for average groundwater compositions along with Animas River samples collected by the USGS ... 51
51. Shallow groundwater samples collected by the EPA and NMED in August 2015 and Animas River samples collected by the USGS ... 52
52. Schematic regional cross sections showing groundwater flowpaths in regional bedrock ... 53
53. Zoomed in view of a losing reach in January 2016 located, 1.5 miles northeast of Aztec ... 54
54. Difference in discharge measured between Cedar Hill and Farmington during non-irrigation season ... 55
55. Observed range in dissolved oxygen concentrations as a function of distance from the river ... 56

Tables

1. Well networks ... 13
2. Continuous recorder sites and type of continuous data recording ... 14
3. Average field parameters for wells sampled multiple times for this study ... 22
4. Field parameters for four wells that were sampled during March 2017 ... 23
5. Field parameters measured on the Animas River, selected ditches, and on the San Juan River ... 24
6. Selected water chemistry with highlighted concentration that exceed U.S. Environmental Protection Agency secondary maximum contaminant levels ... 32–34
7. Average concentrations for selected constituents for all wells sampled ... 35
8. Saturation indices for selected minerals ... 39
9. Tritium and carbon-14 data ... 49

Appendices

(Available in digital format, https://geoinfo.nmt.edu/publications/openfile/details.cfml?Volume=592)

A. Well inventory
B. Water level measurements
C. Water chemistry results
D. Sample collection procedures
E. Water Quality Standards and Health Advisories from the U.S. Environmental Protection Agency and the State of New Mexico

EXECUTIVE SUMMARY

On August 5, 2015 the accidental breech of the Gold King Mine level 7 adit, located in the Silverton Mining District, Colorado, resulted in the movement of millions of gallons of bright orange water through the Animas River into northwestern New Mexico. The water released from the Gold King Mine spill was loaded with dissolved metals and contaminated sediments, which posed a possible risk to groundwater quality in the Animas Valley. As an immediate response to the spill, the New Mexico Environment Department and the U.S. Environmental Protection Agency collaborated with several state and federal agencies, including the U.S. Geological Survey, the New Mexico Office of the State Engineer, and the New Mexico Bureau of Geology and Mineral Resources. Representatives from these groups measured water levels and collected water samples for chemical analysis in over a hundred domestic and irrigation wells in the shallow alluvial aquifer adjacent to the Animas River between Colorado and Farmington, New Mexico. Our team of researchers from the New Mexico Bureau of Geology and Mineral Resources selected a subset of these wells to serve as a monitoring network for the purpose of assessing the spatial and temporal variability of groundwater/surface water interactions, and groundwater quality in the area. The study described in this report uses repeated water level measurements and geochemical analyses sampled between January 2016 and June 2017 to accomplish the following objectives:

- Characterize the hydrogeologic system, which includes the determination of groundwater flow directions, hydraulic gradients, and recharge sources, and the assessment of groundwater/surface water interactions
- Identify areas along the river where the river may be losing water to the shallow aquifer
- Assess the possible impacts of the Gold King Mine spill to shallow groundwater

The Animas River flows from the headwaters in the San Juan Mountains, near Silverton, CO to Farmington, NM, where it feeds into the San Juan River. South of Durango, CO, the shallow subsurface geology and exposed rock that bounds the Animas Valley is composed of sedimentary rocks ranging in age from the late Cretaceous to Paleogene age. The spatial arrangement and orientation of these rock is controlled by the structure of the San Juan Basin. The majority of the New Mexico reach of the Animas River flows over the Nacimiento Formation, which pinches out near Farmington, where the underlying Kirtland Shale is observed at the surface. The Animas River from the Colorado-New Mexico border flows through Quaternary alluvial deposits, which are largely made up of sediment eroded from Paleogene rocks into which the Animas River has incised. While municipal or regional drinking water is largely sourced from the Animas River, most private domestic and irrigation wells in the valley rely on the alluvial aquifer, with well depths of about 30 to 60 feet.

For this study, we measured water levels and collected water samples from existing wells at different seasons, which were determined based on Animas River flow conditions. Flow conditions targeted for data collection events were: Winter baseflow (January 2016 and 2017),

Pre-irrigation (March 2016 and 2017), Peak snowmelt river flow (June 2016 and 2017), and end of irrigation (October 2016). During these events, water levels were measured and water samples were collected in wells that were completed in the alluvial aquifer and were within one mile of the river. For each sampling event, water levels were measured in 50 to 80 wells, and water samples were collected in 16 to 26 wells. We collected some water samples in wells that were farther from the river and completed in bedrock that underlies the alluvium with the intention of characterizing regional groundwater. All water samples were analyzed for major anions and cations, trace metals, and the stable isotopes of hydrogen and oxygen. For major cations and trace metals, total and dissolved constituents were measured. For some wells, water samples were analyzed for the environmental tracers, tritium and carbon-14 in order to determine groundwater ages. A subset of wells was also instrumented with data loggers to continuously collect data at hourly intervals. In 25 wells, continuous measurements included water level, and temperature. For 13 of these wells, specific conductance was measured in addition to water level and temperature.

Groundwater level measurements were used to construct water table maps to assess groundwater flow direction and the hydraulic gradient between groundwater and the river stage. In general, groundwater flows to the southwest (downstream) and towards the river. In most areas, the Animas River is gaining water from the groundwater, as groundwater from the surrounding valley flows downhill, or down gradient, discharging to the river. However, in some areas, water levels in close proximity to the river have a nearly flat hydraulic gradient between groundwater and the river, where small seasonal fluctuations in groundwater levels and river stage can turn a slightly gaining reach to a slightly losing reach. Groundwater levels in the valley are generally lowest in March, before the irrigation season begins, and highest in October, near the end of the irrigation season. High seasonal water level fluctuations were observed near the Cedar Hill and Inca communities, where we observed an apparent reversal in gradient that changes the river in those areas from a gaining stream in the summer during irrigation season to a losing reach in the winter.

The high-resolution groundwater hydrographs observed for wells equipped with data loggers showed distinct patterns that were used to categorize most of the measured wells based on their different hydrograph characteristics. Water levels in wells that exhibit "river-stage-controlled-groundwater" hydrographs have a high correlation to river stage with a distinct increase that correlates to peak snowmelt in the river followed by a rapid drop in groundwater levels through August. Water levels in wells that exhibit "irrigation-controlled" hydrographs begin increasing in late march at the beginning of irrigation season and continue to increase through July and do not begin to decrease until the end of irrigation in late October. This hydrograph type was observed for over 50% of the measured wells. Water levels in wells that exhibit "winter-recharge/summer-evapotranspiration" hydrographs increase slightly during the winter and decrease during the summer months.

General water chemistry, stable isotope, environmental tracer data, and modeling of two-endmember mixing indicate that shallow groundwater is primarily comprised of young river water and older regional groundwater from the underlying Nacimiento Formation. The river water end-member is characterized by low total dissolved solids (less than 500 mg/L), a calcium bicarbonate water type, and high tritium values (above 5 tritium units, modern water). The regional groundwater end-member is characterized by a much higher total dissolved solids concentration (about 10,000 mg/L), a sodium sulfate water type, undetectable

tritium content, and an apparent carbon-14 age of approximately 20,000 years before present. The observed spatial trend of increasing concentrations for sulfate and total dissolved solids in the general groundwater flow direction (southwest) is the result of the upwelling of regional groundwater due to the gradual thinning of the Nacimiento Formation, which pinches out near Farmington. While the river water is by far the most dominant recharge source, accounting for over 80% of the mixture in all water samples collected from the alluvial aquifer, the input of regional groundwater significantly affects water quality by increasing the total dissolved solids content to above 1,000 mg/L in some areas. Groundwater with total dissolved solids concentration over 1,000 mg/L greatly exceeds the secondary maximum contaminant level as defined by secondary EPA drinking water regulations (500 mg/L), and can affect the ability to grow some crops.

Discrepancies between modeled and observed chloride, barium, and strontium concentrations suggest a small degree of mixing with a third endmember component. We hypothesize that this other mixing component is a brine characterized by high chloride, barium, and strontium concentrations, and low sulfate. High-chloride, low-sulfate brines have been observed in the San Juan Basin from Cretaceous rocks that lay beneath the study area. Many brines that have been observed in the San Juan Basin are associated with oil and gas that resides in these geologic formations.

Geochemical data provided direct evidence of the input of river water to the aquifer. In some wells that were equipped with data loggers, an abrupt change in specific conductance and/or temperature trends that correlated with groundwater level increases were clearly indicative of the mixing of river water with local groundwater. Observed temporal variability of dissolved oxygen in wells also provided evidence of river water recharging the groundwater system. Significant increases in dissolved oxygen observed between sampling events in individual wells were usually accompanied by slight decreases in total dissolved solids, indicating the addition river water, which is characterized by high dissolved oxygen and relatively low total dissolved solids concentrations, to the shallow aquifer. Water sampled in many wells sustained low dissolved oxygen concentrations (<3mg/L) over the duration of this study. In contrast, dissolved oxygen concentrations in some wells varied significantly over time (by over 4 mg/L), indicating a more dynamic system in that area where river water recharges the aquifer.

River water primarily recharges the shallow aquifer as a result of irrigation practices in the area. During the growing season (March through October), water is diverted from the river into irrigation ditches and canals that transport water to agricultural fields. Water seeping through the bottoms of canals and ditches and past the root zone in agricultural fields recharges the shallow aquifer, resulting in groundwater levels increasing significantly during irrigation season throughout most of the study area, as was observed from groundwater level measurements in the majority of wells. While the seepage of irrigation water through canal and ditch bottoms and agricultural fields is the primary mechanism by which river water enters the aquifer, there is evidence that water can infiltrate directly from the river into the aquifer in some areas. Therefore, we recommend that in the event of another mine water release, that residents with a well within 300 feet of the river (especially near the communities of Inca and Cedar Hill) discontinue pumping of the well temporarily until the contaminant plume in the river has passed.

Potential groundwater contaminants identified in water and sediments associated with the Gold King Mine spill include iron, aluminum, manganese, lead, copper, arsenic, zinc,

cadmium, and mercury. Measurements for most of the metals mentioned above were either below U.S. Environmental Protection Agency maximum contaminant levels, or were below the reporting limit of the analysis. Several wells in the shallow aquifer produced water that exceeds U.S. Environmental Protection Agency secondary maximum contaminal levels for dissolved iron and manganese. Observed Eh values indicate redox conditions that are favorable for the reduction of manganese resulting in the dissolution of manganese oxides. The lower end of the observed range in Eh values (about 200 millivolts) suggest that small decreases in Eh result in the reduction of iron and the dissolution of iron (hydr)oxides. Most groundwater samples with the highest iron and manganese concentrations exhibit Eh values of less than 200 millivolts, which accounts for about 25% of the water samples collected for this study.

It is difficult to determine the source of iron and manganese. While iron and manganese were observed at high concentrations in the Gold King Mine spill plume and water in the Animas River has relatively high iron and manganese total concentrations (most is likely adsorbed onto colloids and other particulates), these metals are also present in the aquifer sediments. Therefore, the spatial distribution of water that is high in iron and manganese may be controlled by the location where these minerals were dominantly deposited within the alluvial aquifer. In addition, potentially contaminated river sediment (some of which may have been associated with the Gold King Mine spill) deposited in irrigation ditches and canals may also be a source of manganese and iron. As irrigation water infiltrates through these sediments, metals such as iron, manganese and aluminum may be mobilized and transported to the shallow water table. Results from this study do not suggest that the groundwater quality has necessarily been impacted by this mechanism. However, continued monitoring of groundwater quality is recommended. Groundwater in the alluvial aquifer is estimated to be, on average, less than 10 years old and is a mixture of very young water derived from recent spring runoff in the San Juan Mountains and older irrigation recharge from past irrigation seasons. Therefore, it may be several years before an impact to water quality in the shallow aquifer can be observed.

We also need to consider the spatial distribution of reductants, such as organic matter, septic contamination, and possibly hydrocarbons and how it relates to spatial variability of manganese and iron concentrations in groundwater. In areas with an increased amount of reductants, biodegradation can decrease the Eh significantly, resulting in the dissolution of manganese oxides and iron (hydr)oxides at a higher rate. The well that exhibited the highest dissolved iron and manganese concentrations also had the highest chloride and barium content, possibly providing additional evidence of a high-chloride, low-sulfate brine that may be associated with oil or gas that has leaked into the shallow aquifer either by natural or anthropogenic pathways. The biodegradation of leaked hydrocarbons in the aquifer could decrease Eh values significantly, resulting in the observed increased dissolved manganese and iron concentrations in groundwater in this area.

With groundwater pH being fairly neutral and constant between 6.7 and 8.3, and with manganese and iron buffering the redox conditions, it is unlikely that metals associated with the Gold King Mine spill will be contaminants of concern in this groundwater system. However, the potential for contaminants associated with the Gold King Mine spill may still exist due to the possible deposition of contaminated sediments in irrigation ditches. Therefore, continued monitoring of groundwater quality is recommended. Future work should include groundwater quality monitoring and sediment analysis in irrigation ditches.

I. INTRODUCTION

The New Mexico Bureau of Geology and Mineral Resources is a research and service division of New Mexico Institute of Mining and Technology, serving as the state's geologic survey. After the Gold King Mine (Figure 1) released metal and sludge-laden water into Cement Creek and the Animas River on August 5, 2015, the agency began a hydrologic assessment focused on the alluvial aquifer adjacent to the Animas River in New Mexico, from the Colorado state line to Farmington, NM. The purpose of this project was to evaluate possible effects from the mine release on the shallow groundwater near the Animas River. Accomplishing this requires an understanding of the seasonal changes to the surface water-groundwater system and long-term monitoring of the groundwater quality conditions along this reach of the Animas River.

The Gold King Mine Spill and Response

There is a long history of natural acid rock drainage and acid mine drainage in the headwater region of the Animas River, along the western San Juan Mountains near Silverton, Colorado. For at least 9,000 years, acidic and metal-laden waters have drained into

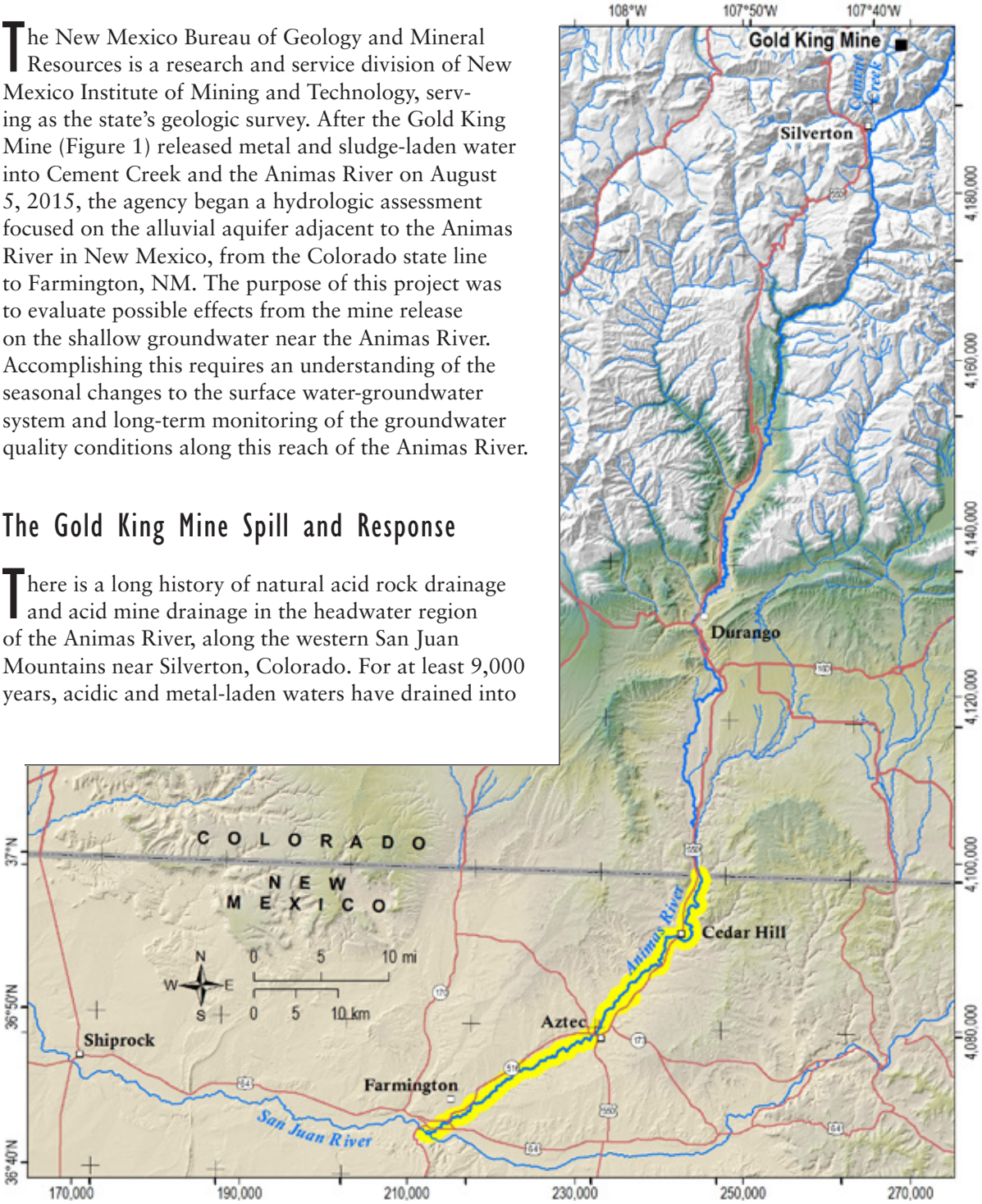

Figure 1. The study area. This study focused on the reach of the Animas River outlined in yellow, from the Colorado-New Mexico state line to Farmington. Also shown on this map is the approximate location of the Gold King Mine, near Silverton, Colorado.

mountain streams, including Cement Creek and the upper Animas River (Church et al., 2007; Yager and et al., 2016). On August 5, 2015, in an attempt to repair drainage issues in the Level 7 adit of the Gold King Mine, workers accidentally breached the earthen plug holding back acidic water in the vertical mine workings. As the mine workings rapidly drained, the released water also gained an estimated 490,000 kg (~540 tons) of metals and sediment from waste rock piles below the mine (U.S. Environmental Protection Agency, 2016). Cement Creek was soon flooded with yellow-orange, sediment laden water from the Gold King Mine and surrounding area. This water-sediment mixture contained high concentrations of iron, aluminum, manganese, lead, copper, arsenic, zinc, cadmium, and some mercury (U.S. Environmental Protection Agency, 2016). Within about 3 days, the yellow water had flowed down the Animas River to Farmington, New Mexico where it entered the San Juan River.

Immediately following the Gold King Mine spill, many questions were asked about the connection of the Animas River to the surrounding groundwater. Could there be contamination of the groundwater aquifer along the river? How exactly do the groundwater and surface water interact? How might Gold King Mine spill sediments deposited in the river bed or irrigation ditches affect groundwater?

In August 2015, in collaboration with the U.S. Geological Survey, New Mexico Office of the State Engineer, and New Mexico Environment Department, the New Mexico Bureau of Geology and Mineral Resources collected groundwater level measurements at over 100 locations along the Animas River. The goal of these measurements was to identify gaining or losing reaches of the river system. Water quality samples were initially collected by the U.S. Environmental Protection Agency and their contractors in August 2015. Using the network of private domestic wells established in August 2015, we developed a repeat sampling program for groundwater quality and groundwater levels along the Animas River valley. The first year of monitoring after the spill was summarized by Timmons et al. (2016). This report presents water level and geochemical results and interpretations of data that was collected over the entire duration of this study.

Geologic Background

The geology of the area described here is summarized from Craigg (2001), which is part of a larger review of the geology found in the San Juan Basin

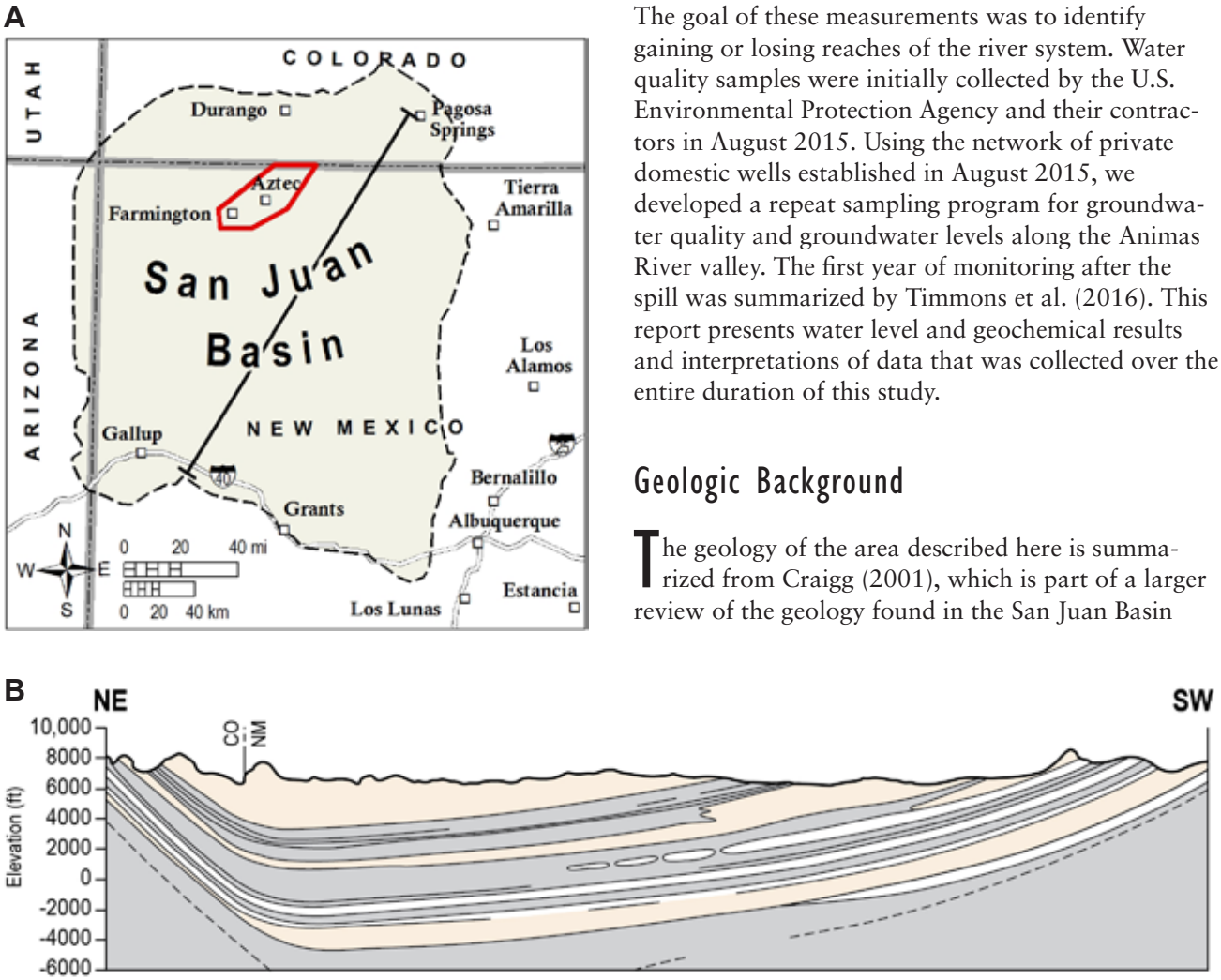

Figure 2. Location of the San Juan Basin and generic geologic cross-section. Modified from Kelley et al. (2014). **A**—The San Juan Basin a large structural depression located mostly in Northeastern New Mexico, but also covers small areas in Colorado, Utah, and Arizona. **B**—This simplified cross-section shows the general arrangement of rocks and the structural framework of the San Juan Basin. The subsurface shape of the San Juan Basin is roughly a large bowl-shape depression, dipping northward.

(Figure 2A). The Animas River in northwest New Mexico flows through the northwestern margin of the San Juan Basin, which is an asymmetric structural depression (Figure 2B) in the Colorado Plateau province. Below and surrounding the alluvial aquifer, the geology along the Animas River from Durango to Farmington consists of sedimentary rocks of late cretaceous to Paleogene age (Figure 3). Near Durango, the Animas River flows over the Animas Formation, which is made up of interbedded tuffaceous sandstone, conglomerate and shale. In the Cedar Hill region, the nearby surrounding hills/mesas are composed primarily of Eocene (~50–55 Ma) San Jose Formation, and Paleocene (~60–65 Ma) Nacimiento Formation. The San Jose is an interbedded very fine to coarse-grained arkosic sandstone. The Nacimiento Formation consists of interbedded gray shale, and discontinuous lenses of sandstone and interfingers with the Paleocene Ojo Alamo Sandstone, which consists of arkosic sandstone and conglomerate. The Ojo Alamo Formation outcrops just north of Farmington, New Mexico. Along the river in the proximity of Farmington, outcrops of late Cretaceous (~75 Ma) Kirtland Shale are found. The Kirtland Shale consists of interbedded repetitive sequences of sandstone, siltstone, shale and claystone. The Kirtland Shale helps cap the Fruitland Formation below, which consists of carbonaceous shale and coal (Craigg, 2001). The majority of the New Mexico reach of the Animas River flows over the Nacimiento Formation. There are no major structural features (i.e. faults or folds) along the river corridor.

The Animas River from the Colorado-New Mexico border flows through Quaternary alluvial deposits. The Quaternary alluvium is largely made up of sediment eroded from Paleogene rocks into which the Animas River has incised. While municipal or regional drinking water is largely sourced from

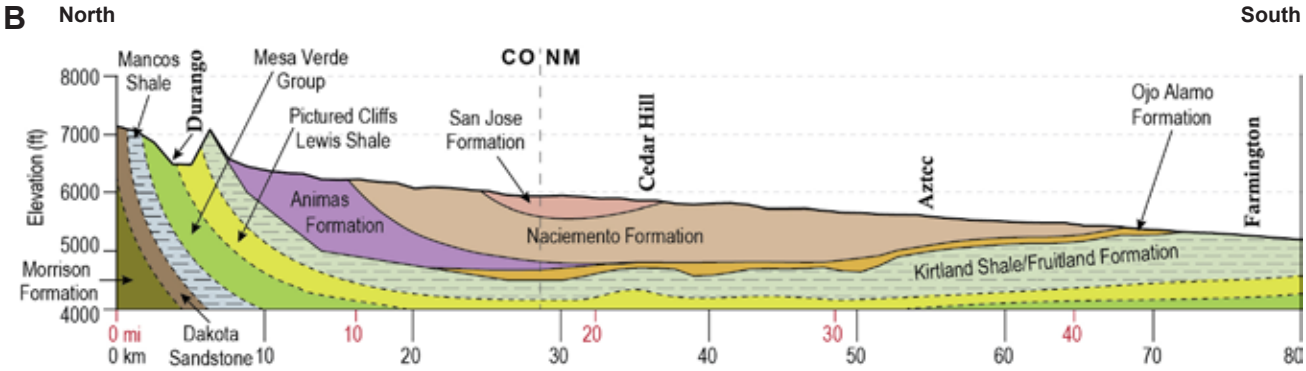

Figure 3. Simplified geologic map and geologic cross-section. **A**—The black line is the location of the cross-section, shown in B, that runs roughly that runs roughly parallel to the Animas River from Durango to Farmington. **B**—The thin layer of quaternary alluvium is not shown in this cross-section (modified from Kelley et al., 2014; Craigg, 2001).

the Animas River, most private domestic wells in the valley rely on the alluvial aquifer, with well depths of about 30 to 60 feet.

The Animas River

The headwaters of the Animas River originate high in the San Juan Mountains, in the Silverton Mining District. Two other main tributaries drain from this mineral rich region and join the Animas River in Silverton, including Cement Creek and Mineral Creek. These mineral-rich streams account for roughly a third of the observed flow measured in Farmington, NM (~80 cubic feet per second (cfs) at baseflow). The Animas flows through the Animas Canyon, between Silverton and Durango (roughly 50 miles), where it is fed by numerous smaller streams that flow into the canyon. By the time the river reaches Durango, it has more than doubled in volume. Just north of the New Mexico-Colorado border, the Florida River feeds into the Animas River. By the time the Animas enters New Mexico the river discharge is roughly equal to the flow measured at Farmington, NM, (~300 cfs at baseflow). The Animas River meanders roughly 40 miles from the New Mexico border, to Farmington, where it joins the San Juan River. The San Juan River flows an additional ~180 miles through New Mexico and Utah before discharging into Lake Powell.

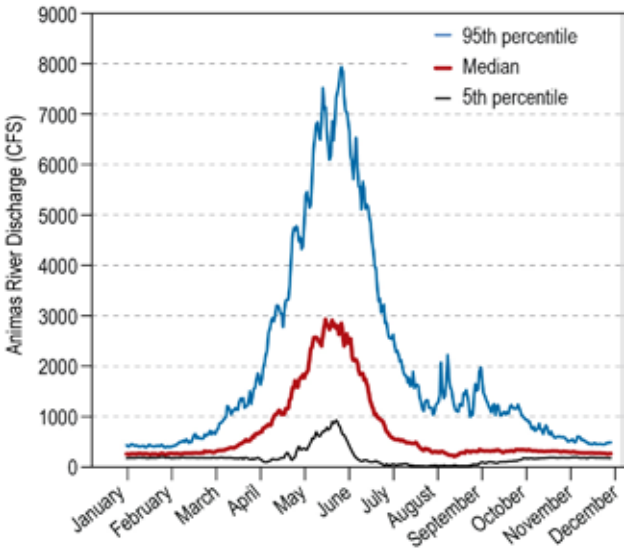

Figure 4. Animas River discharge. Median daily discharge (over 92 years) measured at the U.S. Geological Survey gauge in Farmington, NM (09364500). Also included are the 95th and 5th percentile flows observed at the gauge.

The discharge of the Animas River fluctuates with the seasons. In Farmington, just upstream of where the Animas River discharges into the San Juan River, the U.S. Geological Survey has recorded over 90 years of river discharge measurements (Figure 4). The median daily discharge varies from 208 cfs at its lowest, to nearly 3,000 cfs at its peak. In general, the river discharge begins to rise slowly in April as early snow melt enters the river. Discharge continues to increase throughout May as temperatures in the mountains feeding the headwaters rises, melting more snow. The river typically reaches peak discharge between late May and mid-June as the main pulse of snowmelt moves through the river. The discharge declines through late summer as the snowpack diminishes. Throughout the late summer, river discharge often rises rapidly as a result of monsoon storms, before ebbing back to previous levels. By late August the river has returned to a baseflow. The river is often lowest during early fall as result of diversions for irrigation, and higher evapotranspiration rates. Moving into fall and winter the river remains relatively steady at roughly 300 cfs.

II. DATA AND METHODS

Sample Site Inventory

Sample locations and data discussed in this report are found in Figures 5–7, Tables 1 and 2, and the Appendices. The data include groundwater level measurements, groundwater chemistry data, surface water measurements (water levels and stable isotopes), and continuous records of water levels, temperatures, and in some wells, specific conductance. Data collected by U.S. Environmental Protection Agency from August 2015 are included in our analyses, as well as data from previous years, reported in Timmons et al. (2016). Well sites used in this study were all existing wells, most of them being privately owned domestic or irrigation wells.

Well selection priorities included (1) proximity to the Animas River, (2) proximity to agricultural irrigation ditches, (3) wells that were previously sampled by U.S. Environmental Protection Agency in August 2015, and (4) wells with owners that were cooperative and willing to allow repeated sampling. Selected wells for repeat sampling were completed in the alluvial aquifer, and within approximately 1 mi on either side of the Animas River, from the Colorado state line to Farmington, NM. Wells completed in the alluvium are typically shallow, generally between 30 to 60 feet deep (Table 1). We sampled several wells outside of the valley on the surrounding bluffs (Figure 6). These wells are much deeper and are completed in the Eocene (~50–55 Ma) San Jose Formation and Paleocene (~60–65 Ma) Nacimiento Formation and Ojo Alamo Sandstone. Data collected from each sampling event were used to assess hydrogeologic processes at these locations, for the event season.

Spatial coordinates (easting and northing) for all sample sites were determined using a handheld GPS receiver, and then corrected based on satellite imagery. At each site we photographed the well and documented site-specific information, such as well depth, casing diameter, casing stick-up height, etc. We determined surface elevations at each site and river stage elevations using high resolution elevation data from LiDAR (U.S. Geological Survey, 2015). The dataset collected over the Animas River Valley was delivered as a raster with 1 m^2 resolution, with an elevation accuracy of 7–16 cm. The improved spatial resolution of the LiDAR dataset allowed us to more accurately estimate the water level elevation based on the higher resolution ground surface elevation.

Timing of Groundwater Level Measurements and Sample Collection

For this study, groundwater level measurements and water samples for geochemical analyses were collected during high flows (snowmelt runoff, spring) and low flows (baseflow, winter), as well as irrigation onset and monsoon storm events. Sampling events occurred at the following time periods: January 26–27, 2016; March 14–17, 2016; May 31–June 10; October 17–21, 2016; January 23-February 3, 2017; March 13–24, 2017; and May 29–June 9, 2017 (Figure 8). Groundwater level measurements are found in Appendix B, and chemical data from water sampling are presented in Appendix C.

Water Level Measurements

Water levels were measured following U.S. Geological Survey protocols for a steel tape measurement device with repeat measurements to within 0.02 ft (Cunningham and Schalk, 2011). If water level measurements were not repeatable within 0.02 ft, notes were made and entered into database suggesting that these measurements were of lower data quality. This may happen for various reasons, such as when the well is pumping, recovering, or a nearby site is being pumped. The goal is to obtain a static water level measurement which is confirmed by a repeatable measurement within 0.02 ft. All manual groundwater level measurements are found in Appendix B. Water level data from pressure transducers with data recorders are available from the New Mexico Bureau of Geology and Mineral Resources upon request.

To assess the nature of the seasonal groundwater flow direction, four water table maps were made from the water level monitoring network for each of the unique sampling periods collected in 2016. Water

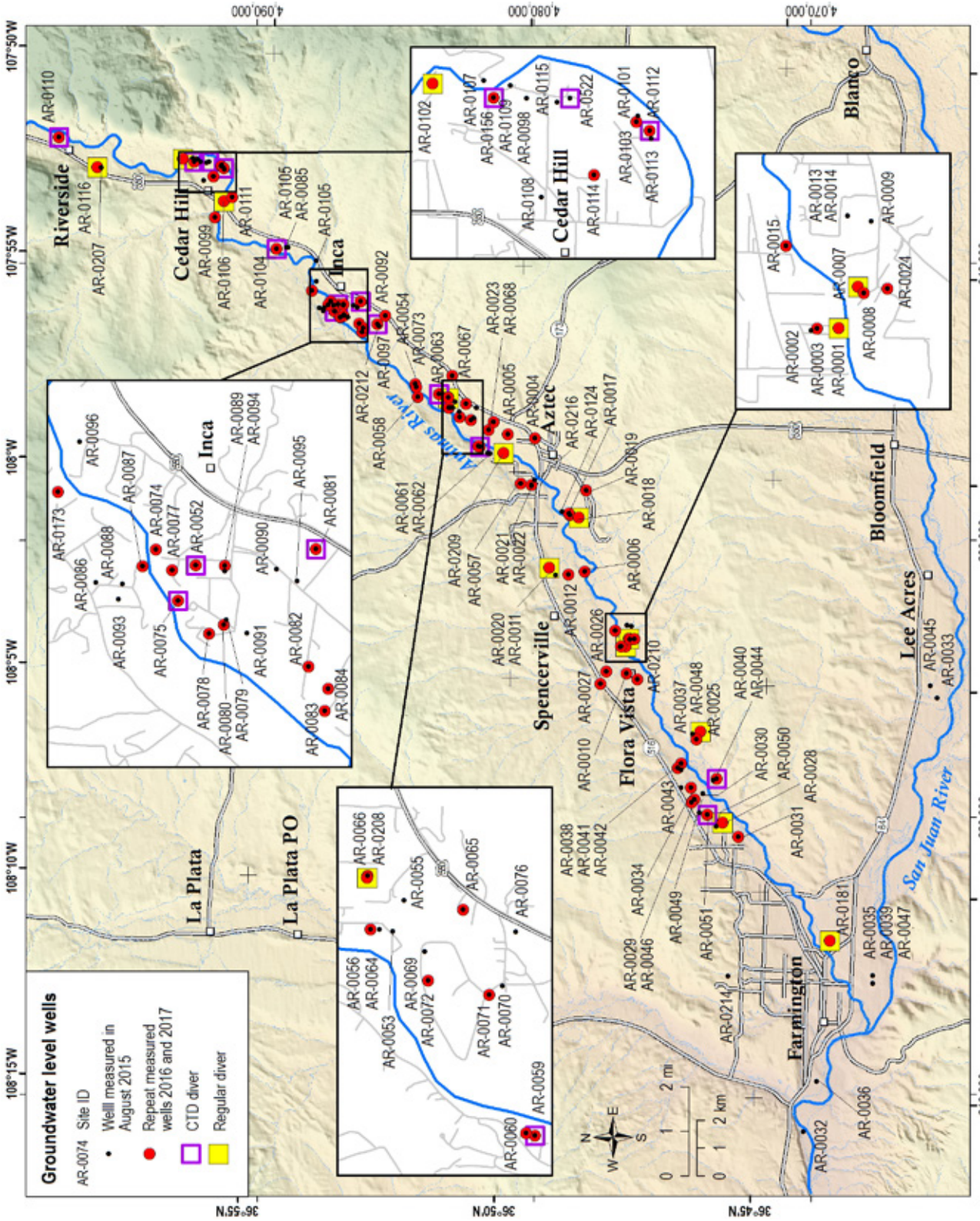

Figure 5. Locations of groundwater level measurement sites. As a response to the Gold King Mine spill, staff from NMBGMR, NMOSE, the USGS and other agencies measured groundwater levels in over 100 wells in August 2015 (small black points). A subset of those wells make up the well network for this study. Wells within this network were measured repeatedly between January 2016 and June 2017 (red circles). Within this well network, 12 wells were equipped regular pressure transducers (Divers) that collect continuous measurements of water level and water temperature (purple squares). A total of 13 wells were equipped with CTD Divers, which measure specific conductance in addition to temperature and water level (yellow squares). Well point IDs used in this study are listed on the map, and can be cross-referenced with data tables in this report. The well inventory is included in Appendix A.

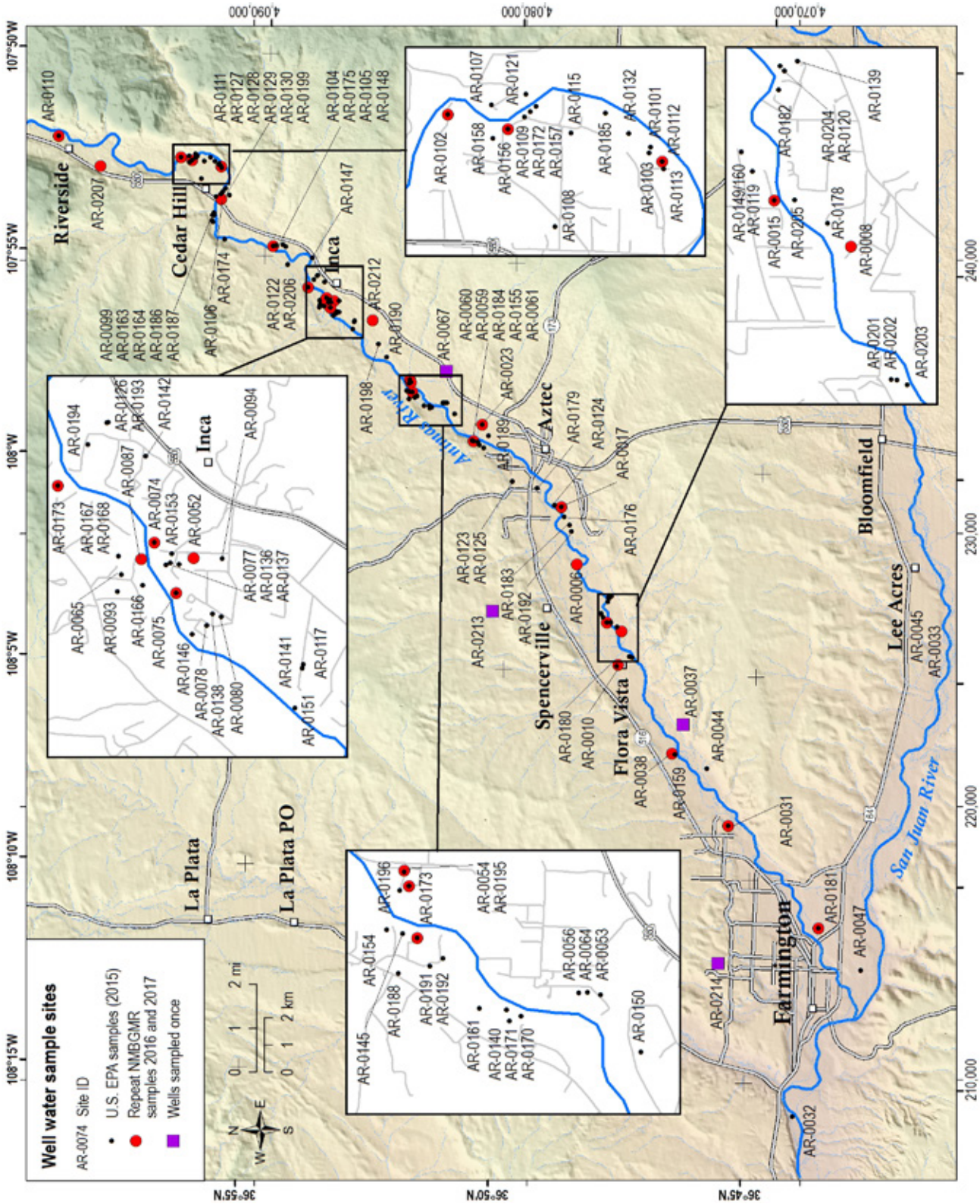

Figure 6. Well water sample sites. As a response to the Gold King Mine Spill, the U.S. Environmental Protection Agency collected over 100 water samples from numerous private domestic and irrigation wells for geochemical analyses in August 2015 (small black points). NMBGMR sampled up to 26 wells on seven different sampling events between January 2016 and June 2017 (red circles). In addition, four wells were sampled only once in March 2017 with the goal of characterizing regional groundwater (purple squares).

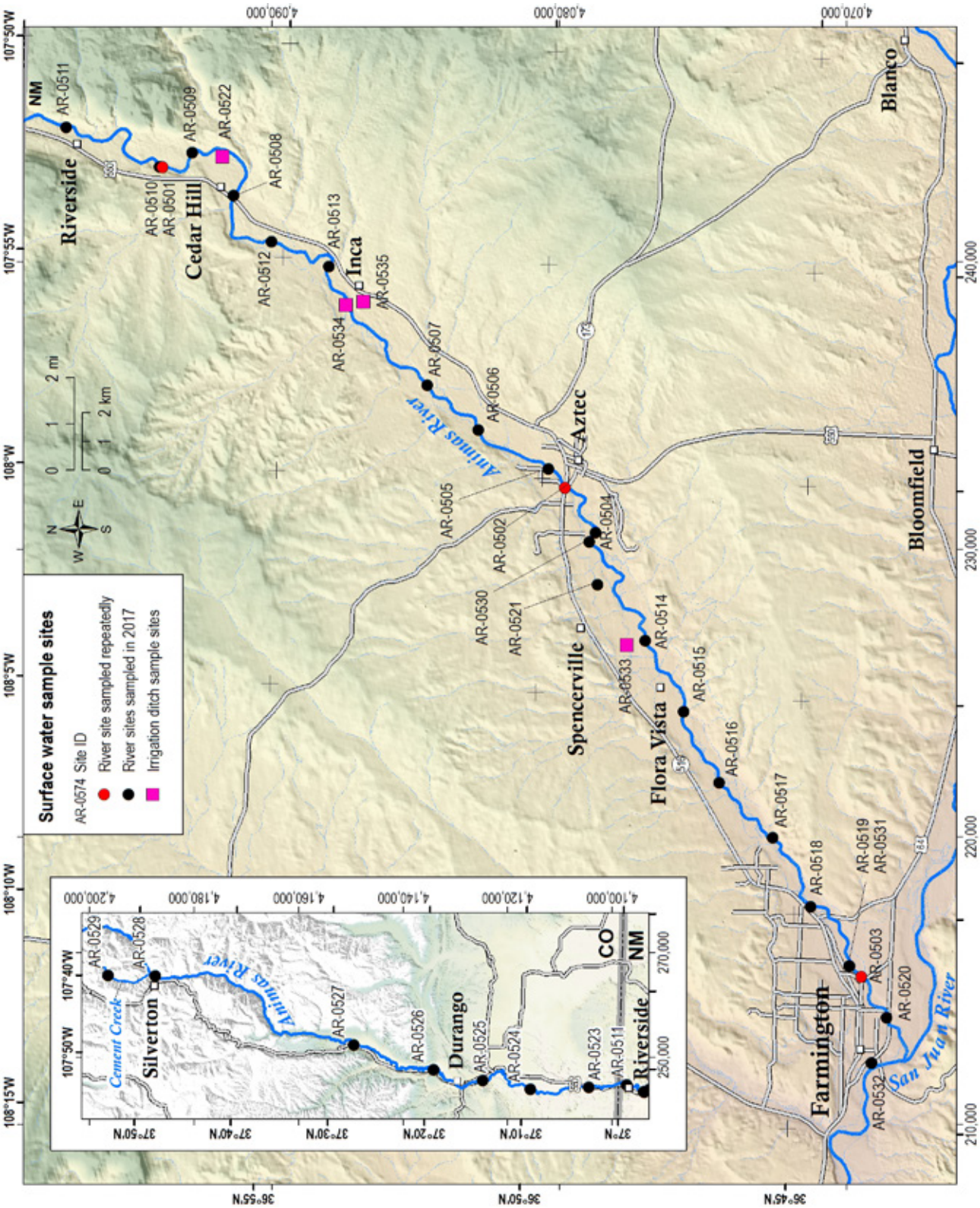

Figure 7. Surface water sample sites. River water samples were collected for stable isotope analysis at three river sites for each sampling event between January 2016 and June 2017 (red circles). River water samples were collected for stable isotope analysis and field parameters at numerous sites along the Animas including 7 sites in Colorado in 2017 (black circles). Four irrigation ditches were sampled for stable isotope analysis and field parameters in June 2017 (pink squares).

Table 1. Well networks. For this study, these are the wells in the water level and water quality monitoring networks.

Site ID	UTM easting NAD83	UTM northing NAD83	Elevation (ft asl)	Distance to river (m)	NMOSE well record	Well depth (ft bls)	Water level network well	Water quality network well
AR-0001	226179	4076700	5496	51	SJ-00186	31	x	
AR-0003	226176	4076850	5497	200		27	x	
AR-0004	233702	4079960	5661	899		58	x	
AR-0005	233838	4080950	5642	668	SJ-03939	62	x	
AR-0006	228880	4078170	5538	58	SJ-03793		x	x
AR-0007	226463	4076570	5505	89	SJ-03663	32	x	
AR-0008	226419	4076530	5504	101	SJ-02653	21	x	x
AR-0010	225194	4076660	5517	547		38	x	x
AR-0012	228771	4078750	5577	620		18	x	
AR-0015	226741	4077060	5512	32		29	x	x
AR-0016	230933	4078710	5573	83	SJ-01722	20	x	
AR-0017	230984	4078740	5571	108	SJ-01722 POD2	17	x	x
AR-0018	230841	4078390	5580	321	SJ-03821	13	x	
AR-0019	231810	4078110	5647	968	SJ-03718	68	x	
AR-0020	229016	4079450	5621	1087	SJ-01310	67	x	
AR-0021	232008	4080090	5630	296	SJ-03790	49	x	
AR-0023	234008	4081640	5643	532	SJ-02814	31	x	x
AR-0024	226448	4076370	5511	259	SJ-02553	25	x	
AR-0025	223102	4073990	5600	866	SJ-03614	48	x	
AR-0026	225273	4077390	5540	969		40	x	
AR-0027	224833	4077610	5567	1409		48	x	
AR-0028	219814	4073190	5413	443		20	x	
AR-0029	220655	4074210	5457	565			x	
AR-0031	219294	4072630	5384	355		14	x	x
AR-0034	221070	4074330	5453	425			x	
AR-0038	221948	4074690	5443	185		35	x	x
AR-0041	221789	4074810	5467	322			x	
AR-0044	221393	4073400	5441	398		39	x	
AR-0046	220537	4074320	5464	706	SJ-02266		x	
AR-0048	222819	4074140	5578	562	SJ-03143 POD2	40	x	
AR-0051	220096	4073740	5429	592	SJ-02792	49	x	
AR-0052	238534	4087080	5740	259			x	x
AR-0054	235654	4084290	5685	211	SJ-02049	26	x	x
AR-0056	234810	4083080	5657	93			x	
AR-0057	232064	4080490	5638	602	SJ-03209	49	x	
AR-0058	235190	4084200	5678	69	SJ-02656	21	x	x
AR-0059	233406	4081960	5659	99	SJ-04130	50	x	x
AR-0060	233423	4082020	5664	101	SJ-04129	60	x	
AR-0063	235309	4083430	5669	388			x	
AR-0065	234946	4082450	5695	602			x	
AR-0066	235177	4083100	5666	440			x	
AR-0067	235954	4082950	5721	1125	SJ-03543	61	x	x
AR-0068	234296	4081460	5654	867		31	x	
AR-0071	234364	4082272	5657	536			x	
AR-0072	234462	4082686	5653	214	SJ-03720	21	x	
AR-0073	235546	4084255	5682	162			x	x
AR-0074	238641	4087350	5743	7	SJ-03124	20	x	x
AR-0075	238293	4087200	5733	2			x	x
AR-0077	238501	4087240	5740	147			x	
AR-0078	238070	4086990	5736	128	SJ-00318	20	x	
AR-0080	238130	4086890	5733	218	SJ-03670	26	x	
AR-0081	238644	4086260	5782	950			x	
AR-0082	237843	4086310	5737	290			x	
AR-0083	237541	4086200	5727	167			x	
AR-0084	237693	4086178	5732	280			x	
AR-0087	238528	4087440	5739	13			x	x
AR-0092	238124	4085370	5791	1089			x	
AR-0094	238533	4086880	5757	402			x	
AR-0099	241689	4091530	5823	112	SJ-02083	23	x	
AR-0102	243793	4092680	5857	100	SJ-03683	23	x	x
AR-0103	243531	4091290	5842	68			x	
AR-0104	240539	4089310	5783	126			x	x
AR-0106	242278	4091200	5825	122			x	x
AR-0110	244588	4097170	5947	97			x	x
AR-0111	242411	4090900	5826	295			x	
AR-0112	243470	4091200	5839	80			x	x
AR-0114	243169	4091580	5859	519	SJ-03778	60	x	
AR-0116	243507	4095780	5953	670		69	x	
AR-0156	243694	4092265	5860	30	SJ-03069	35	x	x
AR-0173	239035	4088019	5797	69	SJ-03324	43	x	x
AR-0181	215547	4069320	5331	387	SJ-00184	30	x	x
AR-0207	243480	4095630	5966	578				x
AR-0208	235162	4083104	5665	424		28	x	
AR-0209	233169	4081107	5642	47		19	x	
AR-0210	224986	4076268	5499	412	SJ-03605	43	x	
AR-0212	237835	4085662	5743	680	SJ-03925	43	x	x

asl–above sea level; bls–below land surface

Table 2. Continuous recorder sites and type of continuous data recording.

Site ID	UTM easting NAD83	UTM northing NAD83	Site type	Water level and Temp	Water level, temp and sp. Cond.
AR-0001	226179	4076700	Well	x	
AR-0007	226463	4076570	Well	x	
AR-0018	230841	4078390	Well	x	
AR-0020	229016	4079450	Well	x	
AR-0025	223102	4073990	Well	x	
AR-0028	219814	4073190	Well	x	
AR-0044	221393	4073400	Well		x
AR-0051	220096	4073740	Well		x
AR-0052	238534	4087080	Well		x
AR-0059	233406	4081960	Well		x
AR-0063	235309	4083430	Well		x
AR-0075	238293	4087200	Well		x
AR-0081	238644	4086260	Well		x
AR-0102	243793	4092680	Well	x	
AR-0104	240539	4089310	Well		x
AR-0106	242278	4091200	Well	x	
AR-0110	244588	4097170	Well		x
AR-0112	243470	4091200	Well		x
AR-0116	243507	4095780	Well	x	
AR-0156	243694	4092265	Well		x
AR-0181	215547	4069320	Well	x	
AR-0208	235162	4083104	Well	x	
AR-0209	233169	4081107	Well	x	
AR-0212	237835	4085662	Well		x
AR-0522	243691	4091744	Irrigation ditch		x

table elevation contours were drawn by hand using the river stage elevation, modeled during each period, along with the water level measurements. Where not enough data existed, contours were approximated based on basic hydrogeologic properties.

Continuous Data Recorders

We use the term "continuous" to mean that data were collected at regular time intervals by instruments installed in the field. For this study, most continuous data were collected hourly. Continuous measurements of pressure and temperature were recorded using Van Essen "Divers" and "Baros" to measure and record pressure data in wells and the atmosphere respectively. We processed these data using software provided by Van Essen, which subtracts atmospheric pressure from total pressure measured in the wells and accounts for water temperature to convert pressure readings to water head that is equal to the depth of water above the pressure transducer. These continuous water level data were then adjusted based on manual water level measurements that were done at the time of the download. These adjustments that are based on the difference between the manual water level measurement and the corresponding instrument measurement (recorded at the time closest to that of the manual measurement) were applied to continuous water level data going backward in time, to the previous site download/measurement.

As noted in Table 2, a subset of these data recorders (CTD Divers) measured specific conductance in addition to temperature and pressure. Throughout the duration of this study, the factory calibrated instruments yielded specific conductance measurements within 5% of measurements made independently in the field with instruments that had been recently calibrated against known standards. Therefore the recalibration of the CTD Divers was not necessary.

Water Sampling

Sampling protocols used by New Mexico Bureau of Geology and Mineral Resources are described in more detail by Timmons et al. (2013), and as specified in the New Mexico Bureau of Geology and Mineral Resources protocols for clean sampling (Appendix D). The goal was to collect water samples that were chemically representative of local groundwater from existing domestic and irrigation wells that were equipped with pumps. Most of these wells are used regularly, and therefore well bore water is mobile and likely does not reside in the well casing long enough for the chemical composition of the water to change significantly. However, we still took extra precautions to ensure the integrity of the water sample. General water sampling procedures include purging the well until field parameters (pH, dissolved oxygen, specific conductivity, oxidation-reduction potential (ORP), and temperature), which are being monitored in real time, stabilize before collecting the sample. In order to prevent contamination of the samples from external sources and cross-contamination from other samples, we followed a strict sampling protocol (Appendix D). All sampling equipment was cleaned using laboratory soap and rinsed with deionized water immediately prior to each sampling event and at

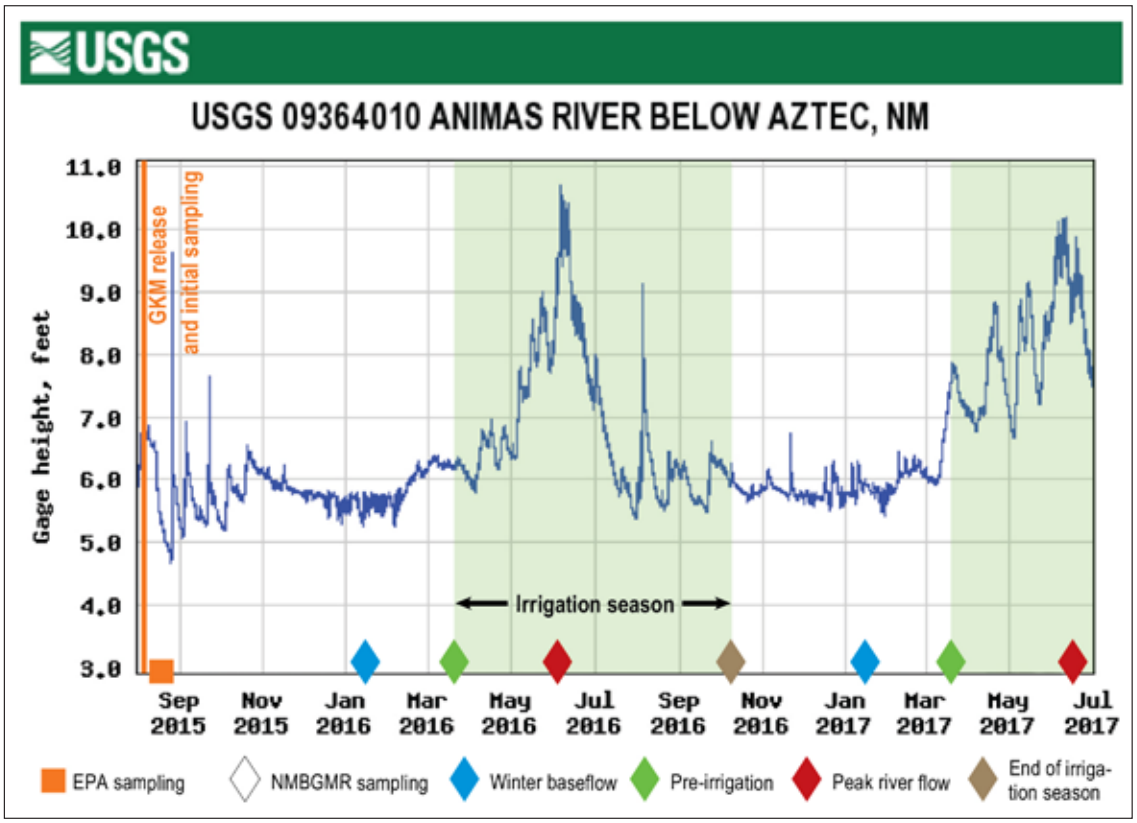

Figure 8. Timing of sampling events. Graph shows U.S. Environmental Protection Agency sampling, and New Mexico Bureau of Geology and Mineral Resources sampling, with U.S. Geological Survey gage height (used to infer surface water flow) of Animas River just below Aztec, New Mexico.

the end of each day during the sampling event. A separate clean sampling manifold and tubing was used for each well and Nitrile gloves were worn during the sampling procedure.

All groundwater samples were analyzed for major cations and anions, trace metals, and the stable isotopes of oxygen and hydrogen. For trace metals and major cations, total and dissolved concentrations were determined. Water to be analyzed for dissolved trace metals and cations was filtered (0.45 micron filters) and acidified with nitric acid in the field. Water samples to be analyzed for total trace metals and cations were also acidified but were not filtered so that any constituent of interest that was adsorbed to colloids and small particulates would be included in the analysis. For a small subset of wells, extra samples were collected for the analysis of the environmental tracers, carbon-14 and tritium. Water samples collected from the river and irrigation ditches, were analyzed only for the stable isotopes of oxygen and hydrogen. Samples collected for stable isotope, carbon-14, and tritium analyses were not filtered or treated in any way in the field prior to submitting samples to analytical laboratories. All water samples, with the exception of the stable isotope samples, were stored in a cool environment with a goal of maintaining temperatures below four degrees Celsius. Samples for stable isotopic analysis were stored at room temperature in a small box. All water samples were tracked using chain-of-custody documentation. Analyses for trace metals, major ions and stable isotopes of oxygen and hydrogen were performed at the Chemistry Lab at New Mexico Bureau of Geology and Mineral Resources. Samples to be analyzed for environmental tracers were sent to Beta Analytic (carbon-14) and Miami Tritium Lab (tritium).

Measuring the water level in a well just south of the New Mexico-Colorado border on a cold day in January 2016.

III. RESULTS AND INTERPRETATIONS

Water Level Measurements

Well network description

The initial water level measurement period in August 2015 included 111 wells during monsoon and irrigation seasons (Figure 5). Building from the original network of wells, the monitoring network established by the New Mexico Bureau of Geology and Mineral Resources consisted of 50 to 80 wells measured during the following periods: baseflow (late-January), initial snowmelt/onset of irrigation season (mid-March), peak snowmelt/extended irrigation season (early-June), and at the end of irrigation season (mid-October). Occasionally, wells were not measured during one or more of the measurement campaigns due to scheduling conflicts, freezing conditions, or if well owners opted out of the program (Appendix B). Figure 9 shows the magnitude of annual fluctuations recorded from each well's water level measurements in 2016. In general, wells located farther from the river have greater fluctuation. The reach between Aztec and Inca is where we see the largest annual fluctuation. Areas that experience significant fluctuation are susceptible to changes in groundwater flow direction.

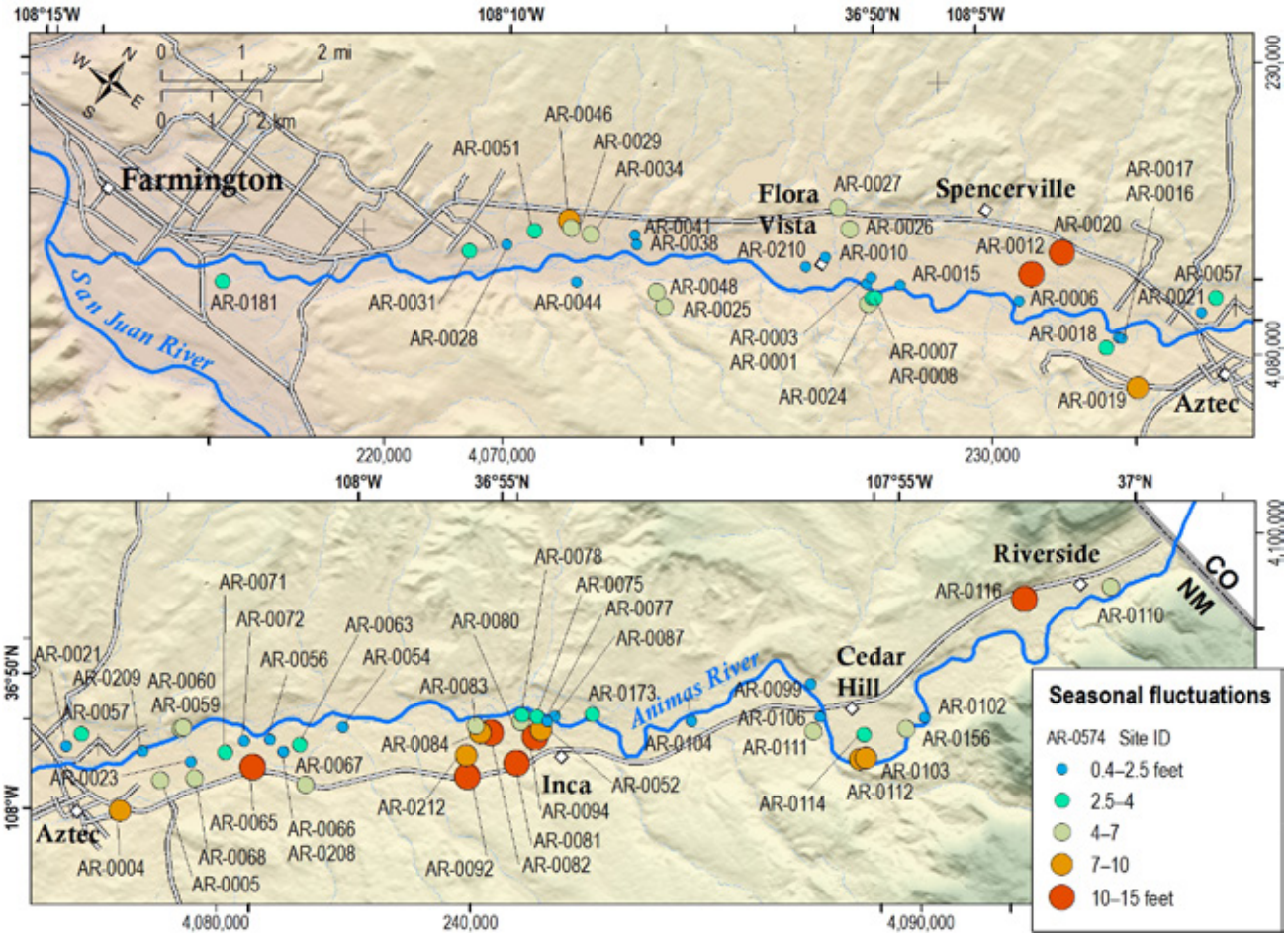

Figure 9. Map showing the seasonal range in water level fluctuations. The color and size of the point represents the difference between the maximum and minimum water level elevations observed at each well in 2016.

Water table analysis

Groundwater level measurements were used to construct water table elevation maps that can help determine the direction of groundwater flow and observe seasonal changes in the hydraulic gradient. Our observations show that in a broad sense, the Animas River is gaining water from the groundwater, as groundwater from the surrounding valley flows downhill, or down gradient, discharging to the river. However, by looking at the water levels in close proximity to the river, we found that the water table gradient can be nearly flat (low gradient). In some locations (indicated as red points on the water table maps, Figure 10), we observed that the water table elevation is below river elevation, suggesting that the

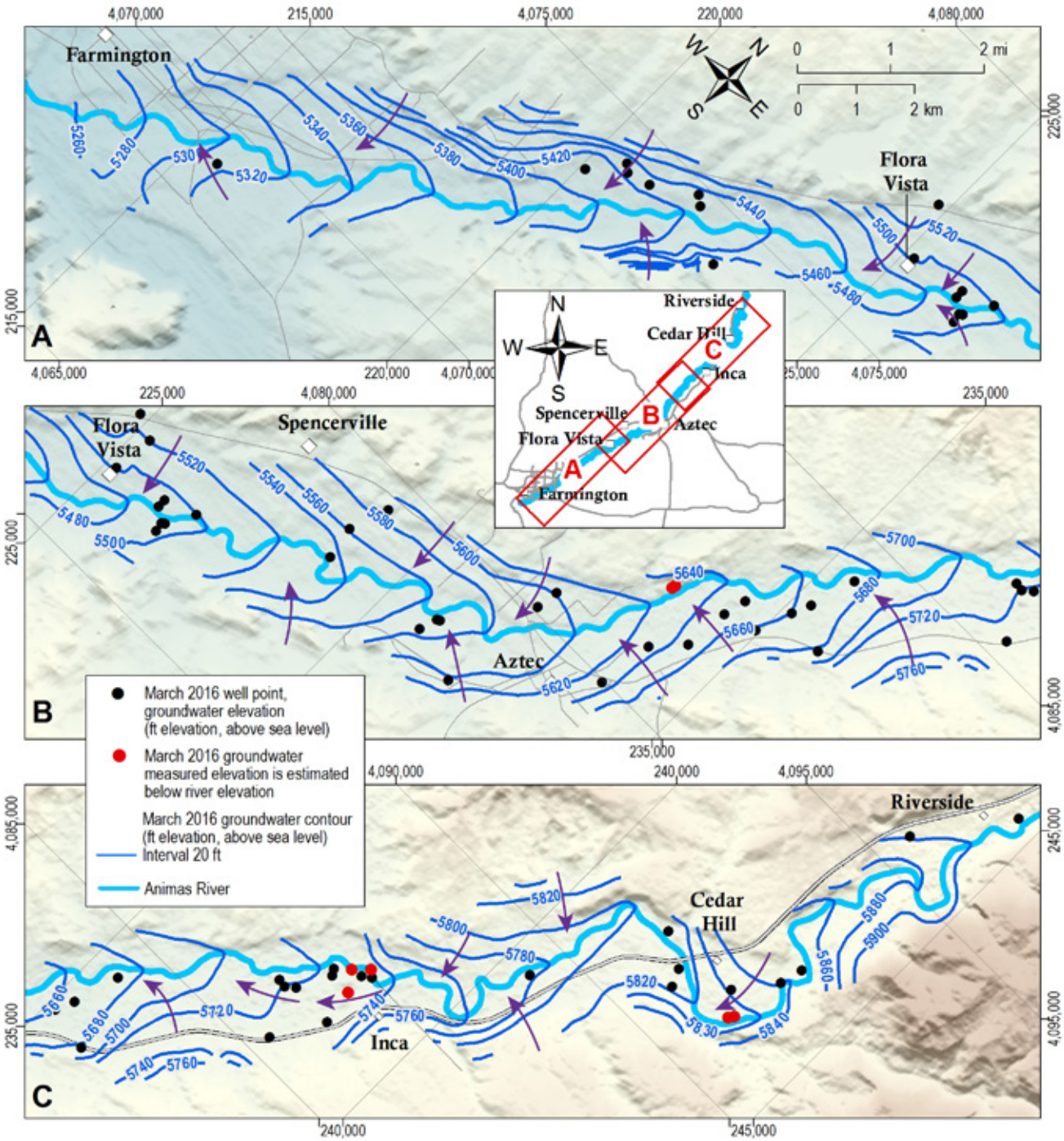

Figure 10. Water table map based on water level measurements during March 2016. The purple arrows indicate approximate groundwater flow directions.

river could add water to the aquifer (a losing river). With a flat or nearly flat water table, fluctuations in the river stage can turn a slightly gaining reach to a slightly losing reach. The difference between groundwater elevations and the river stage elevation, in places, is small (less than 1 ft), so it may not be detected by coarse resolution water table mapping.

Groundwater levels in the valley were generally lowest in March, before the irrigation season begins, and highest in October, near the end of the irrigation season. Therefore, by comparing the water table map contoured from the March data to the map based on October water level data, we can better understand seasonal changes in groundwater flow conditions. Two areas that show the largest seasonal variations are the Cedar Hill area (Figure 11A), and the Inca area (Figure 11B). Looking closely at the water table changes in the Cedar Hill area, the hydraulic gradient between the river and the aquifer reverses from losing conditions (river recharging aquifer) in March, which was seen in specific wells that are close to the river and are highlighted in red, to gaining conditions (groundwater discharging to river) in October.

The Inca area shows the largest seasonal groundwater level fluctuation. From the water table contoured using the March water level measurements, the hydraulic gradient near Inca dramatically flattens during the winter/non-irrigation period. While it isn't uncommon that the water table gradient flattens out during this period, the flat gradient extends farther from the river, and to a greater degree than other locations along river. Once the irrigation season begins, the system shift back to gaining conditions.

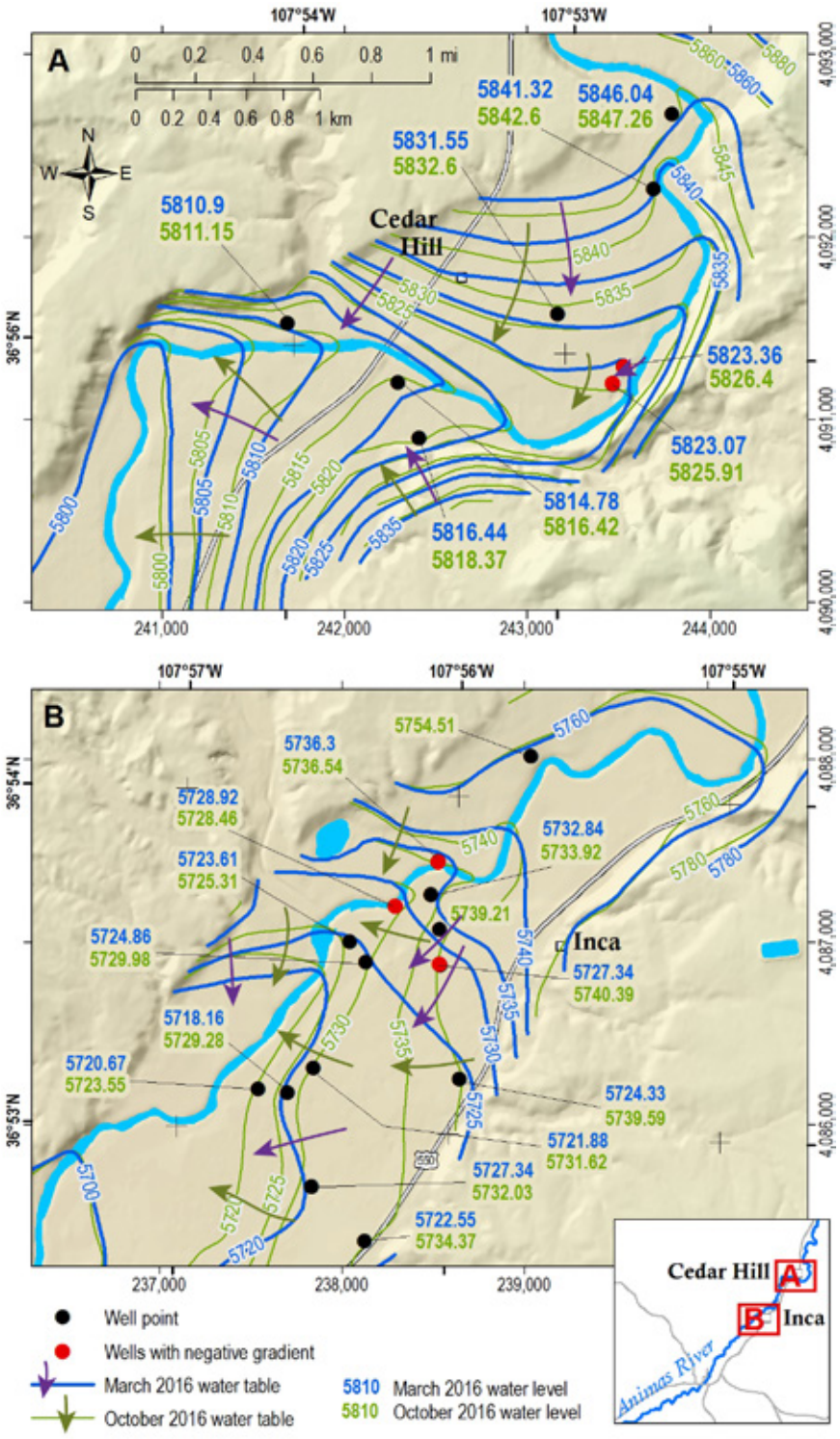

Figure 11. Water table maps showing water level elevation contours and arrows that indicate approximate groundwater flow directions for March 2016 (blue contours, purple arrows) and October 2016 (green contours and green arrows). **A**—In the Cedar Hill region, March and October water level elevation contours differ slightly. Observed localized losing conditions in March near wells indicated by red points change to gaining conditions by October. **B**—Near Inca, March and October water level contours differ dramatically with a flatter gradient and observed localized losing conditions in March. By October, this reach of the river is observed to be gaining water from the aquifer.

Hydrograph trends

To better understand the hydrodynamics of the alluvial aquifer, we

examined observed temporal fluctuations in water levels and how these fluctuations vary throughout the study area. Continuous water level measurements in many wells (Table 2) showed clear seasonal water level fluctuations. From the groundwater monitoring network, 75 wells had at least three manual measurements from which to assess seasonal fluctuations. We used continuous water level data to help fill in the gaps between sampling periods for manual water level datasets to better assess fluctuations that were missed between sampling events. Additionally, this allowed us to more effectively define and group the manual hydrographs into distinguishable trends.

The trends are characterized by the magnitude of the seasonal fluctuations, and the timing of the peak in groundwater level. From studying the continuous pressure records we identified three main hydrograph trends: 1) river-stage-controlled, 2) irrigation-controlled, and 3) winter-recharge/summer-evapotranspiration (Figure 12).

The first hydrograph trend, the ***river-stage-controlled*** hydrographs (Figure 13) indicates a hydraulic connection to the river. These records correlate with the stage of the Animas River, and represent 22 of the 70 wells with distinguishable hydrograph trends. In general, these wells fluctuate rapidly, mimicking the stage of the river. The most distinct feature in the river-stage-controlled water hydrographs is the rise in water level in early June, which coincides with peak snowmelt moving through the valley. This peak is generally followed by a rapid drop in groundwater level through August. By late September, groundwater levels have stabilized and remain relatively flat through the winter. Wells that have the river-stage-controlled trend are typically closest to the river (median distance of 320 ft) and exhibit a median annual water level fluctuation of 3.5 ft. These wells are very shallow with a median total depth of 31 ft, and a median depth-to-water of about 9.4 ft below ground surface. The close proximity of these wells to the river plays a large part in the fluctuations that characterize this group. Moving farther away from the Animas River, the effect of the stage of the river is muted and the impact of irrigation can also be distinguished.

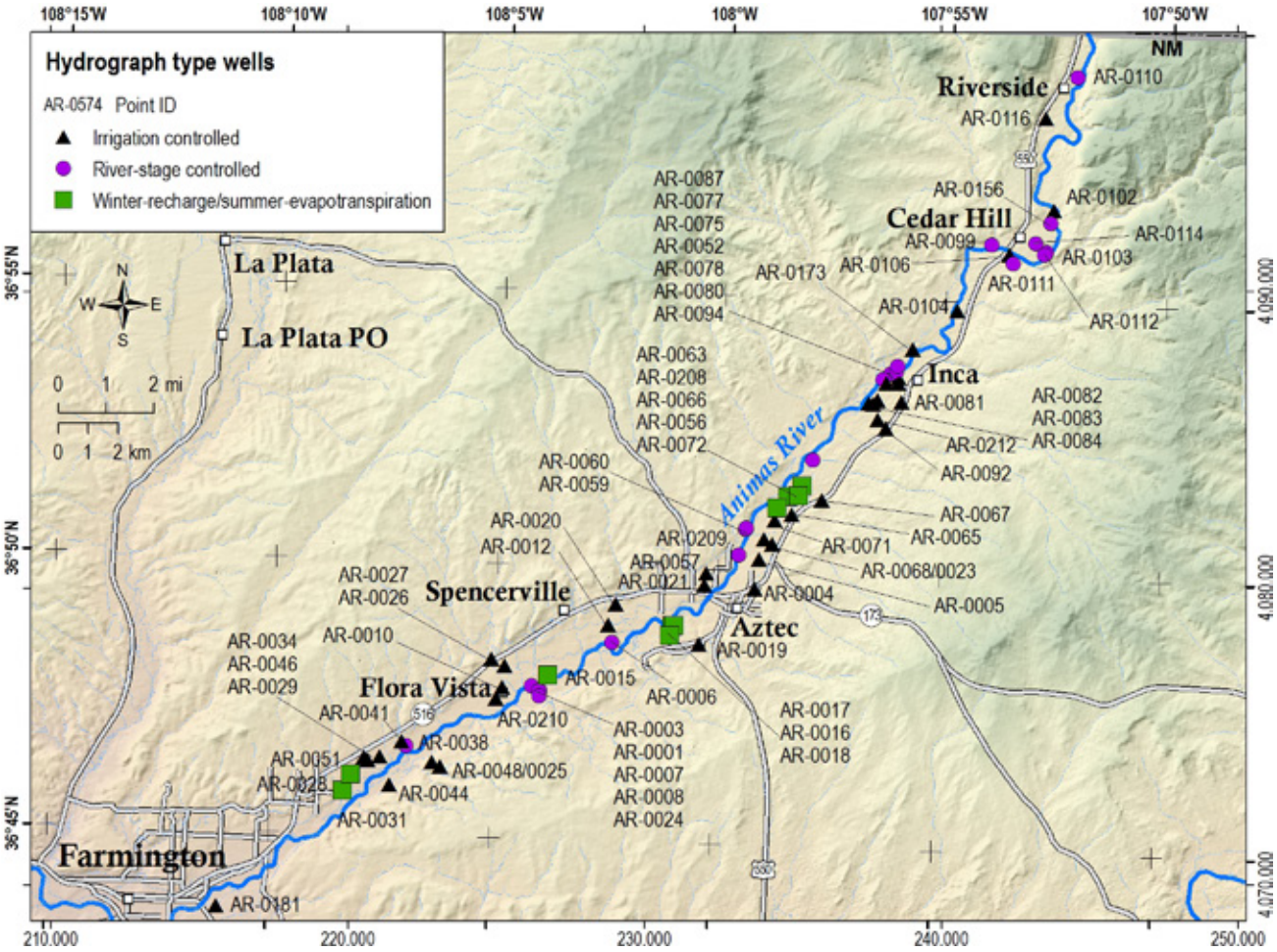

Figure 12. Locations of different hydrograph type wells.

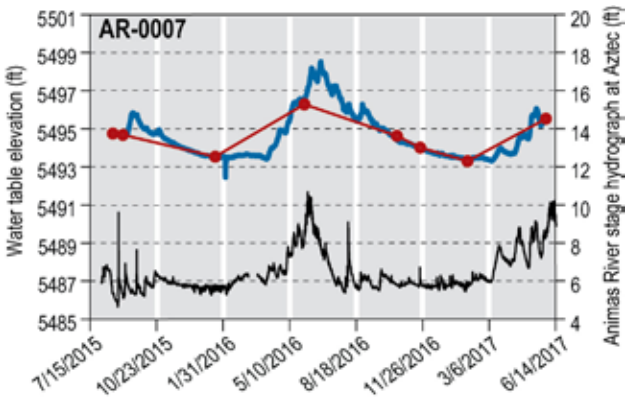

Figure 13. Example of a river-stage-controlled hydrograph (AR-0007). Both the manually collected water level measurements (red points) and the continuous pressure transducer (blue line) data sets are shown. The black line represents Animas River stage measured by the U.S. Geological Survey at Aztec, New Mexico (09364010). These data are available through the USGS data portal (https://waterdata.usgs.gov/nwis/uv?09364010).

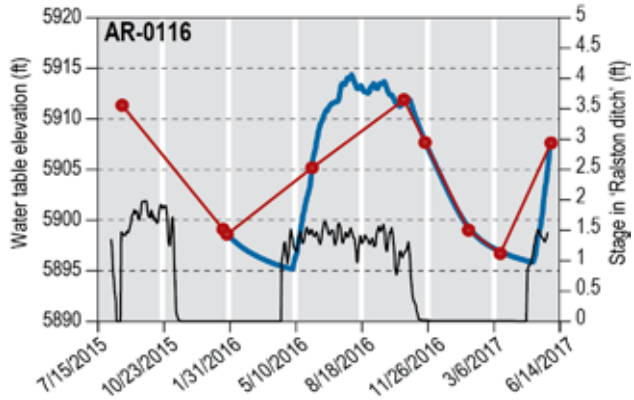

Figure 14. Example of an irrigation-controlled hydrograph (AR-0116). Both the manual water level measurements (red points) and the continuous pressure transducer (blue line) data sets are shown. Ralston ditch stage, in feet, is show by the black line. The intake of the Ralston ditch, where it takes its water from the Animas River, is located in the northern end of the study area, 1.3 miles south of the Colorado border. This data is available from the New Mexico Office of the State Engineer (meas.ose.state.nm.us).

The ***irrigation-controlled*** hydrograph trend is the most prevalent amongst the wells measured (38 of 70 wells), and is heavily influenced by the irrigation season (Figure 14). These wells clearly show the alluvial aquifer being recharged during the irrigation season. Where the river-stage-controlled hydrographs are generally prone to sharp spikes in water levels as they respond to the irregular flow of the river, the irrigation-controlled trend is characterized by smooth seasonal fluctuations. When the ditches are first filled in late March, the groundwater level begins to rapidly rise, similar to how the river-stage-controlled-groundwater wells respond to early snow melt runoff floods. What distinguishes the rise in water level seen in the irrigation-controlled hydrographs is the timing and magnitude of the change. While the river-stage-controlled-groundwater hydrographs peak rapidly in June before declining, the irrigation-controlled trend rises through June, and generally doesn't reach its maximum until late July. Water levels typically remain elevated in these wells until the end of the irrigation season, when the ditches are shut off. At this point, there is a sharp drop in water levels as the ditches are no longer supplying water to the alluvial aquifer. The declining leg of these hydrographs begins flattening as the water level appears to approach equilibrium before the irrigation season begins again. Wells that have this irrigation-controlled trend are much farther away from the river than the wells that exhibit the other hydrograph types (median distance of 1,810 ft). These wells also display the largest annual change in water level, with a median fluctuation of 5.7 ft. These wells are typically deeper with a median total depth of 43 ft and a median depth-to-water of about 14.7 ft below ground surface.

The irrigation season is important both for the economy of the area and the recharge of the alluvial aquifer. The return groundwater flow from irrigated land and the water lost through the base of the irrigation ditches supports the water table. This in turn contributes to gaining river conditions seen throughout the valley.

The third hydrograph trend is much more subtle. A smaller portion of the wells in the study area show the impact of ***winter-recharge/summer-evapotranspiration*** (10 of 70 wells). Unlike wells that exhibit the other hydrograph trends, these wells have an increase in water level in the winter (Figure 15). In some of these hydrographs, we can distinguish recharge events that are associated with individual snow storms. These brief sharp increases in water level are best observed in AR-0028. During the summer these wells typically show water level declines that are likely the result of increased evapotranspiration. Wells that show this winter-recharge/summer-evapotranspiration trend are generally located within the flood plain, a median distance of 1,160 ft away from the river. This trend shows the smallest seasonal variability, with a median annual fluctuation of 2.1 ft. These wells are typically very shallow with a median total depth of about 20 ft and a median depth-to-water of about 2.5 ft below ground surface. The shallow nature of the water table where these wells are found plays a large role in the seasonal fluctuations. Because the water table is so close to the surface in these areas, plant roots are in direct contact with the aquifers. As result,

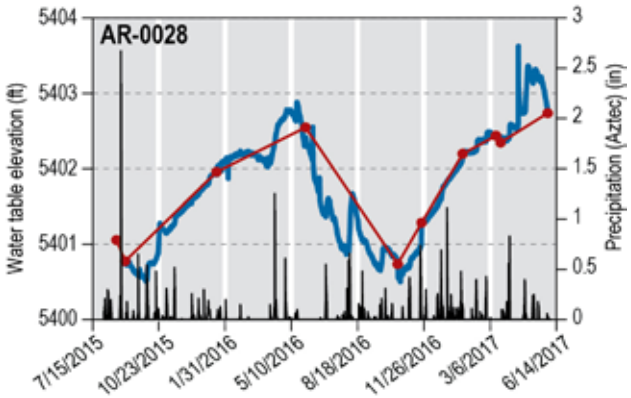

Figure 15. Example of a winter-recharge/ summer-evapotranspiration hydrograph (AR-0028). Both the manually collected water level measurements (red points) and the continuous pressure transducer (blue line) data sets are shown. The black bars represent daily precipitation in inches recorded in Aztec (GHCND:USC00290692). These data are available from NOAA's Climate Data Online portal (ncdc.noaa.gov/cdo-web).

in the summer months we see declines, followed by a rebound in water levels during the winter, when the vegetation is dormant.

Groundwater Chemistry

Field parameters

Field parameters, including pH, specific conductance (SC), temperature, dissolved oxygen (DO), and oxidation reduction potential (ORP), were measured in the field for all wells sampled as part of the sample collection procedure. Table 3 shows mean, maximum, and minimum field parameters for wells that were sampled multiple times. Table 4 shows field parameters for wells that were sampled only once, in March 2017, for the purpose of characterizing regional

Table 3. Average field parameters for wells sampled multiple times for this study. The number of samples and timing of sampling for each well is also shown. Oxidation reduction potential (ORP) values are voltages vs. a silver: silver-chloride reference electrode.

	SAMPLING EVENTS							DISSOLVED OXYGEN (mg/L)			pH			SPECIFIC CONDUCTANCE (µS/cm)			TEMPERATURE (°C)			OXIDATION REDUCTION POTENTIAL (mV)		
Site ID	Jan-16	Mar-16	Jun-16	Oct-16	Jan-17	Mar-17	Jun-17	Mean	Max	Min	Mean	Max	Min	Mean	Max	Min	Mean	Max	Min	Mean	Max	Min
AR-0006	x	x	x	x	x	x	x	0.54	1.50	0.04	7.09	7.24	6.81	756	889	602	11.25	13.50	10.10	-91.2	-52.5	-137.5
AR-0008	x	x	x	x	x	x	x	1.66	1.97	0.78	7.16	7.30	6.89	1575	1799	1286	14.95	15.80	13.95	67.4	117.6	-5.0
AR-0010	x	x	x	x	x	x	x	2.32	3.54	1.50	7.15	7.36	6.73	1164	1399	958	15.58	16.10	14.78	107.0	170.0	4.0
AR-0015	x	x	x	x	x		x	1.02	0.45	2.18	7.21	7.40	6.92	1180	1388	993	13.83	15.50	13.10	81.8	148.2	-101.6
AR-0017	x	x	x	x	x		x	0.30	0.07	0.53	7.13	7.34	6.77	1434	1743	1169	12.66	14.40	11.50	-0.8	49.6	-57.9
AR-0023			x	x		x	x	0.29	0.47	0.06	7.27	7.41	6.95	753	843	614	12.99	13.20	12.68	-10.7	23.5	-35.5
AR-0031			x	x			x	1.34	1.75	0.86	6.81	6.96	6.57	2260	2822	1535	14.00	16.00	13.00	94.1	108.0	85.5
AR-0038	x	x	x	x	x	x	x	1.66	3.34	0.74	7.03	7.21	6.78	1203	1417	989	15.10	16.40	14.67	84.0	173.8	53.0
AR-0052				x		x	x	6.14	8.58	4.79	7.25	7.46	6.94	624	693	561	14.94	15.80	14.42	65.4	94.7	43.7
AR-0054				x	x	x	x	1.16	1.16	0.07	7.04	7.07	6.86	959	997	898	13.51	15.10	13.31	194.8	194.8	98.4
AR-0058		x	x	x	x	x	x	1.95	5.89	0.45	7.10	7.32	6.77	1063	1305	719	12.24	14.40	11.48	43.7	144.9	-74.7
AR-0059	x	x	x	x	x	x	x	2.66	4.96	0.75	7.36	7.52	7.06	822	1175	628	13.88	15.00	12.89	17.2	56.7	-90.9
AR-0073	x	x						2.01	3.79	0.22	7.28	7.36	7.19	681	698	663	11.60	12.00	11.20	100.7	109.2	92.2
AR-0074	x	x	x	x		x	x	2.55	7.20	0.30	7.49	8.32	6.84	647	844	527	11.84	16.30	9.67	-16.8	62.4	-65.8
AR-0075	x	x	x	x	x	x	x	5.10	10.12	10.12	7.48	7.78	6.97	790	1322	330	9.74	14.30	7.30	-85.5	-64.2	-113.9
AR-0087				x	x	x	x	2.83	5.93	5.93	7.17	7.31	6.82	864	1016	684	13.17	16.00	11.82	0.0	30.4	-26.2
AR-0102	x	x	x	x	x	x	x	0.85	1.72	0.22	7.14	7.37	6.71	807	918	662	12.56	13.70	12.00	73.8	120.9	32.9
AR-0104				x	x	x	x	0.31	0.49	0.13	7.20	7.42	6.77	956	968	949	11.59	12.90	11.05	-50.3	-13.7	-79.9
AR-0106	x	x	x	x	x	x	x	1.01	4.69	0.05	7.38	7.61	6.87	556	649	447	13.05	16.00	11.54	62.7	196.5	-38.6
AR-0110		x	x	x		x	x	3.97	6.27	1.31	7.21	7.47	6.83	854	969	741	15.38	16.00	13.90	97.1	123.0	70.6
AR-0112	x	x	x	x	x	x	x	0.58	1.20	0.02	7.44	7.79	6.96	554	680	431	12.26	13.70	11.30	-67.3	126.7	-135.0
AR-0156	x	x	x	x	x	x	x	5.42	7.11	1.97	7.14	7.37	6.81	700	927	500	13.39	15.40	12.50	77.4	154.2	-87.7
AR-0173				x	x	x	x	7.25	8.61	6.03	7.22	7.34	6.94	938	968	897	14.45	14.61	14.20	67.9	96.7	34.9
AR-0181	x	x	x	x	x	x	x	1.74	4.31	0.24	7.12	7.29	6.87	797	893	694	16.32	17.00	15.30	180.6	271.5	140.2
AR-0207	x	x	x	x	x	x	x	5.03	8.14	3.38	7.19	7.44	6.75	713	823	587	13.71	15.70	11.84	389.6	576.7	127.7
AR-0212				x	x	x	x	3.40	6.89	1.94	7.21	7.32	7.02	674	721	593	14.16	14.61	13.96	140.6	157.8	125.8

Table 4. Field parameters for four wells that were sampled during March 2017. These wells were chosen based on total depth and representation of regional water that is not influenced by river water or irrigation.

Site ID	Sample date	Dissolved oxygen (mg/L)	pH	Specific conductance (µS/cm)	Temperature (°C)	Oxidation reduction potential (mV)
AR-0037	3/13/2017	7.9	7.12	860	14.08	135
AR-0067	3/14/2017	3.9	7.29	982	19.94	165.3
AR-0213	3/16/2017	0.36	7.64	12049	16.5	-111.9
AR-0214	3/20/2017	1.98	6.99	3512	17.37	117.9

groundwater. AR-0037 is on the south side of the river half way between Aztec and Farmington and has a total depth of 320 ft. AR-0067 is located north of Aztec with a total depth of 61 ft. AR-0213 and AR-0214 are deep wells on the north side of the river between Aztec and Farmington, outside of the floodplain, with total depths of 500 ft and 370 ft respectively. All of these wells, according to driller's logs, appear to be completed in bedrock below the alluvial fill. However, as will be discussed below, AR-0213 and AR-0214 were the only wells that appears to produce regional groundwater that were clearly geochemically distinct compared all other groundwater samples. Field parameters were measured for the Animas River and selected irrigation ditches during March and June 2017 (Figure 16, Table 5). Water temperature and specific conductance were also measured continuously with data loggers installed in several wells throughout the study area (Figure 5).

Dissolved oxygen—While dissolved oxygen was measurable in all wells for all sampling events, measured dissolved oxygen in the shallow groundwater varied considerably spatially from one well to another and temporally within some individual wells. Because dissolved oxygen concentration can have a significant effect on water quality, specifically on the solubility of metals, we used the observed variability in dissolved oxygen to group wells into different categories that will be used in analyses discussed below. Figure 17 shows the range of dissolved oxygen concentration for each well as a function of the maximum measured dissolved oxygen, as well as the different dissolved oxygen categories. Wells were categorized as ***low dissolved oxygen*** wells, with concentrations below 3 mg/L for all samples collected at different times, and with small variability over time. ***Mixed dissolved oxygen*** wells had concentrations both less than and greater than 3 mg/L. Mixed dissolved oxygen wells that have similar values for the maximum and range

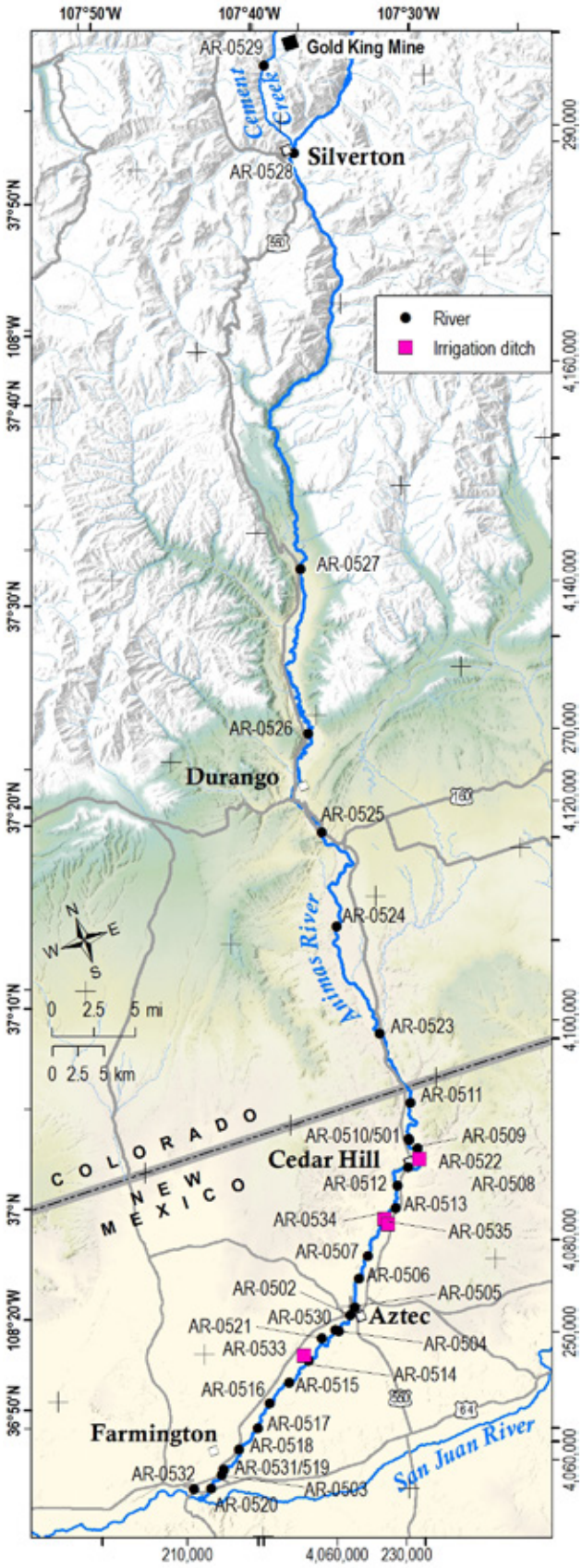

Figure 16. River (black points) and ditch (pink squares) locations sampled for field parameters and stable istotopes. Data are in Table 5 and Appendix C.

Table 5. Field parameters measured on the Animas River, ditches, and the San Juan River just below Farmington. Map locations shown in Figure 16.

Site ID	Site location	Collection date	Specific Conductance (µS/cm)	Dissolved Oxygen (mg/L)	Oxidation Reduction Potential (mV)	pH	Temperature (°C)
AR-0520	Animas	3/15/2017	393	9.7	218.1	8.04	13.27
AR-0519	Animas	3/15/2017	429	9.9	238.5	8.19	12.52
AR-0518	Animas	3/15/2017	513	8.35	303.9	8.11	14.99
AR-0517	Animas	3/15/2017	399	10.5	271.5	8.13	12.09
AR-0516	Animas	3/15/2017	400	9.99	202.3	8.16	11.8
AR-0515	Animas	3/15/2017	401	10.16	277.1	7.88	9.76
AR-0515	Animas	3/15/2017	401	10.16	277.1	7.88	9.76
AR-0514	Animas	3/15/2017	396	10.51	303.3	8.04	8.95
AR-0514	Animas	3/15/2017	396	10.51	303.3	8.04	8.95
AR-0521	Animas	3/15/2017	386	10.11	196.8	8.17	11.34
AR-0504	Animas	3/14/2017	407	11.32	253.9	7.9	8.06
AR-0505	Animas	3/14/2017	261	11.86	197.3	8.14	8.84
AR-0506	Animas	3/14/2017	414	8.97	172.8	8.16	10.4
AR-0507	Animas	3/14/2017	409	9.6	22.5	8.17	9.39
AR-0513	Animas	3/14/2017	388	9.79	380.2	7.08	10.38
AR-0512	Animas	3/14/2017	366	10.6	288	8.12	10.91
AR-0508	Animas	3/14/2017	385	8.67	296.2	7.49	9.42
AR-0509	Animas	3/14/2017	284	13.08	248.9	8.14	10.07
AR-0509	Animas	3/14/2017	284	13.08	248.9	8.14	10.07
AR-0510	Animas	3/14/2017	378	11.06	278	8.12	11.17
AR-0511	Animas	3/14/2017	373	9.88	254.9	7.75	10.67
AR-0501	Animas	6/7/2017	169	11.09	213.2	7.74	11.03
AR-0502	Animas	6/7/2017	179	11.12	226	7.55	12.08
AR-0503	Animas	6/7/2017	188	11.34	197.3	7.48	10.58
AR-0507	Animas	6/6/2017	178.4	9.73	299.4	7.93	11.8
AR-0508	Animas	6/6/2017	170.5	9.45	189	7.73	11.6
AR-0515	Animas	6/6/2017	188.5	9.73	284.5	8.03	12.8
AR-0517	Animas	6/6/2017	189.7	9.22	270.8	7.94	13.1
AR-0523	Animas	6/5/2017	150.5	10.73	267.1	7.16	11.4
AR-0524	Animas	6/5/2017	144.2	11.33	234.6	7.42	9.6
AR-0525	Animas	6/5/2017	143.1	11.42	260.8	7.45	8.1
AR-0526	Animas	6/5/2017	146	10.89	255.7	7.12	7.9
AR-0527	Animas	6/5/2017	119.8	10.79	291.2	7.4	8.6
AR-0528	Animas	6/5/2017	149.4	9.61	116.1	6.91	7.1
AR-0529	Animas	6/6/2017	230.9	10.85	320.9	4.9	2.5
AR-0530	Animas	6/6/2017	183.4	9.49	252	7.78	12.3
AR-0531	Animas	6/6/2017	146.3	9.37	217.8	7.83	13.5
AR-0533	Ditch	6/7/2017	315.7	9.18	176.8	7.66	11.6
AR-0534	Ditch	6/7/2017	186.8	9.7	242.5	7.46	11.5
AR-0535	Ditch	6/7/2017	186.8	9.42	211.1	7.62	14.6
AR-0522	Ditch	6/7/2017	175	11.13	207.3	7.57	11.11
AR-0532	San Juan	6/6/2017	210	9.65	258.1	7.75	12.7

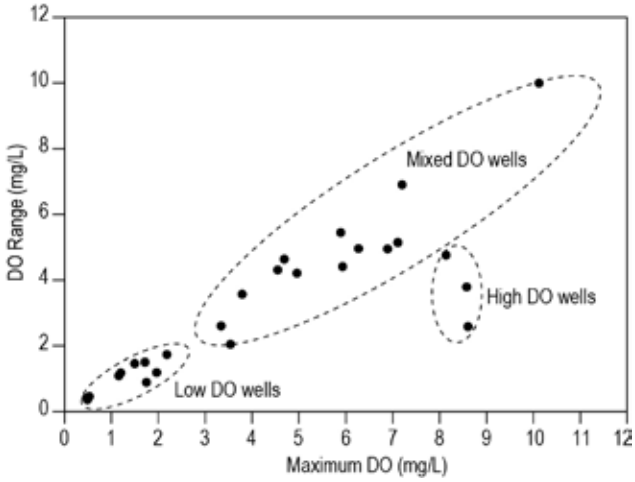

Figure 17. The range of dissolved oxygen (DO) concentrations as a function of the maximum dissolved oxygen value for each well with 2 or more measurements at different times. Most wells with higher maximum dissolved oxygen concentrations also exhibit a larger range in dissolved oxygen. Low dissolved oxygen wells had concentrations below 3 mg/L for all samples collected from that well between January 2016 and June 2017. Mixed dissolved oxygen wells exhibited at least one dissolved oxygen concentration greater than 3 mg/L. The higher range in concentrations for mixed dissolved oxygen wells suggests a more dynamic biogeochemical system. High dissolved oxygen wells had concentrations higher than 3 mg/L for all samples collected over the period of the study.

of dissolved oxygen concentrations have a minimum dissolved oxygen concentration close to zero. This high temporal variability indicates a dynamic biogeochemical system and has implications for the mobilization of some contaminants in the shallow alluvial aquifer. The three wells categorized as ***high dissolved oxygen*** wells had concentrations greater than 3 mg/L for all samples collected. Figure 18 shows the location of the different wells categorized based on dissolved oxygen concentrations as described above. All dissolved oxygen concentrations measured for the Animas River samples were high (>8 mg/L) due to exposure to the atmosphere.

pH values—Water from all wells had relatively neutral pH values that ranged between 6.71 and 8.32. With the exception of the well AR-0074, water from each well varied by less than 0.83 pH units. AR-0074 had the highest pH value of 8.32 in March 2016.

Specific Conductance—The specific conductance (SC) of a water sample is the electrical conductivity of that water at 25°C and correlates to the amount of dissolved minerals in the water. For wells sampled repeatedly (Table 3), average specific conductance values ranged from 554 to 2,260 µS/cm, and the

observed range of specific conductance values in individual wells over time varied between 19 and 1,287 µS/cm. In other words, specific conductance was very constant over time in some wells, while in other wells, this value was observed to vary significantly over the time span of this study. Large temporal fluctuations in specific conductance likely indicates the mixing waters with very different specific conductance values or the occurrence of processes that affect the concentration of dissolved minerals, such as mineral dissolution or evaporation. For the regional wells (Table 4), all specific conductance values are on the high end of the observed range of values with water from AR-0213 exhibiting the highest specific conductance by an order of magnitude (12,049 µS/cm). AR-0214 showed the next highest specific conductance at 3,512 µS/cm.

The specific conductance of the Animas River samples collected during March 2017 in many locations in New Mexico averaged 384 µS/cm. For samples collected all along the river, including some locations in Colorado in June 2017, specific conductance averaged 179 µS/cm. The lower values in June are due to the spring runoff water being mostly snowmelt from mountain streams. The higher values in March, just before the spring runoff, indicate some degree of base flow conditions where groundwater discharge contributed a significant amount of water to the river. While specific conductance values in the river can vary substantially throughout the year, they are significantly less than the specific conductance measured in most groundwater in the study area.

Continuous specific conductance measurements in most wells with data loggers had fairly constant values over time. However, a few continuous specific conductance datasets showed fluctuations indicative of the mixing different source waters. Figure 19 shows continuous water level and specific conductance data for AR-0075, which is located near Inca and less than ten feet from the river. The continuous data set spans about six months between November 2016 and June 2017. During the winter, the water level and specific conductance were fairly constant. U.S. Geological Survey stream discharge data for the Animas River below Aztec showed spring runoff began in early March 2017. The water level in the well strongly correlated with river discharge. Shortly after the water level rose, specific conductance dropped significantly, indicating an input of river water with relatively low specific conductance to the aquifer in the nearby river bank.

Figure 20 shows continuous water level and specific conductance data for four wells and an irrigation

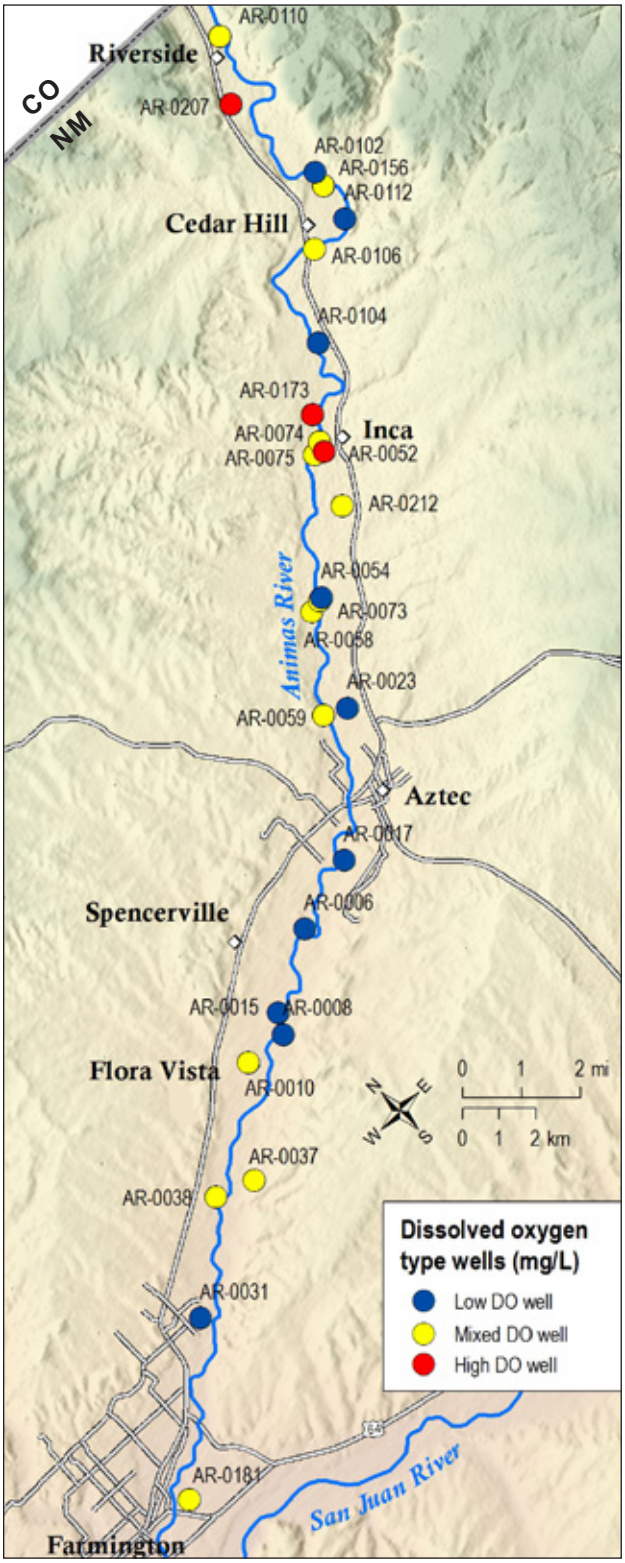

Figure 18. Locations of wells categorized by observed maximum dissolved oxygen (DO) concentration and temporal variability of dissolved oxygen concentrations. Low DO wells exhibited dissolved oxygen measurements less than 3 mg/L, mixed DO wells had DO values both less than and greater than 3 mg/L, and high DO wells exhibited dissolved oxygen values greater than 3 mg/L.

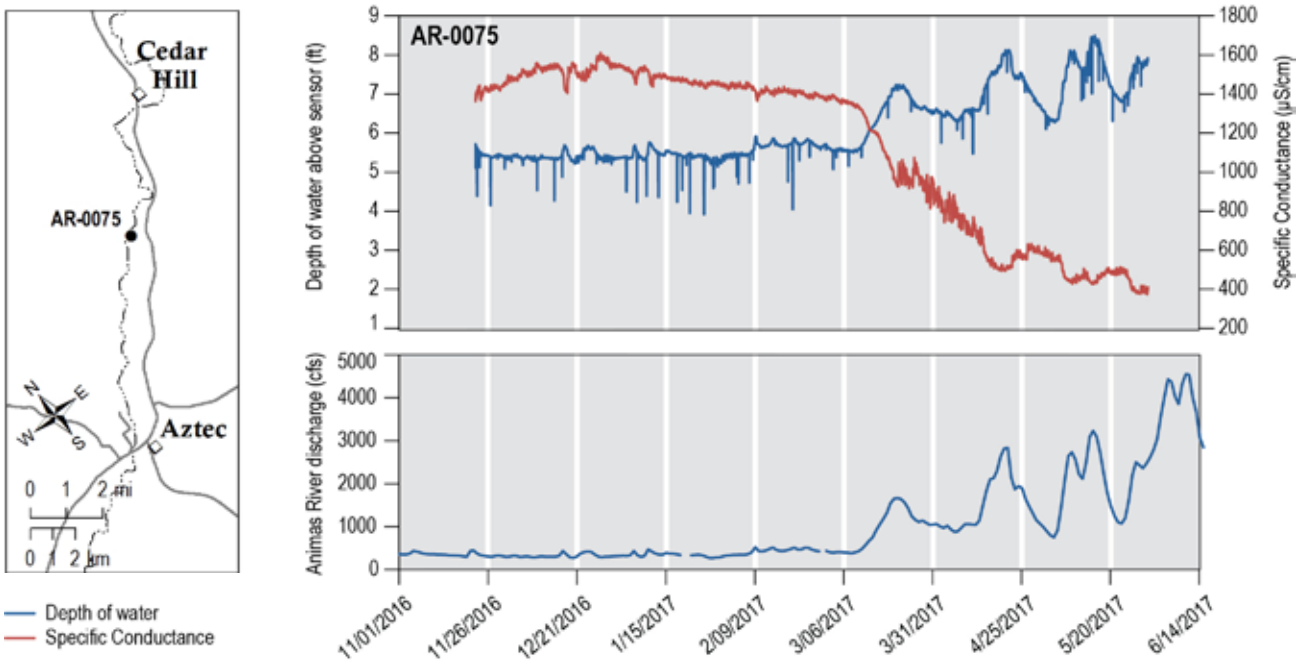

Figure 19. Continuous water level and specific conductance data for AR-0075 and river discharge data from the USGS gauge below Aztec (09364010). The water level in the well (depth of water above the sensor) correlates strongly with river discharge. A significant decrease in specific conductance values, which coincides with spring runoff, indicates that river water is entering the aquifer near that well and affecting the water quality. (https://waterdata.usgs.gov/nm/nwis/uv?site_no=09364010)

ditch. The abrupt increase in water level and specific conductance in the ditch (AR-0522) indicates the beginning of the irrigation season in mid-April. Specific conductance values observed for the water in the ditch, which is river water that was diverted to the irrigation canals, are significantly lower than those observed in groundwater. Groundwater wells AR-0044, AR-0052, AR-0059, and AR-0112 are approximately 1,337; 849; 332; and 256 feet from the river, respectively. For these four wells, there is an inverse correlation between specific conductance and the water level in the well. Between November 2016 and April 2017, water levels decline slowly while specific conductance values increase slightly. Observed increases in water levels are apparently due to the initiation of irrigation season, which coincides with decreases in specific conductance. This observation indicates the input of fresher river water (via irrigation) into the aquifer, diluting the groundwater that has higher ion concentrations than river water used for irrigation.

Temperature—Water temperatures varied significantly both spatially and temporally, ranging from 7.30 to 17.34 °C. It should be noted that the lowest water temperature was exhibited by AR-0075, which is less than ten feet from the river as discussed above (Figure 19). In March 2016 and March 2017, water temperatures in well AR-0075 were 7.92 °C and 7.30 °C respectively, were significantly less than temperatures observed in all other wells. In March 2017, measured river water temperatures ranged from 8 °C to 15 °C (Table 5). The low temperature observed in AR-0075 is likely due to local recharge to the shallow aquifer from the river.

Continuous temperature data from data loggers helps to explain the variability we observed for water temperatures during sampling. Figure 21 shows continuous water temperatures for AR-0028 from September 2015 to May 2017 along with average monthly air temperatures measured at the Farmington Four Corners Regional Airport. Air temperature data shows the expected sinusoidal seasonal fluctuations with the highest temperatures in the summer and the lowest temperatures in the winter. Water temperature data exhibit sinusoidal seasonal fluctuations with a wavelength similar to that observed for air temperatures (one year) but with a significant phase shift and a smaller amplitude. These seasonal water temperature fluctuations are controlled by the air temperature and are due to conductive heat transfer between the atmosphere and the subsurface. The magnitude of the phase shift (lag time) and the degree to which the amplitude of water temperature fluctuations is decreased or dampened depends on the thermal characteristics of the soil and the depth at which temperatures are being measured. Therefore, because water temperature was measured at different depths, and in

different areas of the aquifer, a large range of water temperatures is observed at any given time.

This water temperature trend cannot be identified with measurements being taken at time intervals longer than one month. However, with continuous measurements, this seasonal water temperature trend (or the deviation from this trend) may be used to provide evidence of the mixing of source waters. Figure 22 shows continuous water level and temperature data for AR-0181, located near Farmington, approximately 386 feet from the river. The water temperature in this well shows a slight increase in November 2016 and then begins to decrease by January 2017 and continues to decrease throughout the rest of the record. Temperature data from November 2016 through late March 2017 can be explained by conductive heat transfer between the atmosphere and the subsurface as described above. The temperature decrease that begins in early April 2017 deviates from this trend and exhibits a much higher rate of cooling than observed prior to that time. This steep cooling trend, which coincides with increased water levels that are associated with the start of irrigation season, strongly suggests that irrigation water of cooler temperatures is recharging the shallow aquifer and decreasing the water temperature in this area. Not all continuous temperature data had such a straight forward explanation. Most continuous data records for this study are just a little over six months long. Multi-year continuous water temperature records for different wells can provide important information about the local hydrologic system.

Oxidation Reduction Potential—Oxidation reduction potential (ORP) measurements reflect the oxidizing or reducing tendency or "redox state" of the water. The redox state of the shallow alluvial aquifer near the Animas River is particularly important because it controls the reactivity and mobility of many important elements and metals. Figure 23 shows what is known as the "redox ladder," as illustrated in Langmuir (1997), along with box and whisker plots for calculated Eh values for all well samples collected for this study. While the redox state is a factor that controls many important biogeochemical reactions, Eh measurements provide limited information about specific redox reactions that are taking place. Because many redox reactions between

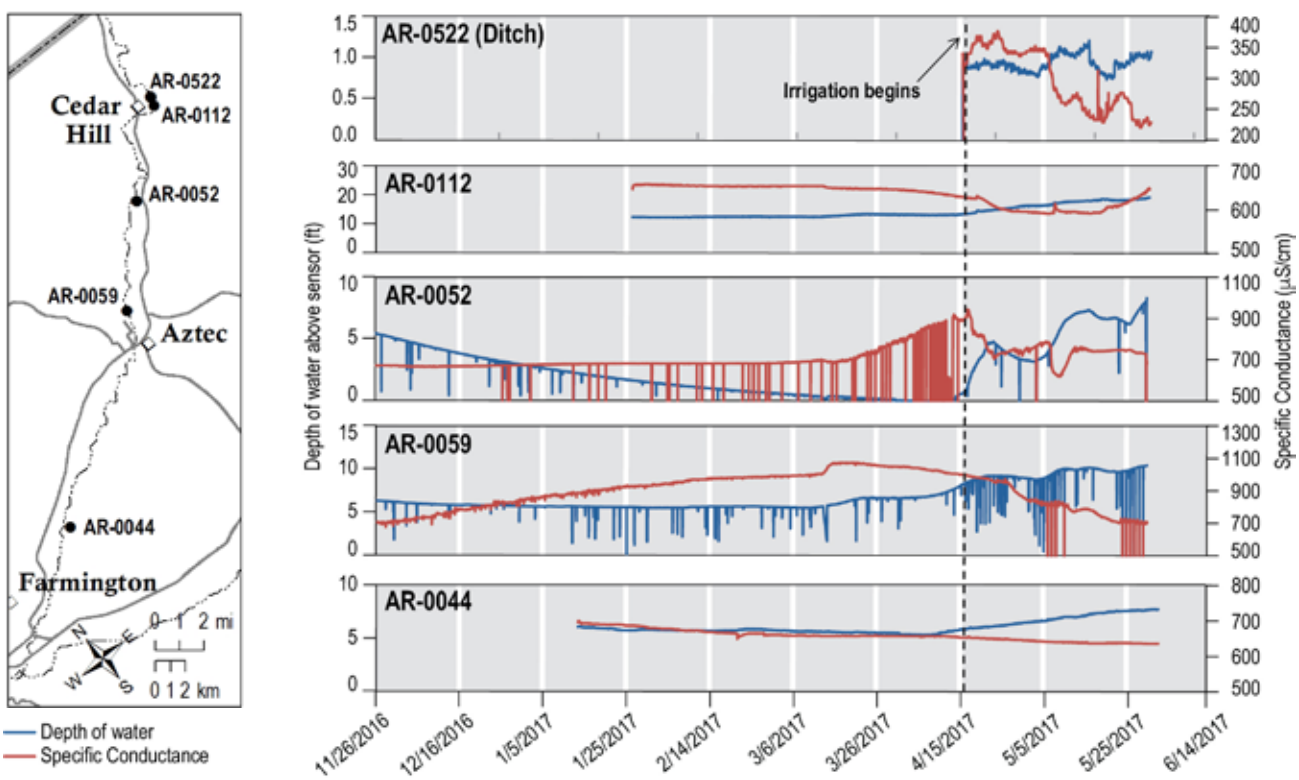

Figure 20. Continuous water level and specific conductance data in four wells and an irrigation ditch. The onset of data collection for the ditch corresponds to the time when irrigation began. In general, there is an inverse correlation between specific conductance and water levels in the wells. The instantaneous decreases (vertical lines) in water level and specific conductance are caused by pumping. Specific conductance decreases to near zero when water level drops below the sensor.

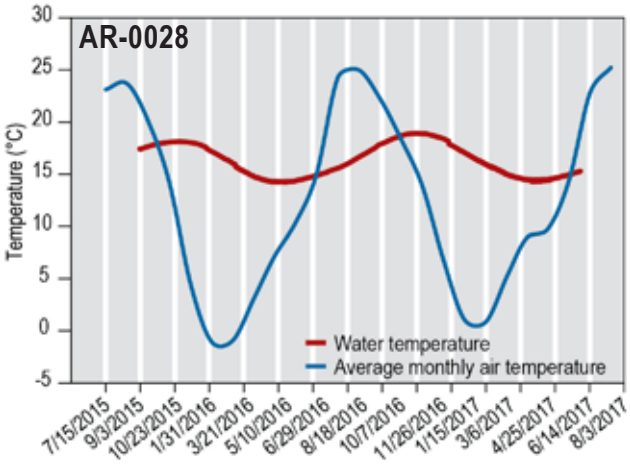

Figure 21. Continuous water temperature data for AR-0028 and monthly average air temperatures at the Farmington Four Corners Regional Airport are shown. Sinusoidal seasonal water temperature fluctuations are a result of conductive heat transfer between the atmosphere and the subsurface.

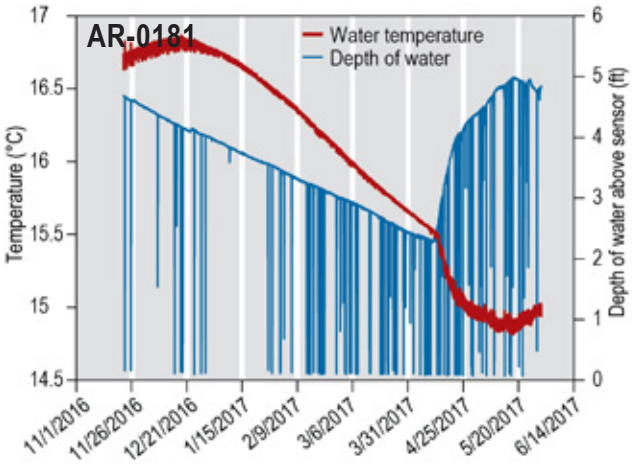

Figure 22. Continuous water level and temperature data for AR-0181 is shown. The abrupt increase in the water cooling rate in early April 2017 that coincides with the beginning of irrigation season (as seen by the increase in the water level) indicates the mixing of cooler irrigation water into the shallow aquifer in this area.

different redox pairs are occurring, it is not possible to measure a unique Eh for a particular geochemical system (Stumm and Morgan, 1996). Slow redox reaction rates also complicate matters because in many natural systems many redox pairs are not in equilibrium and many of the reactions are not reversible. It can be seen in Figure 23 that while all water samples were observed to have measurable amounts of dissolved oxygen, most Eh values indicate an anaerobic system. The hatched area (710 mV < Eh < 814 mV) shows the range of Eh values for an aerobic system where organic matter is oxidized by aerobic respiration. For some of the high dissolved oxygen samples (dissolved oxygen >3 mg/L), Eh plots in this area where Eh is greater thatn 710 mV. As mentioned above, the large temporal variability of measured dissolved oxygen concentrations in some wells has implications for the mobilization of some potential contaminants, such as metals that may be related to the Gold King Mine Spill, due to the resulting change in redox state. This topic will be discussed more below.

Water Quality

The U.S. Environmental Protection Agency water quality standards discussed in this section are provided simply for comparison of privately owned domestic well water samples and are not enforceable for private wells. According to water chemistry data for the measured constituents, all water samples exhibited chemical concentrations below the "maximum contaminant levels" (MCLs) as defined by the EPA

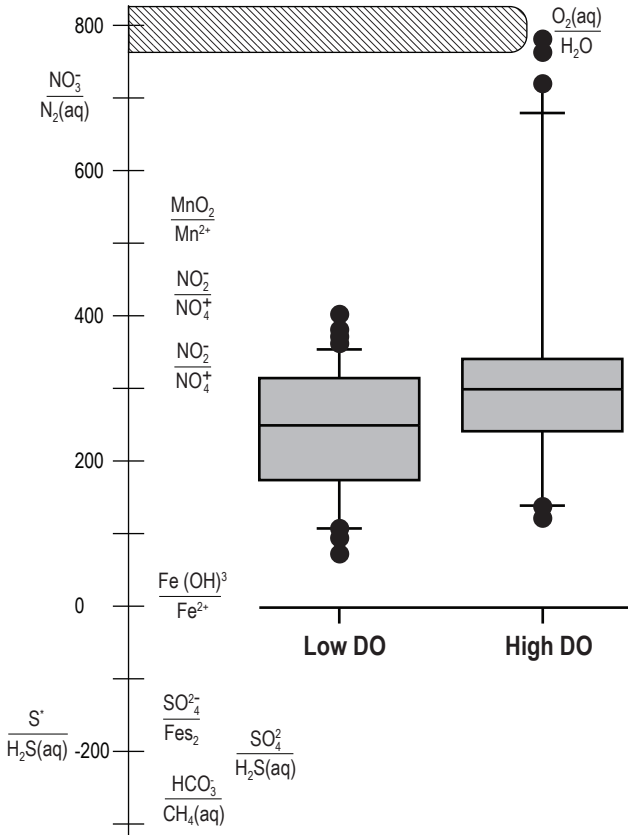

Figure 23. Redox ladder as shown in Langmuir (1997) shows important redox pairs for different Eh values. Box and whisker plots for all water samples collected for this study are divided into two categories based on the measured dissolved oxygen (DO) concentration in the sample. It should be noted that the low dissolved oxygen (DO <3 mg/L) and the high dissolved oxygen (DO >3 mg/L) categories in this figure describe individual samples, not the well categories described in the text. Therefore, many wells are represented in both categories.

National Primary Drinking Water Regulations that were established to protect against consumption of drinking water contaminants that present a risk to human health. For the following discussion, we evaluate groundwater quality by comparing water chemistry results to secondary maximum contaminant levels (SMCLs) as defined by the U.S. Environmental Protection Agency secondary drinking water regulation, which is a non-enforceable guideline regarding cosmetic or aesthetic effects. While these contaminants are not health threatening, if present at levels above the SMCLs, these constituents may cause the water to appear cloudy or colored, or to taste or smell bad. Please see Appendix E for a more complete list of U.S. Environmental Protection Agency and New Mexico water quality standards and health advisories. Constituents for which measured concentrations were observed to exceed the SMCLs include total dissolved solids (TDS), sulfate, chloride, iron, manganese and aluminum. Table 6 shows selected water chemistry data for all samples, and identifies individual analyses that showed chemical concentrations exceeding the SMCL for the analyte of interest. A complete summary of all water chemistry results are available in Appendix C.

Most wells produced water with total dissolved solids concentrations exceeding the MCL of 500 mg/L, possibly resulting in mineral deposition in pipes and water heaters, colored water, and a salty taste. Total dissolved solids concentrations above the SMCL are common in groundwater in New Mexico, due to the dissolution of soluble minerals such as calcite and gypsum. Some wells that were sampled produced water with total dissolved solids concentrations well above 1000 mg/L, which can affect some crops if being used for irrigation. Sulfate concentrations exceeding the SMCL of 250 mg/L were also observed in many water samples. The sample with the highest total dissolved solids and sulfate concentrations is from the well AR-0213. AR-0213 was also the only well that produced water with chloride and fluoride concentrations that exceed the SMCLs. AR-0213 and AR-0214, which are completed in the bedrock that underlies the alluvial aquifer, have total depths of 500 and 370 feet respectively and will be discussed in more detail below due to their distinct chemical signatures.

For the metals manganese, iron, and aluminum, both dissolved and total concentrations are listed in Table 6. The total concentration includes the amount of the analyte that was in solution when the sample was collected and the amount of that analyte that was adsorbed onto particulates and colloids in the sample. The dissolved concentration only accounts for the portion of the analyte that was in solution when the sample was collected. Several wells produced water that exceeded the SMCL for iron and manganese. While manganese, by oral route, is considered one of the least toxic elements, some studies suggest that long-term exposure to manganese in drinking water may cause some adverse health effects (WHO, 2011). Most of these studies focused on drinking water with manganese concentrations that are at least an order of magnitude greater than those observed in this study. AR-0075 exhibited the highest manganese concentrations and consistently showed manganese concentrations that exceed the SMCL. Iron in drinking water poses no health threats (WHO, 2003).

Measureable dissolved aluminum was detected in 50% of groundwater samples, with AR-0214 being the only well producing water with dissolved aluminum concentrations that exceed the SMCL of 0.05 mg/L. A total of 88% of groundwater samples exhibited measureable total aluminum,while only three wells (AR-0110, AR-0156, and AR-0214) had concentrations greater than the SMCL. With the exception of AR-0214, dissolved aluminum concentrations in shallow groundwater are below or within the normal range for natural waters with near neutral pH values as reported by the WHO (2010), of between 0.001 and 0.05 mg/L. Water sampled from AR-0214 showed a significantly high dissolved aluminum concentration of 0.161 mg/L. The presence of measureable total aluminum in most water samples indicates potential for the dissolution of aluminum in groundwater in the Animas valley. However, with the observed pH values, this is unlikely. The effects of long-term exposure to dissolved aluminum in drinking water are debated. While some studies suggest the possibility of an association between Alzheimer disease and aluminum in groundwater, other studies have not produced the same results (WHO, 2010).

Figure 24 shows the locations of wells that produced water that exceeded groundwater SMCLs for total dissolved solids, sulfate, total iron, total manganese and total aluminum. While SMCLs refer to dissolved constituents, we included total concentrations for iron, manganese, and aluminum because the presence of colloidal or particulate forms of theses metals may indicate potential dissolution of these metals. Most of the wells that produce water with sulfate concentrations exceeding the SMCL are located south of Aztec. This spatial trend will be discussed more below.

While there are no enforceable standards on water hardness, Table 6 shows that most

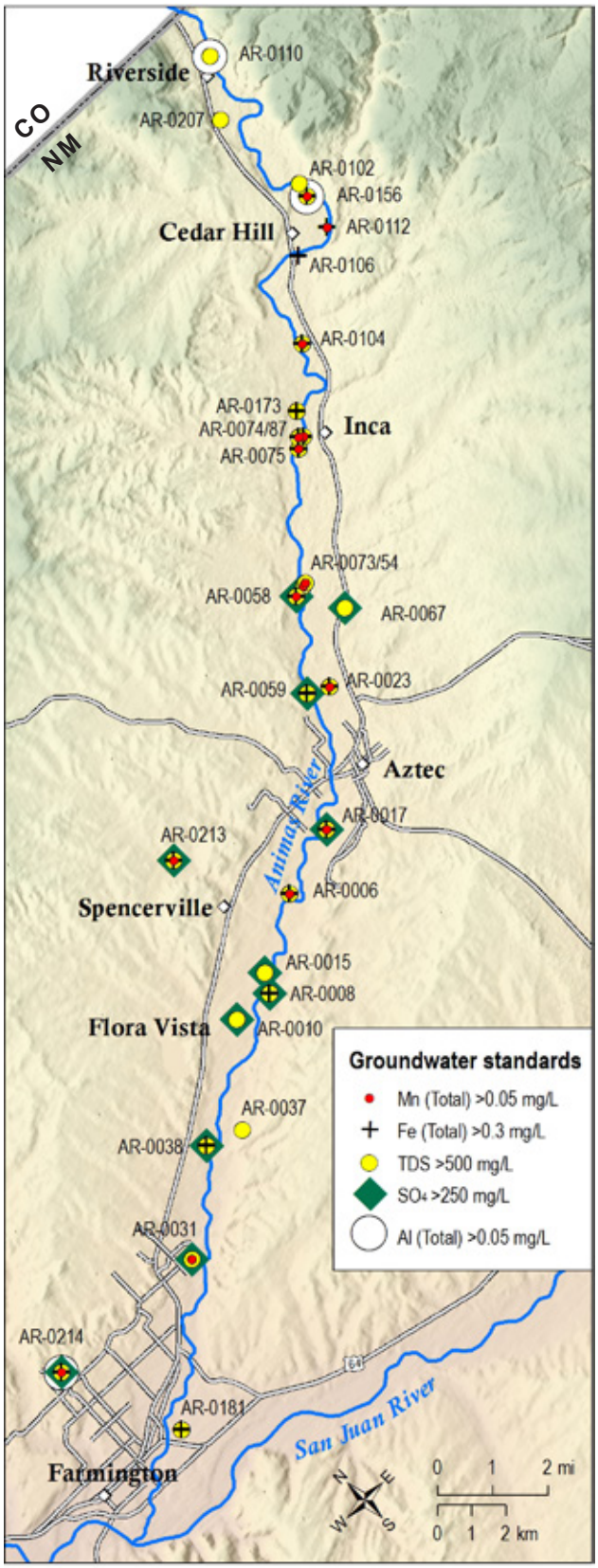

Figure 24. Location of wells that produced water exceeding U.S. EPA secondary maximum contaminant levels for total dissolved solids (TDS), total iron (Fe), total manganese (Mn), sulfate (SO_4) and total aluminum (Al).

groundwater in the study area is considered to be very hard, with values above 300 mg/L. Hardness, which is a result of the dissolution of minerals that contain calcium and magnesium, is not a health concern, but can be a nuisance by causing mineral buildup in plumbing and water heaters.

General Water Chemistry

The concentration of the major cations (sodium (Na), calcium (Ca), magnesium (Mg) and potassium (K)) and anions (sulfate (SO_4), bicarbonate (HCO_3), and chloride (Cl)) in groundwater depends on the types of rocks or sediments that comprise the aquifer, the amount of time water spends in the aquifer, the length of the flow path, and the geochemical processes that are taking place. In this section we describe the major ion chemistry, identify spatial and temporal trends for the major cations and anions and other chemical constituents, and identify the different water types. Table 7 shows average concentrations of selected ions and other constituents for wells that were sampled multiple times during this study, with the exception of regional samples shown in Table 4, which were sampled only once.

Spatial Variability—Several spatial trends for groundwater chemistry were observed. Average total dissolved solids (TDS) concentrations in repeat samples show a weak trend of increasing values from the northeast to the southwest (down river) (Figure 25B). Sulfate concentrations show the same but stronger trend (Figure 25C). Figure 25A shows a very strong linear correlation between total dissolved solids and sulfate concentrations. Sulfate concentration can be used as a proxy for total dissolved solids concentration and is the focus of the discussion about mixing processes below. Trends in the same direction can be seen for other constituents as well (Figure 26A and B). Strontium concentrations increase in the downstream direction while barium concentrations decrease in the downstream direction. No spatial trend for chloride was observed (Figure 26C).

Temporal changes in dissolved oxygen and total dissolved solids—In the above discussion about field parameters, wells were categorized based on dissolved oxygen concentrations and the observed range in values measured in individual wells over the course of the study. Higher dissolved oxygen concentrations are likely due to the input of river water which is usually saturated with respect to oxygen due to being exposed to the atmosphere (see Table 5). This is

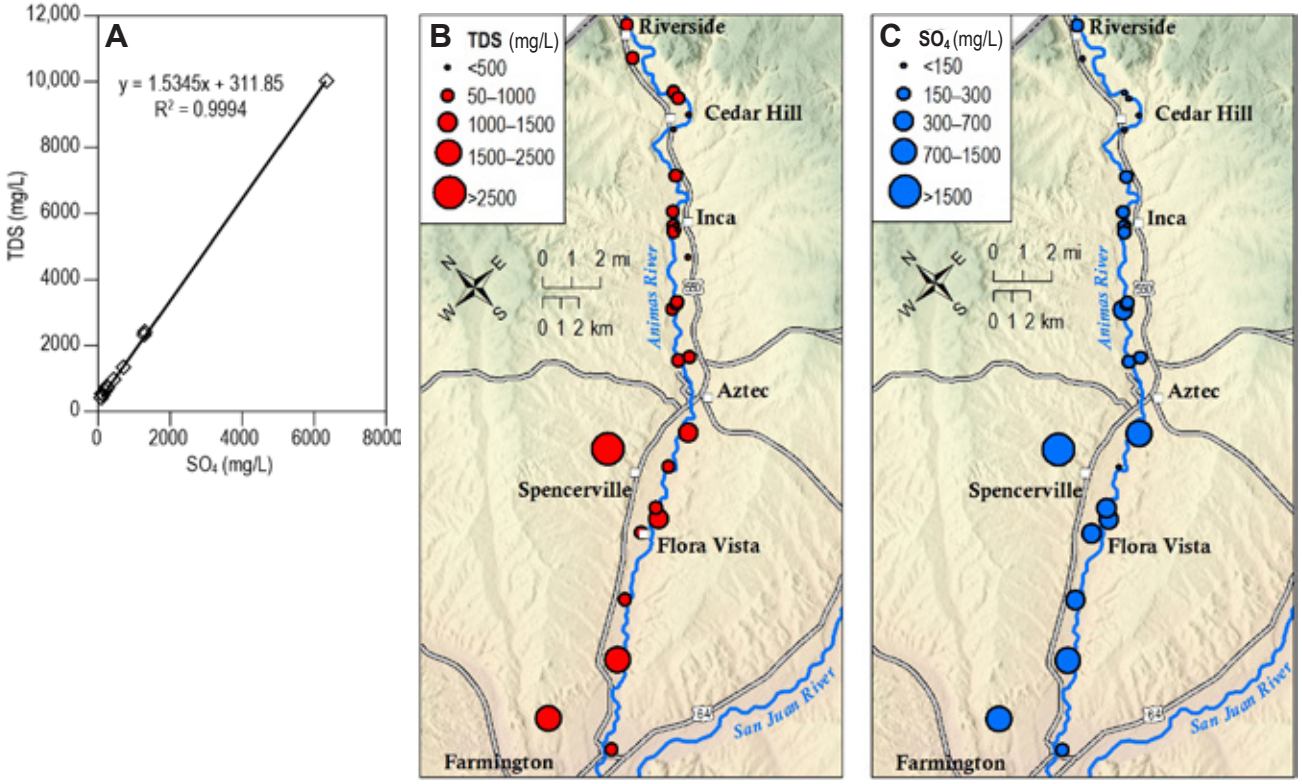

Figure 25. Trends of total dissolved solids and sulfate. **A**—Total dissolved solids (TDS) as a function of SO_4 has a strong linear correlation. **B**—Average total dissolved solids concentrations show a general trend of increasing in the downstream (southwest) direction. **C**—Average SO_4 concentrations show a general trend of increasing in the downstream (southwest) direction.

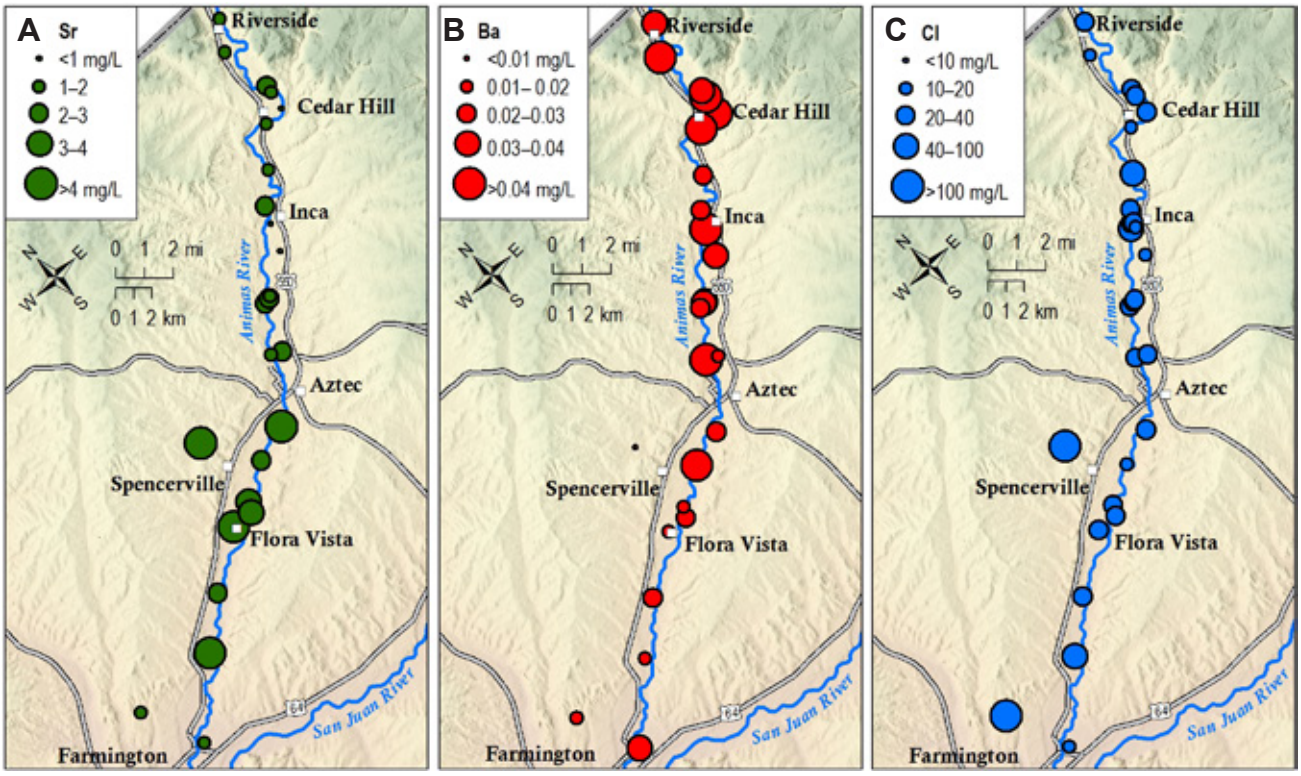

Figure 26. Spatial variability observed for strontium (Sr), barium (Ba), and chloride (Cl). Concentrations are average values. **A**—Strontium concentrations in groundwater increase in the down-gradient direction (northeast to southwest). **B**—Barium concentrations in groundwater decrease in the down-gradient direction. **C**—No spatial trend was observed for chloride concentrations in groundwater.

Table 6. Selected water chemistry with highlighted concentrations that exceed U.S. Environmental Protection Agency secondary maximum contaminant levels (SMCLs). The U.S. Environmental Protection Agency secondary drinking water regulation is a non-enforceable guideline regarding cosmetic and aesthetic effects. The SMCL for each constituent is shown in the top row. The limit for hardness is not a regulation but is provided for reference only. All concentrations are given in mg/L.

U.S. Environmental Protection Agency Secondary maximum contaminant level						250 mg/L		250 mg/L	500 mg/L	300 mg/L (for reference only, not a standard)	2 mg/L	0.3 mg/L		0.05 mg/L		0.05 mg/L	
Site ID	Collection date	Calcium Ca	Magnesium Mg	Sodium Na	Potassium K	Sulfate SO_4	Bicarbonate HCO_3	Chloride Cl	Total Dissolved Solids, TDS	Hardness HRD	Fluoride F	Dissolved Iron Fe	Total Iron Fe	Dissolved Manganese, Mn	Total Manganese Mn	Dissolved Aluminium, Al	Total Aluminum Al
January 2016																	
AR-0006	1/26/16	144	16.8	29.4	2.11	131	419	17.4	565	429	0.36	1.11	1.27	0.109	0.114	<0.0025	<0.0025
AR-0008	1/27/16	222	29	142	2.97	653	312	24.6	1250	673	0.28	<0.1	1.13	<0.005	0.008	<0.0025	0.0026
AR-0010	1/27/16	233	15.7	57	1.8	452	281	32.2	967	647	0.4	<0.1	<0.02	<0.005	<0.005	<0.0025	<0.0025
AR-0015	1/27/16	207	23.5	92.4	1.88	478	312	30	1010	613	0.61	<0.1	0.022	0.007	0.007	<0.0025	0.0104
AR-0017	1/27/16	335	22.6	65.9	1.64	702	302	22.4	1330	929	0.47	0.313	0.676	0.214	0.218	<0.0025	<0.0025
AR-0038	1/25/16	234	25.6	51	2.33	407	367	32.9	959	689	0.39	<0.1	0.168	0.005	0.005	<0.0025	<0.0025
AR-0059	1/26/16	119	15.1	76	2.05	264	250	28.8	646	360	0.35	<0.1	0.163	0.008	0.008	<0.0025	<0.0025
AR-0073	1/26/16	153	23.3	46.2	1.69	176	413	24.6	657	478	0.34	<0.1	0.049	0.559	0.57	<0.0025	<0.0025
AR-0074	1/27/16					157	317	28.6			0.66		0.781		0.796		<0.0025
AR-0075	1/27/16	174	24.6	73.3	3.88	245	354	123	849	536	0.35	3.34	4.58	6.4	6.48	<0.0025	<0.0025
AR-0102	1/26/16	131	26.9	41.9	3.53	151	400	32.3	606	438	0.54	<0.1	0.051	<0.005	<0.005	<0.0025	<0.0025
AR-0106	1/26/16	102	14.9	19.7	2.78	101	286	17.5	412	316	0.42	<0.1	0.06	0.009	0.009	<0.0025	<0.0025
AR-0112	1/26/16	91.3	12.5	25.4	1.91	95.8	250	22.6	388	280	0.43	1.84	1.79	1.01	1.03	<0.0025	<0.0025
AR-0156	1/27/16	127	25.1	47.9	3.7	151	400	33.3	603	419	0.31	<0.1	2.94	<0.005	0.087	<0.0025	0.064
AR-0181	1/25/16	144	22.4	37.5	2.66	170	390	21.8	610	453	0.53	<0.1	<0.02	<0.005	<0.005	<0.0025	<0.0025
AR-0207	1/26/16	127	21.4	28.2	2.06	118	382	22.1	528	406	0.37	<0.1	0.062	<0.005	<0.005	<0.0025	0.0032
March 2016																	
AR-0006	3/15/16	160	18.8	32.4	2.19	151	439	23.1	621	476	0.38	0.87	1.12	0.109	0.107	<0.0005	0.0009
AR-0008	3/14/16	249	32.4	152	2.99	720	307	26	1360	755	0.26	<0.1	0.131	0.001	0.002	<0.0005	0.002
AR-0010	3/14/16	214	14.6	54.1	1.74	404	284	28.8	891	594	0.43	<0.1	0.183	<0.001	0.003	0.0006	0.0019
AR-0015	3/16/16	202	23.1	90.9	1.79	467	302	29.8	985	599	0.62	<0.1	<0.1	0.004	0.003	0.0012	0.0058
AR-0017	3/15/16	336	22	66.5	1.46	705	299	22.2	1330	930	0.46	0.304	1.02	0.15	0.148	0.0005	0.0016
AR-0038	3/17/16	229	25.5	48.7	2.38	410	362	32.1	953	678	0.42	<0.1	<0.1	0.005	0.004	0.0005	0.0008
AR-0058	3/15/16	153	15	64.6	2.13	257	349	21.4	702	444	0.31	<0.1	0.574	0.001	0.004	0.0005	0.0083
AR-0059	3/15/16	138	17.6	101	2.29	328	284	35.5	780	416	0.34	0.249	0.644	0.016	0.024	<0.0005	0.0009
AR-0073	3/15/16	148	22.8	44.9	1.63	178	409	24.2	648	463	0.36	<0.1	<0.1	0.508	0.502	0.0005	0.0007
AR-0074	3/16/16	109	14.6	34.6	2.08	155	263	32.7	490	332	0.7	0.388	3.77	0.645	1.18	0.0006	0.0024
AR-0075	3/16/16	124	17.7	59.3	3	175	305	67.2	621	382	0.4	2.48	2.8	4.52	4.46	<0.0005	0.0008
AR-0102	3/17/16	131	27.3	43.3	3.34	157	406	34	617	439	0.59	<0.1	0.1	0.007	0.006	0.0005	0.0028
AR-0106	3/17/16	100	15	19.9	2.6	97.6	286	17.5	407	312	0.42	<0.1	<0.1	0.009	0.009	0.0013	0.0006
AR-0110	3/17/16	106	23.7	88.3	2.18	206	344	36.9	660	361	0.47	<0.1	<0.1	<0.001	0.005	0.0025	0.0899
AR-0112	3/16/16	88.9	12.5	26.6	1.61	110	232	23.7	392	273	0.48	1.78	1.8	0.961	0.935	0.001	0.0033
AR-0156	3/16/16	126	25	47.6	3.54	158	393	33.9	606	416	0.37	<0.1	0.706	0.004	0.016	0.0011	0.0214
AR-0181	3/14/16	137	21.3	35.7	2.57	172	375	21.2	592	429	0.62	<0.1	<0.1	<0.001	<0.001	<0.0005	0.0009
AR-0207	3/17/16	131	22.3	28.2	1.98	128	388	23.5	548	420	0.41	<0.1	<0.1	<0.001	0.021	0.0006	0.0011
June 2016																	
AR-0006	6/1/16	151	17.8	31.5	2.18	132	458	16.1	593	451	0.39	1.09	1.09	0.101	0.105	<0.0005	0.0006
AR-0008	6/1/16	299	39.7	180	3.26	906	331	28.1	1640	909	0.23	<0.1	<0.1	0.001	0.001	0.0005	0.0008
AR-0010	5/31/16	249	16.8	59.4	1.8	486	279	32.9	1020	690	0.4	<0.1	<0.1	<0.001	0.001	0.0005	0.0009
AR-0015	6/1/16	199	22.8	91.3	1.72	460	311	29.8	978	591	0.66	<0.1	<0.1	0.001	0.001	0.0007	0.0019
AR-0017	6/1/16	340	22.1	66.3	1.39	702	313	21.5	1330	941	0.47	0.221	0.334	0.122	0.125	<0.0005	0.0006
AR-0023	6/3/16	137	15.3	32.9	0.854	182	285	26.5	553	406	0.46	<0.1	<0.1	0.081	0.084	0.0005	0.0008
AR-0031	5/31/16	564	56.8	116	2.93	1330	378	89.5	2380	1640	1.1	<0.1	0.107	1.07	1.08	0.0006	0.0026
AR-0038	5/31/16	242	26.2	49.2	2.39	428	367	30.4	983	711	0.4	0.101	0.241	0.009	0.011	0.0007	0.0006
AR-0058	6/1/16	150	14.5	60.8	1.96	228	365	21	670	434	0.32	<0.1	0.151	<0.001	0.002	<0.0005	0.0017

Table 6. Continued.

Site ID	Collection date	Calcium Ca	Magnesium Mg	Sodium Na	Potassium K	Sulfate SO_4	Bicarbonate HCO_3	Chloride Cl	Total Dissolved Solids, TDS	Hardness HRD	Fluoride F	Dissolved Iron Fe	Total Iron Fe	Dissolved Manganese, Mn	Total Manganese Mn	Dissolved Aluminium, Al	Total Aluminum Al
AR-0059	6/1/16	103	12.9	58.8	1.83	185	256	20.7	523	309	0.36	<0.1	0.363	0.007	0.006	0.0005	0.0011
AR-0074	6/3/16	106	14.5	37.1	2.28	148	256	35.9	481	323	0.65	0.38	0.444	0.632	0.639	0.0006	0.0008
AR-0075	6/2/16	61.9	8.71	32.3	2.39	73.4	210	14.3	315	191	0.47	1.12	1.63	2.23	2.25	<0.0005	0.0008
AR-0102	6/2/16	131	26.7	41.3	3.43	152	386	32.7	596	437	0.54	<0.1	<0.1	<0.005	0.001	<0.0005	0.0006
AR-0106	6/2/16	100	15	20	2.57	97.4	285	15.6	402	313	0.39	<0.1	<0.1	0.007	0.007	0.0005	<0.0005
AR-0110	6/3/16	129	30	58.5	2.23	205	357	34.8	668	446	0.41	<0.1	<0.1	<0.001	<0.001	0.0006	0.0027
AR-0112	6/2/16	93.6	13	24.1	1.65	92.1	269	17.6	387	287	0.4	1.85	1.86	0.885	0.884	0.0008	0.0009
AR-0156	6/2/16	95.1	19.3	28	3.07	98.2	305	18.4	425	317	0.46	<0.1	<0.1	0.001	0.001	<0.0005	0.0005
AR-0181	5/31/16	138	21.5	36	2.53	168	367	19.8	583	434	0.56	<0.1	<0.1	<0.001	<0.001	0.0005	0.0005
AR-0207	6/3/16	133	22.7	26.1	2.05	123	401	18.9	540	426	0.35	<0.1	0.14	0.001	0.006	0.0058	0.012
October 2016																	
AR-0006	10/18/16	131	15.6	30.6	2.1	123	370	16	517	392	0.44	0.964	1.06	0.086	0.09	<0.0005	0.0007
AR-0008	10/17/16	190	25.7	143	2.9	545	306	20.3	1100	581	0.35	0.128	2.47	0.006	0.028	<0.0005	0.0091
AR-0010	10/17/16	251	17.2	62.2	1.72	477	276	32.3	1010	698	0.44	<0.1	0.12	<0.001	0.001	0.0005	0.0012
AR-0015	10/19/16	196	22.4	91.5	1.82	430	306	28.8	944	582	0.68	<0.1	<0.1	0.001	0.001	0.0018	0.0024
AR-0017	10/21/16	334	22.3	78.2	1.51	717	299	21.1	1350	927	0.57	0.298	0.613	0.144	0.156	<0.0005	<0.0005
AR-0023	10/18/16	131	14.8	35.2	0.776	185	274	27.3	551	389	0.5	<0.1	0.155	0.072	0.073	0.0006	0.0012
AR-0031	10/17/16	494	51	115	2.9	1140	355	81.4	2100	1440	1.32	<0.1	<0.1	0.821	0.83	<0.0005	0.0012
AR-0038	10/17/16	222	24.9	49.1	2.37	396	362	26.9	927	657	0.47	<0.1	0.503	0.006	0.012	<0.0005	0.0014
AR-0052	10/20/16	102	13.6	16.3	1.56	92.3	269	14.8	387	312	0.36	<0.1	<0.1	0.001	0.004	0.0007	0.0017
AR-0054	10/18/16	140	21.4	35.9	1.49	161	414	20.2	611	437	0.38	<0.1	<0.1	0.257	0.349	<0.0005	0.0018
AR-0058	10/19/16	174	17.1	72	2.4	312	331	25.3	785	505	0.35	<0.1	1.76	0.004	0.066	<0.0005	0.003
AR-0059	10/18/16	80.7	10.2	36.8	1.52	124	221	14.6	392	243	0.41	<0.1	0.417	0.005	0.009	0.0007	0.0019
AR-0074	10/20/16	123	16.4	40.3	3.09	142	335	25.2	531	374	0.68	0.354	0.421	0.692	0.712	<0.0005	0.0006
AR-0075	10/20/16	144	20.3	61.9	3.88	197	317	86.5	700	444	0.47	2.49	2.69	5.3	5.23	<0.0005	0.0018
AR-0087	10/19/16	113	19.7	56.9	1.97	165	345	28.7	574	363	0.46	0.394	3.92	0.075	0.234	<0.0005	0.0066
AR-0102	10/21/16	119	24.3	38.8	3.35	139	375	27.1	558	398	0.64	<0.1	<0.1	<0.001	0.002	<0.0005	0.0007
AR-0104	10/20/16	98.6	14.4	98.3	1.11	189	313	41.3	613	305	0.58	0.302	0.424	0.535	0.615	0.0009	0.0017
AR-0106	10/19/16	92.5	13.7	19	2.83	79	276	13.4	370	288	0.45	0.263	0.323	0.007	0.007	<0.0005	<0.0005
AR-0110	10/21/16	104	24	56.9	2.08	164	322	27.1	562	359	0.48	<0.1	<0.1	<0.001	0.001	0.0007	0.0099
AR-0112	10/19/16	105	14.7	21.6	1.91	84.2	323	16.4	421	324	0.42	2.24	2.3	0.961	0.995	0.001	0.0014
AR-0156	10/21/16	113	22.4	34	3.66	125	351	24	512	375	0.48	<0.1	<0.1	<0.001	0.001	<0.0005	0.0026
AR-0173	10/20/16	120	25	61	1.24	178	322	26.1	629	401	0.58	<0.1	0.28	0.001	0.002	0.0006	0.0009
AR-0181	10/17/16	123	19.2	34.6	2.6	158	332	18.9	539	387	0.7	<0.1	<0.1	<0.001	<0.001	0.0015	0.0011
AR-0207	10/21/16	116	20.3	24.8	1.83	102	357	13.9	476	373	0.46	<0.1	<0.1	<0.001	<0.001	<0.0005	0.0008
AR-0212	10/18/16	96.3	13.5	16.8	1.03	70.3	291	8	368	296	0.4	<0.1	<0.1	<0.001	0.003	<0.0005	0.0008
January 2017																	
AR-0006	1/24/17	146	17.9	30.5	2.15	134	409	16.6	567	439	0.36	1.07	1.39	0.102	0.102	0.0006	0.0007
AR-0008	1/23/17	223	31.5	156	3.11	666	324	25.1	1280	685	0.27	0.069	1.3	0.002	0.019	0.0005	0.0122
AR-0010	1/31/17	225	15.7	62.9	1.78	452	271	31.1	956	626	0.4	<0.02	0.083	<0.001	<0.001	0.0006	0.0011
AR-0015	1/23/17	205	23.1	93.6	1.8	479	298	28.5	1000	607	0.6	<0.02	<0.02	0.001	<0.001	0.0005	0.0014
AR-0017	1/25/17	328	22.6	78.3	1.57	698	308	21.8	1330	912	0.48	0.381	0.379	0.206	0.208	<0.0005	0.0007
AR-0038	1/31/17	246	27.5	52.9	2.53	432	365	29.5	997	727	0.41	0.119	0.178	0.009	0.008	<0.0005	0.0007
AR-0054	1/31/17	150	22.9	37.9	1.42	167	330	20	588	470	0.27	0.036	<0.02	0.253	0.254	0.0009	0.0007
AR-0058	1/24/17	205	20.1	91.5	2.43	417	385	26	972	594	0.27	0.065	0.338	0.001	<0.001	0.0005	0.0014
AR-0059	1/25/17	127	17	93.8	2.14	315	265	32.7	736	386	0.34	0.062	0.545	0.014	0.016	0.0005	0.0008
AR-0075	1/25/17	178	24.8	92	3.99	239	422	116	895	547	0.38	3.12	3.52	6.48	6.59	<0.0005	0.0009
AR-0087	1/24/17	123	23	64.2	1.96	196	338	35.2	629	403	0.39	0.496	1.07	0.042	0.082	0.0005	0.0011
AR-0102	1/26/17	124	25	40.4	3.3	144	376	28.3	571	413	0.59	0.025	0.171	0.001	0.004	<0.0005	0.0203
AR-0104	2/1/17	91.6	13.1	116	1.28	204	312	43.4	640	283	0.53	0.24	0.471	0.527	0.64	<0.0005	0.0007
AR-0106	2/1/17	95.8	14.5	19.3	2.6	89.8	277	16.6	389	299	0.43	0.181	0.221	0.005	0.004	<0.0005	<0.0005
AR-0112	1/25/17	91.9	13.1	24.9	1.76	96.2	254	22.2	391	283	0.45	1.76	1.77	0.948	1.01	0.0009	0.0025
AR-0156	1/26/17	121	24.6	46	3.63	136	375	29.7	574	402	0.36	<0.02	0.134	0.001	0.003	0.0005	0.0083
AR-0173	2/1/17	114	22.9	59	1.27	171	316	29.4	599	378	0.54	0.064	0.411	0.001	0.005	<0.0005	0.0017
AR-0181	1/24/17	135	21.6	36.3	2.66	171	357	19.8	582	427	0.63	<0.02	0.696	0.001	0.003	0.0006	0.0017
AR-0207	1/26/17	124	21.1	26.6	1.82	119	368	21	517	396	0.4	<0.02	0.021	<0.001	<0.001	0.0025	0.0084
AR-0212	1/31/17	117	16.7	18.4	0.995	95.4	343	13.6	450	361	0.38	<0.02	0.223	0.001	0.007	<0.0005	0.0012

Table 6. Continued.

Site ID	Collection date	Calcium Ca	Magnesium Mg	Sodium Na	Potassium K	Sulfate SO_4	Bicarbonate HCO_3	Chloride Cl	Total Dissolved Solids, TDS	Hardness HRD	Fluoride F	Dissolved Iron Fe	Total Iron Fe	Dissolved Manganese, Mn	Total Manganese Mn	Dissolved Aluminium, Al	Total Aluminum Al
March 2017																	
AR-0006	3/13/17	155	17.3	28.9	1.99	139	410	16.1	579	459	0.37	0.933	1.06	0.102	0.104	<0.0005	0.0005
AR-0008	3/14/17	242	31	164	2.89	701	328	25.9	1350	731	0.26	0.116	1.36	0.002	0.011	<0.0005	0.0102
AR-0010	3/13/17	210	15	61.1	1.73	404	284	29.9	894	586	0.41	<0.02	<0.02	<0.001	<0.001	<0.0005	<0.0005
AR-0015	3/13/17	203	24.2	97.5	1.8	479	297	28.4	1000	607	0.6	<0.02	<0.02	<0.001	<0.001	<0.0005	0.001
AR-0023	3/16/17	115	13.8	37.1	0.768	142	275	25.8	491	344	0.47	0.309	0.386	0.015	0.017	<0.0005	0.001
AR-0037	3/13/17	129	30.1	24	1.59	125	410	17	556	447	0.8	0.064	0.108	0.003	0.003	<0.0005	0.0006
AR-0038	3/20/17	233	27.4	52.5	2.5	440	366	31	994	695	0.39	0.098	0.111	0.006	0.006	<0.0005	0.0005
AR-0052	3/21/17	110	14.5	18	1.53	97.3	290	18.5	430	334	0.33	0.025	0.137	0.001	0.003	0.0006	0.002
AR-0054	3/14/17	152	23.3	37.7	1.38	170	409	20.1	634	474	0.34	<0.02	<0.02	0.248	0.257	<0.0005	<0.0005
AR-0058	3/15/17	197	18.3	87.6	2.3	358	391	28.2	903	566	0.28	0.082	0.193	0.001	0.002	<0.0005	0.0006
AR-0059	3/21/17	132	17.9	107	2.37	328	298	33.9	787	404	0.32	0.074	0.333	0.016	0.015	<0.0005	0.0009
AR-0067	3/14/17	125	16.2	81.2	1.21	256	293	19.7	674	378	0.42	<0.02	0.228	0.001	0.004	0.0009	0.0008
AR-0074	3/21/17	102	15.5	36.6	2.53	124	304	22.1	469	320	0.68	1.01	2.54	0.641	0.74	<0.0005	0.0021
AR-0075	3/21/17	135	19.8	72.9	3.44	171	360	64.3	671	418	0.36	2.54	2.66	4.98	5.12	<0.0005	0.0005
AR-0087	3/15/17	129	24	65.3	1.93	200	346	36.1	651	422	0.38	0.598	0.717	0.041	0.05	<0.0005	0.0013
AR-0102	3/16/17	125	27.1	43.1	3.47	147	380	30.8	585	424	0.58	0.022	0.216	0.004	0.006	0.0006	0.0005
AR-0102	3/16/17	125	25.7	41.1	3.28	148	382	30.9	582	417	0.58	<0.02	0.093	0.004	0.004	<0.0005	0.0009
AR-0104	3/15/17	115	16.4	76.9	0.999	203	314	40.9	625	355	0.51	0.266	0.556	0.652	0.678	<0.0005	0.0008
AR-0106	3/15/17	99.1	15	20.1	2.61	91.3	274	17	394	309	0.42	0.06	0.065	0.005	0.006	<0.0005	0.0005
AR-0110	3/16/17	107	24.3	72.2	2.1	195	331	35	624	367	0.44	0.027	0.161	0.002	0.026	0.0019	0.0713
AR-0112	3/21/17	87.4	12.9	27.5	1.7	108	233	24.2	393	272	0.46	1.6	1.65	1.01	1	0.0011	0.0017
AR-0156	3/14/17	123	24	53.2	3.43	148	377	34.8	598	406	0.35	0.111	1.22	0.002	0.036	<0.0005	0.008
AR-0173	3/15/17	115	24.6	64.8	1.41	175	320	33	613	388	0.52	0.075	0.238	0.001	0.002	<0.0005	0.001
AR-0181	3/20/17	131	21.4	35.6	2.57	166	356	18.4	569	416	0.63	<0.02	0.048	<0.001	0.001	<0.0005	0.0008
AR-0207	3/16/17	125	21.9	26.2	1.86	121	372	20.9	522	403	0.4	<0.02	0.035	<0.001	0.001	0.0021	0.0051
AR-0212	3/14/17	120	18.1	20.4	1.08	96.3	354	13.1	463	373	0.37	<0.02	<0.02	<0.001	<0.001	<0.0005	<0.0005
AR-0213	3/16/17	409	25.3	2880	10.4	6320	109	280	10000	1130	1.55	0.391	0.424	1.67	1.75	<0.0025	0.0084
AR-0214	3/20/17	103	9.04	687	3.04	1320	100	208	2410	295	2.92	<0.04	1.51	0.454	0.459	0.161	2.97
June 2017																	
AR-0006	5/31/17	140	17.6	31	2.06	136	394	16.2	554	422	0.36	0.796	0.735	0.096	0.098	0.0007	0.0009
AR-0008	5/30/17	232	34.1	157	3.11	693	325	24.6	1330	719	0.26	0.046	0.158	0.002	0.001	0.001	0.0026
AR-0010	5/30/17	174	13.3	55.5	1.61	329	292	28.3	777	488	0.4	<0.02	<0.02	<0.001	<0.001	0.0009	0.0009
AR-0015	5/30/17	199	23.8	97.3	1.73	464	300	28.1	985	595	0.62	<0.02	<0.02	<0.001	<0.001	0.0013	0.0016
AR-0017	5/31/17	328	22.2	77.9	1.49	722	306	20.4	1350	909	0.43	0.109	0.094	0.102	0.11	<0.0005	0.0008
AR-0023	5/31/17	123	14.5	34.9	0.723	166	283	26.6	525	367	0.44	0.059	0.075	0.13	0.142	0.0008	0.0139
AR-0031	6/1/17	570	64.6	130	3.21	1380	393	109	2490	1690	1.1	0.056	0.09	1.18	1.19	<0.001	0.0016
AR-0038	5/30/17	242	28.4	52.1	2.53	444	361	31.3	1010	722	0.4	0.117	0.153	0.007	0.008	0.004	0.0009
AR-0052	6/6/17	91.8	12.1	15	1.33	70.2	257	12	351	279	0.37	0.054	0.125	0.004	0.007	0.0008	0.0026
AR-0054	5/31/17	152	23.5	38	1.35	162	418	20.3	643	476	0.32	<0.02	<0.02	0.206	0.229	<0.0005	0.001
AR-0058	6/1/17	166	17	83.1	2.15	307	374	26.2	803	484	0.28	0.075	0.137	0.001	0.001	<0.0005	0.0011
AR-0059	6/1/17	101	12.5	54.6	1.63	175	257	20	508	303	0.34	0.045	0.09	0.003	0.003	0.0005	0.0009
AR-0074	6/6/17	102	13.5	27.8	2.44	101	296	16.1	423	310	0.67	0.488	0.469	0.572	0.569	0.0005	0.0013
AR-0075	6/6/17	46	6.53	23.9	2.01	52.3	169	7.26	243	142	0.47	0.94	1.02	1.87	1.81	0.0007	0.0014
AR-0087	6/1/17	128	22.7	63.6	1.85	193	351	33.5	636	412	0.33	0.274	0.432	0.059	0.062	0.0014	0.0037
AR-0102	6/5/17	122	26.6	43.4	3.29	149	378	37.4	590	415	0.58	<0.02	<0.02	<0.001	<0.001	<0.0005	0.0012
AR-0104	6/5/17	115	16.8	74.1	0.987	201	319	37.1	619	356	0.51	0.171	0.221	0.696	0.663	0.0011	0.0014
AR-0106	6/5/17	101	14.9	18.9	2.48	96.9	286	17.2	405	313	0.39	<0.02	<0.02	0.016	0.005	0.0006	0.0009
AR-0110	6/5/17	107	26.5	58.7	2.04	178	331	34.3	600	377	0.42	<0.02	<0.02	<0.001	0.003	0.0006	0.0078
AR-0112	6/6/17	102	14.6	25	1.69	88.3	295	21.2	415	316	0.38	1.98	1.96	0.921	0.898	0.0007	0.0029
AR-0156	6/6/17	79.8	15.7	21.8	2.74	77.6	265	12.7	352	264	0.53	<0.02	<0.02	<0.001	<0.001	<0.0005	0.0009
AR-0156	6/6/17	78.9	15.6	21.1	2.71	77.2	261	12.5	352	261	0.53	<0.02	<0.02	0.001	<0.001	0.0006	0.0005
AR-0173	6/1/17	113	23.9	61.2	1.24	177	319	32	606	380	0.51	0.062	0.112	0.001	0.001	0.0036	0.001
AR-0181	5/30/17	133	20.6	34.9	2.38	160	352	19.9	564	418	0.63	<0.02	<0.02	<0.001	<0.001	0.0009	0.0012
AR-0207	6/5/17	122	21.6	23.5	1.77	112	382	16.3	505	394	0.39	<0.02	<0.02	<0.001	<0.001	0.0029	0.0037
AR-0212	5/31/17	114	16.6	18.8	0.948	91.2	347	12.4	444	353	0.34	<0.02	<0.02	<0.001	0.001	0.001	0.0008

important when considering potential impacts of the Gold King Mine spill, or other water contaminants in the Animas River. Areas in the aquifer that show a large range of dissolved oxygen concentrations over time are probably very dynamic with frequent periods of recharge by high dissolved oxygen river water. Specific conductance data in Table 3 and Table 5 indicate that river water has lower total dissolved solids concentrations than those observed in most groundwater in the study area. Therefore, the hypothesis that increases in dissolved oxygen concentrations in groundwater was due to the input of river water was tested by examining temporal changes in dissolved oxygen and total dissolved solids for mixed-dissolved oxygen wells.

An inverse linear correlation was identified for some of the mixed-dissolved oxygen wells (Figure 27). However, many of these correlations were weak, and we did not observe this linear relationship for many of the mixed-dissolved oxygen wells. Time series graphs of total dissolved solids and dissolved oxygen for many of the mixed-dissolved oxygen wells

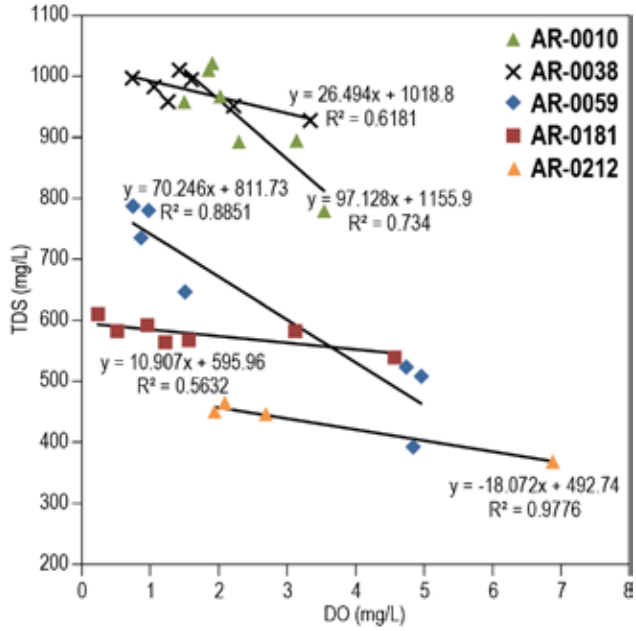

Figure 27. Linear regressions for total dissolved solids (TDS) as a function of dissolved oxygen (DO) for selected wells show an inverse correlations. When dissolved oxygen concentrations in groundwater increase, total dissolved solids concentrations decrease.

Table 7. Average concentrations for selected constituents for all wells sampled (all concentrations in millgrams per liter).

Site ID	Ca	Mg	Na	Cl	HCO_3	SO_4	K	ALK	B	Ba	Cu	Li	Mn	NO_3	Si	Sr	Zn
AR-0006	147	17	31	17	414	135	2.1	339	0.085	0.053	0.0007	0.039	0.101	0.2	4.9	2.1	0.0017
AR-0008	237	32	156	25	319	698	3.0	261	0.093	0.026	0.0025	0.043	0.002	2.4	5.8	3.3	0.0083
AR-0010	222	15	59	31	281	429	1.7	230	0.090	0.020	0.0015	0.032	0.001	15.5	5.8	4.8	0.0099
AR-0015	201	23	93	29	305	463	1.8	250	0.126	0.015	0.0015	0.023	0.003	2.6	6.1	3.6	0.0321
AR-0017	334	22	72	22	305	708	1.5	250	0.111	0.022	0.0016	0.023	0.156	1.7	7.3	6.6	0.0032
AR-0023	127	15	35	27	279	169	0.8	229	0.082	0.018	0.0009	0.027	0.075	2.3	5.8	2.1	0.0083
AR-0031	543	57	120	93	375	1283	3.0	308	0.253	0.010	0.0027	0.094	1.024	4.3	10.9	6.1	0.0036
AR-0038	235	27	51	31	364	422	2.4	299	0.089	0.023	0.0016	0.051	0.007	4.8	7.3	2.5	0.0029
AR-0052	101	13	16	15	272	87	1.5	223	0.048	0.057	0.0020	0.034	0.002	8.6	4.3	0.7	0.0104
AR-0054	149	23	38	20	409	170	1.4	335	0.096	0.035	0.0012	0.022	0.248	7.6	6.8	2.0	0.0009
AR-0058	174	17	77	25	366	313	2.2	300	0.116	0.029	0.0010	0.034	0.002	2.6	4.7	2.4	0.0199
AR-0059	114	15	75	27	262	246	2.0	214	0.071	0.046	0.0011	0.034	0.010	1.2	5.5	1.8	0.0194
AR-0073	151	23	46	24	411	177	1.7	337	0.103	0.034	0.0013	0.024	0.534	8.0	6.3	2.1	0.0026
AR-0074	108	15	35	27	295	138	2.5	242	0.058	0.042	0.0010	0.038	0.636	0.2	4.6	1.0	0.0069
AR-0075	123	17	59	68	305	165	3.2	250	0.059	0.123	0.0007	0.044	4.540	0.2	7.4	1.1	0.0215
AR-0087	123	22	63	33	345	189	1.9	283	0.082	0.039	0.0008	0.041	0.054	3.7	5.2	2.0	0.0011
AR-0102	126	26	42	32	385	148	3.4	316	0.091	0.032	0.0010	0.061	0.004	2.3	6.1	2.0	0.0106
AR-0104	105	15	91	41	315	199	1.1	255	0.073	0.030	0.0028	0.030	0.603	0.1	5.2	1.7	0.0113
AR-0106	99	15	20	16	281	93	2.6	231	0.050	0.042	0.0054	0.042	0.008	0.2	4.4	1.2	0.0018
AR-0110	111	26	67	34	337	190	2.1	276	0.077	0.030	0.0028	0.025	0.002	12.9	5.2	1.6	0.0277
AR-0112	94	13	25	21	265	96	1.7	217	0.045	0.110	0.0007	0.028	0.957	0.2	4.6	0.7	0.0035
AR-0156	108	21	37	25	341	121	3.3	279	0.086	0.044	0.0013	0.042	0.002	4.3	4.9	1.3	0.0057
AR-0173	116	24	62	30	319	175	1.3	262	0.095	0.028	0.0015	0.030	0.001	29.7	5.4	2.6	0.0052
AR-0181	134	21	36	20	361	166	2.6	296	0.062	0.034	0.0030	0.036	0.001	1.9	5.5	1.2	0.0128
AR-0207	125	22	26	20	379	118	1.9	310	0.062	0.044	0.0022	0.028	0.001	4.3	5.4	1.5	0.0103
AR-0212	112	16	19	12	334	88	1.0	274	0.053	0.040	0.0038	0.028	0.001	2.4	5.9	0.9	0.0204
AR-0213	409	25	2880	280	109	6320	10.4	89	0.914	0.008	0.0053	0.250	1.670	0.5	4.1	6.8	0.0127
AR-0214	103	9	687	208	100	1320	3.0	82	0.584	0.014	0.0023	0.070	0.454	4.3	6.5	1.7	0.0132

that did exhibit this linear relationship (Figure 28) confirm this inverse relationship by clearly showing that for most increases in dissolved oxygen concentrations between sampling events, there were correlating decreases in total dissolved solids concentrations.

This same general trend was also seen for most mixed-dissolved oxygen wells, even if there was not a linear correlation between dissolved oxygen and total dissolved solids (Figure 29). However, this inverse correlation between total dissolved solids and dissolved oxygen concentrations was not observed for all wells, as can be seen for AR-0106 (Figure 29). We identified the direction of change for total dissolved solids and dissolved oxygen concentrations between sampling events for all samples that were sampled at least four consecutive sampling events to evaluate how often the direction of change for total dissolved solids was opposite to that of dissolved oxygen. Figure 30 shows that for mixed-dissolved oxygen wells, slightly over 70% of coincident changes in

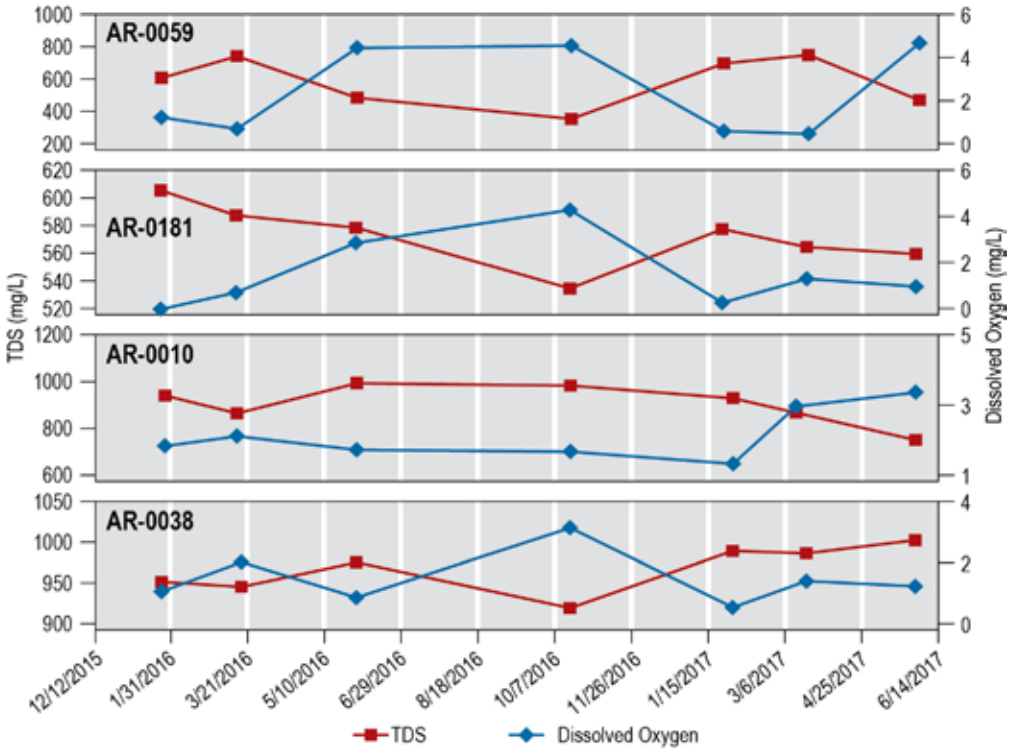

Figure 28. Time series graphs of total dissolved solids and dissolved oxygen for selected mixed-dissolved oxygen wells that show a inverse linear relationship between total dissolved solids and dissolved oxygen. For most increases in dissolved oxygen a correlating decrease in total dissolved solids concentrations was observed.

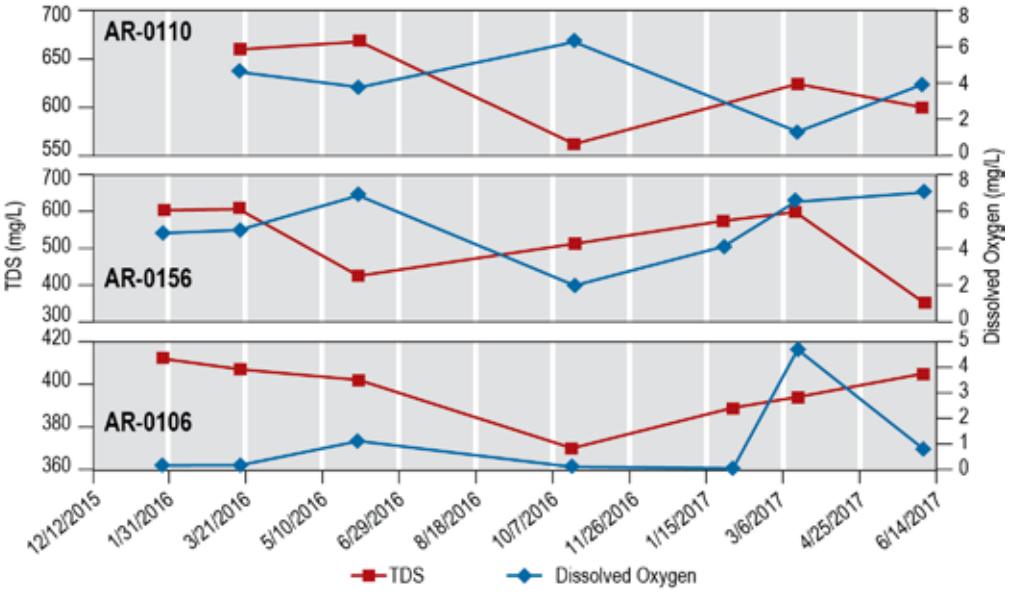

Figure 29. Time series graphs of total dissolved solids and dissolved oxygen for selected mixed-dissolved oxygen wells that do not show a linear relationship between total dissolved solids and dissolved oxygen. Well AR-0110 shows inverse correlation in the direction of change for total dissolved solids and dissolved oxygen concentrations. For AR-0156, some fluctuations in total dissolved solids and dissolved oxygen show this inverse correlation while others do not. For AR-0106, this inverse correlation is not consistent.

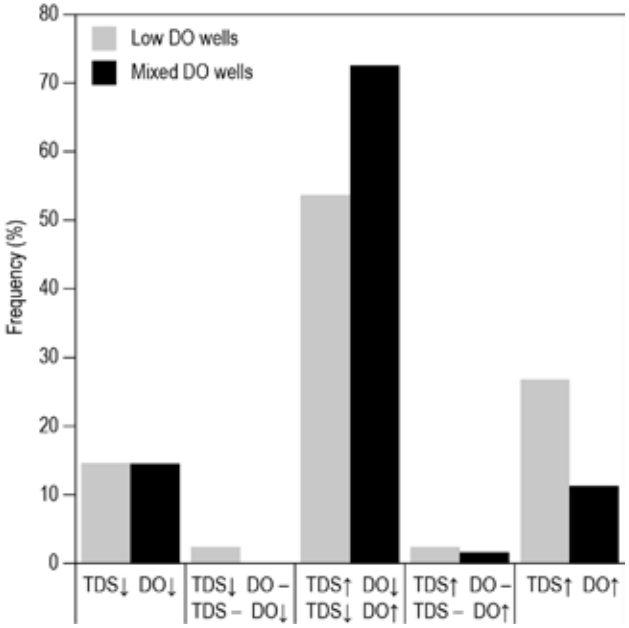

Figure 30. Analysis of the direction of change in dissolved oxygen (DO) and total dissolved solids (TDS) between sample events. An up-arrow indicates an increase; a down-arrow indicates a decrease; a dash indicates no change. Most increases in dissolved oxygen are accompanied by a decrease in total dissolved solids and vice versa for both mixed-dissolved oxygen wells and low-dissolved oxygen wells. This trend suggests that increases in dissolved oxygen concentrations in groundwater are usually due to the input of high-dissolved oxygen, low-total dissolved solids irrigation water.

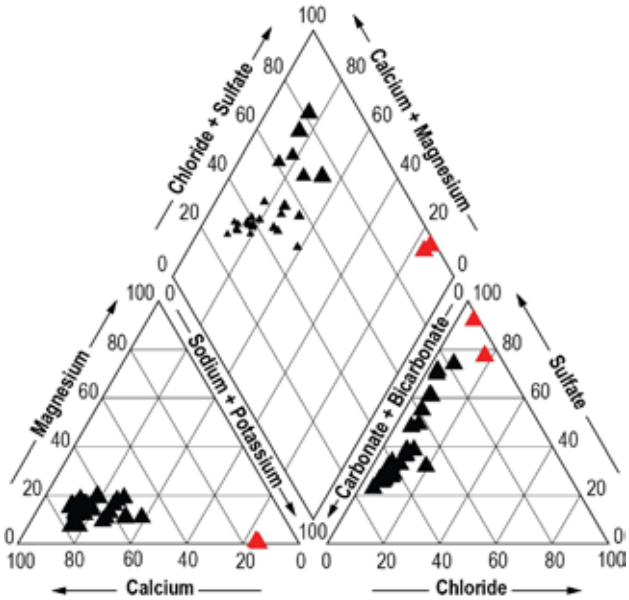

Figure 31. Piper diagram showing relative cation (left ternary plot) and anion (right ternary plot) concentrations for repeated samples (black triangles) and the deep, regional wells AR-0213 and AR-0214 (red triangles). The size of each data point in the middle diamond graph is proportional to the sulfate concentration.

total dissolved solids and dissolved oxygen between sampling events occurred in opposite directions. Interestingly, for low-dissolved oxygen wells, slightly over 50% of coincident changes in total dissolved solids and dissolved oxygen between sampling events occurred in the opposite direction. If the causes of change in dissolved oxygen and total dissolved solids over time were not related, and the occurrence of the coincident changes in dissolved oxygen and total dissolved solids in opposite direction was random, we would expect to see this occur about 25% of the time. Therefore, temporal fluctuations in dissolved oxygen in groundwater are very likely indicative of oxygenated, lower total dissolved solids river water recharging the shallow aquifer in that area. These mixing processes are discussed below in detail.

Water type—The Piper diagram shown in Figure 31 is used to group different types of water based on relative concentrations of the major cations and anions. Data points shown on Figure 31 are average values for samples collected multiple times (black triangles). The two deeper wells, AR-0213 and AR-0214 are shown as red triangles and were only sampled once. On the ternary plot on the bottom left, which shows relative cation concentration, for all repeated samples calcium (Ca) is the dominant cation, accounting for more than 50% of equivalents per liter of cations. Data for AR-0213 and AR-0214 shows that the dominant cation is sodium (Na), which accounts for over 80% of cations. For the anions shown in the ternary plot on the right, almost all repeated samples exhibit relative chloride (Cl) concentrations of less than 10% and plot in a linear fashion between bicarbonate (HCO_3) and sulfate (SO_4), ranging from 67% bicarbonate to 75% sulfate. Again, AR-0213 and AR-0214 stand out with sulfate being the dominant anion. For AR-0213, sulfate accounts for over 90% of anions. Figure 32 shows the location of all the wells that were sampled and indicates the water types as calcium – bicarbonate, calcium – sulfate, and sodium – sulfate, which identifies the dominant cation and anion in the water sample. All wells exhibiting a calcium – sulfate water type are located south of Aztec.

Water/Mineral interactions—Mineral/water interactions largely control the concentrations and relative distribution of dissolved constituents in groundwater. The types of minerals present in the aquifer, their solubility, and the residence time of the water determines the relative amount of major ions in

Figure 32. Location of wells, identified by their water type as defined by relative cation and anion concentrations.

solution. Therefore, the geochemical composition of groundwater can help to determine the type of rocks or sediments with which the water has interacted. As discussed above, the major ions present are calcium, bicarbonate, and sulfate, indicating the dissolution of calcium carbonate (limestone, dolomite, or calcite cements) and gypsum. Figure 33 shows that for all water samples the main anions (sulfate and bicarbonate on the y-axis) and cations (calcium and magnesium on the x-axis) mostly control the charge balance of the solution, with the data plotting close to the 1:1 line. However, all data plots slightly above the 1:1 line, indicating a slight deficit of cations to maintain a charge balance. This observation is likely due to cation exchange, where sodium ions that are bound to clay mineral surfaces exchange with calcium and magnesium in solution. The presence of sodium and chloride in groundwater is usually primarily due to the dissolution of halite (NaCl), which has a molar ratio (Na/Cl) of 1, represented by the 1:1 line in Figure 34A, which shows sodium concentration as a function of chloride concentration. Almost all the data shows an excess of sodium relative to chloride. Figure 34B shows that the cation deficit shown in Figure 33 is roughly equal to the sodium excess, confirming the occurrence of cation exchange. Some of the observed excess sodium may also be a result of the mixing of the sodium sulfate water shown in Figure 31 and Figure 32.

Geochemical modeling with PHREEQC (Packhurst and Appelo, 1999) was used to determine saturation indices for different minerals. Saturation indices for selected minerals based on average groundwater chemistry data are included in Table 8. Most groundwater sampled ranged from saturated to super-saturated with respect to calcite, aragonite, dolomite, barite, and quartz. This indicates that this water cannot dissolve these minerals and can potentially precipitate them. Almost all water samples were under-saturated with respect to gypsum, indicating the potential to dissolve gypsum. Saturation indices for minerals not shown in Table 8 are less than zero, indicating under-saturation.

Wells AR-0213 and AR-0214, both of which appear to produce water from bedrock underlying alluvial sediments, are chemically distinct as high-TDS sodium-sulfate type waters. These water samples are also distinct isotopically and are much older than any other waters sampled in the study area, as will be discussed below. High total dissolved solids sodium-sulfate type water is found in the Nacimiento, Ojo Alamo, and Animas Formations (Phillips et al., 1989; Kelley et al., 2014). Phillips et al. (1989) sampled water from the Ojo Alamo and Nacimiento Formations that is chemically similar to that sampled from AR-0213 and AR-0214, with high

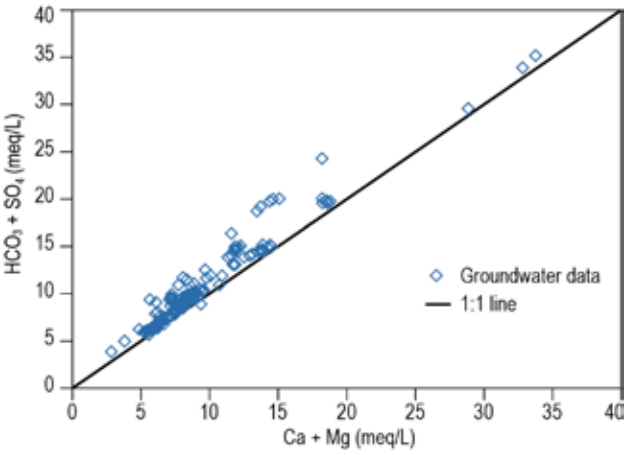

Figure 33. Graph of bicarbonate and sulfate vs. calcium and magnesium helps to evaluate controls on water chemistry. Data that plots along the 1:1 line indicates that the dissolution of limestone, dolomite, and gypsum are the primary factors controlling the major ion chemistry. Data that plots slightly above the 1:1 line indicates a cation deficit for maintaining a charge balance. The unit milliequivalent per liter is the amount of millimoles per liter multiplied by the valence of the ion.

sulfate and sodium and low calcium and magnesium. Geochemical modeling showed that the chemical evolution of this water involved the dissolution of gypsum and sodium/calcium ion exchange that drove calcite into the dissolution. These processes cause sulfate and sodium to build up and for calcium to be depleted due to cation exchange.

Mixing processes—explained by progressive water/mineral interactions that cause the water chemistry to evolve over time resulting in the observed sodium-sulfate water, as described by Phillips et al. (1989). However, the mixing of the high-total dissolved solids, sodium – sulfate water and fresher calcium – bicarbonate water could also explain the observed trend. Temporal trends in dissolved oxygen and total dissolved solids discussed above suggest that river water, characterized by low total dissolved solids and high dissolved oxygen, mixes with groundwater at certain times, causing the dissolved oxygen to increase and the groundwater total dissolved solids to decrease slightly. While the timing of these observed coincidental changes in total dissolved solids and dissolved oxygen varies from well to well, it appears to happen slightly more often between March and June, indicative of recharge during irrigation season. It is seen in Figure 35 that there is an inverse relationship between the observed range in dissolved oxygen concentrations in groundwater and relative sulfate concentrations. High dissolved oxygen wells and mixed dissolved oxygen wells with the highest dissolved oxygen concentrations, which have more direct river input, exhibit low relative sulfate concentrations (as a proportion of anions). The range in observed dissolved oxygen concentrations decreases as relative sulfate concentrations increase towards values

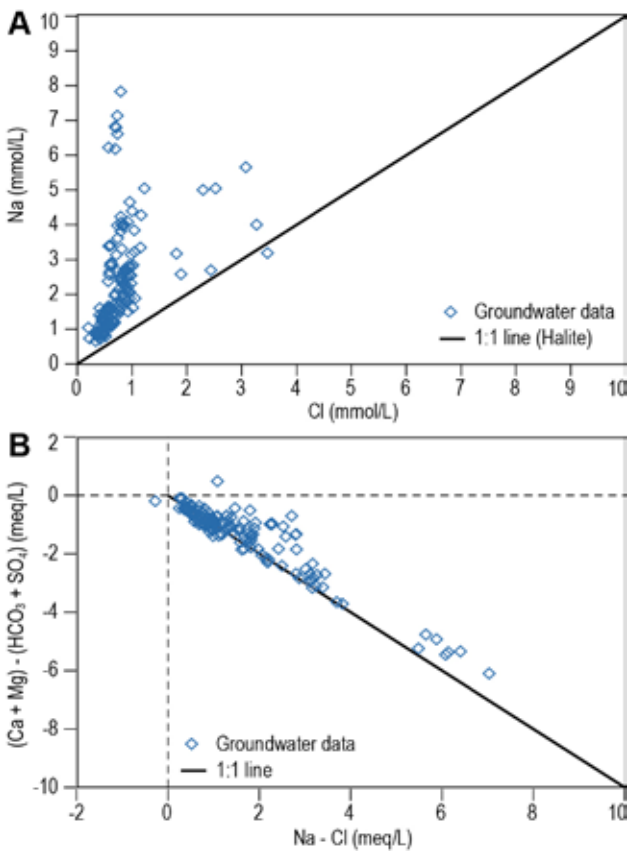

Figure 34. Graphs of major ions to assess water-mineral interactions. **A**—Sodium molar concentrations as a function of chloride molar concentrations show that the presence of sodium is due to processes other than just the dissolution of halite. **B**—The cation deficit ((Ca + Mg) – (HCO_3 – SO_4)) plotted as a function the sodium – chloride cation surplus (Na – Cl) is used to assess the occurrence of cation exchange. Data that plot on or near the line with a slope of -1 indicates that the cation exchange is occuring. The unit milliequivalent per liter is the amount of millimoles per liter multiplied by the valence of the ion.

Table 8. Saturation indices for selected minerals.

	ARAGONITE	BARITE	CALCITE	DOLOMITE	GYPSUM	QUARTZ
Site ID	**$CaCO_3$**	**$BaSO_4$**	**$CaCO_3$**	**$CaMg(CO_3)_2$**	**$CaSO_4$: $2H_2O$**	**SiO_4**
AR-0006	0.97	0.35	1.12	1.46	-1.25	0.1
AR-0008	0.89	0.38	1.04	1.41	-0.54	0.12
AR-0010	0.87	0.14	1.03	1.11	-0.7	0.11
AR-0015	0.86	0.07	1.01	1.28	-0.71	0.16
AR-0017	0.96	0.33	1.12	1.23	-0.4	0.26
AR-0023	0.77	-0.04	0.92	1.09	-1.2	0.15
AR-0031	1.1	0.04	1.25	1.72	-0.1	0.41
AR-0038	0.99	0.21	1.14	1.55	-0.69	0.22
AR-0052	0.71	0.21	0.87	1.06	-1.53	-0.02
AR-0054	0.95	0.19	1.1	1.58	-1.17	0.21
AR-0058	0.93	0.32	1.09	1.32	-0.88	0.07
AR-0059	0.68	0.46	0.84	0.97	-1.1	0.11
AR-0073	0.95	0.23	1.1	1.55	-1.15	0.2
AR-0074	0.72	0.29	0.88	1.05	-1.32	0.06
AR-0075	0.69	0.83	0.85	0.97	-1.22	0.31
AR-0087	0.84	0.3	0.99	1.42	-1.19	0.1
AR-0102	0.89	0.13	1.04	1.57	-1.28	0.17
AR-0104	0.58	0.25	0.73	0.78	-1.21	0.12
AR-0106	0.72	0.15	0.87	1.1	-1.51	0.03
AR-0110	0.8	0.15	0.95	1.48	-1.24	0.06
AR-0112	0.67	0.59	0.82	0.96	-1.5	0.06
AR-0156	0.81	0.22	0.96	1.4	-1.4	0.07
AR-0173	0.78	0.1	0.93	1.39	-1.25	0.09
AR-0181	0.9	0.14	1.05	1.53	-1.21	0.07
AR-0207	0.9	0.18	1.05	1.52	-1.36	0.1
AR-0212	0.83	0.06	0.98	1.32	-1.5	0.13
AR-0213	0.07	0.05	0.22	-0.55	0.05	-0.04
AR-0214	-0.03	0.17	0.12	-0.58	-0.73	0.13

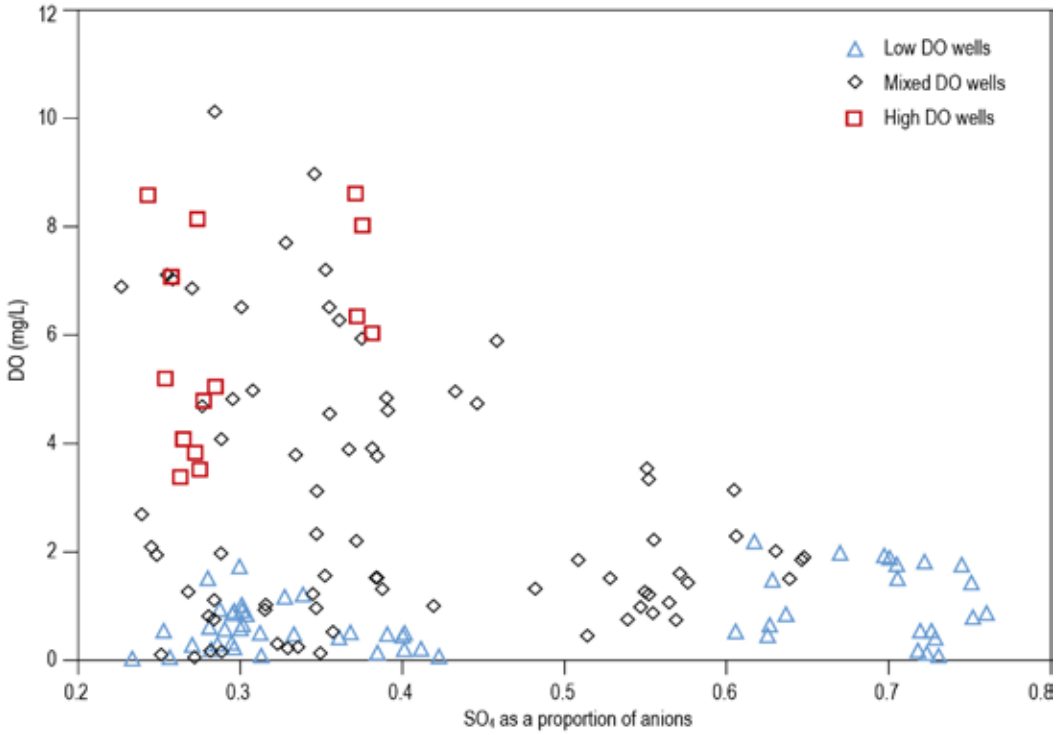

Figure 35. Dissolved oxygen (DO) concentrations plotted as a function of relative sulfate (SO_4) concentrations. This graph shows that water from high dissolved oxygen wells and mixed dissolved oxygen wells with the largest observed range in dissolved oxygen concentrations exhibit lower relative sulfate concentrations. Wells that produce water with higher relative sulfate concentrations exhibit a smaller range in in dissolved oxygen concentrations over time.

observed in AR-0213. This observation supports the hypothesis that the linear trend observed for anions in the piper diagram (Figure 31), which correlates to the spatial trends observed for sulfate and total dissolved solids (Figure 25), is a result of the mixing of fresher water that ultimately originates as river water and high-TDS sodium-sulfate waters observed in the Nacimiento Formation at depths between 300 and 500 feet.

We modeled the mixing of fresh calcium-bicarbonate type river water and high-total dissolved solids sodium-sulfate groundwater in PHREEQC. Well AR-0212, which had one of the lowest sulfate concentrations, was used as the fresh water endmember and AR-0213 water was used as the high-total dissolved solids endmember. The modeled endmembers based on our water chemistry data were combined at different mixing proportions. The resulting modeled mixtures were equilibrated with respect to calcite and barite. The mixing curve shown in Figure 36 plots the relative sulfate concentration as a function of the absolute sulfate concentration. Almost all of the groundwater chemistry data fits this curve remarkably well.

This mixing model suggests that the spatial trend observed for sulfate with increasing concentrations to the southwest (Figure 25) is due to an increased input of regional high-total dissolved solids sodium-sulfate water in the southwest portion of the study area, south of Aztec. For the minor constituents of barium and strontium, which also exhibit the spatial trend in the same direction (Figure 26), groundwater concentrations as a function of relative sulfate concentrations follow the basic shape of the mixing curve, but mostly plot above the mixing line (Figure 37, Figure 38). For barium, most water samples are super saturated with respect to barite. The fresh water endmember on the mixing model shows the concentration that most of the low-sulfate groundwater would exhibit if the solution was at equilibrium with respect to barite. For chloride, which does not exhibit a spatial trend (Figure 26), but usually serves as a conservative tracer, most groundwater concentrations plot slightly above the mixing line (Figure 39). While this mixing trend appears to be the primary process that defines the major ion concentrations in groundwater in the study area, chloride, which makes up a small proportion of anions in both endmembers, appears to be affected by another process. Excess barium, strontium, and chloride concentrations that cannot be explained by the two endmember mixing model presented, suggest that there is likely at least

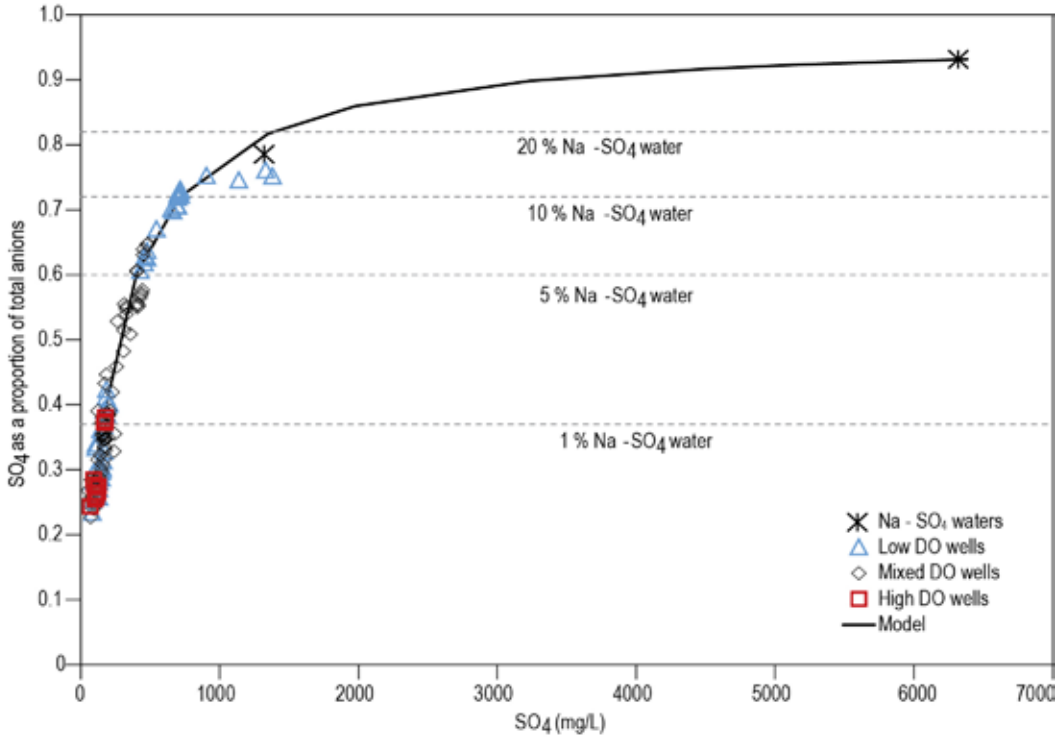

Figure 36. Modeled mixing curve. This mixing curve represents the theoretical mixing of fresher calcium-bicarbonate water with high total dissolved solids sodium-sulfate water, and it matches observed water chemistry data. High dissolved oxygen water and mixed dissolved oxygen water that show evidence of river input plot closer to the fresh water endmember, while waters that plot more towards the high total dissolved solids endmember are low dissolved oxygen wells and do not show evidence of frequent river input.

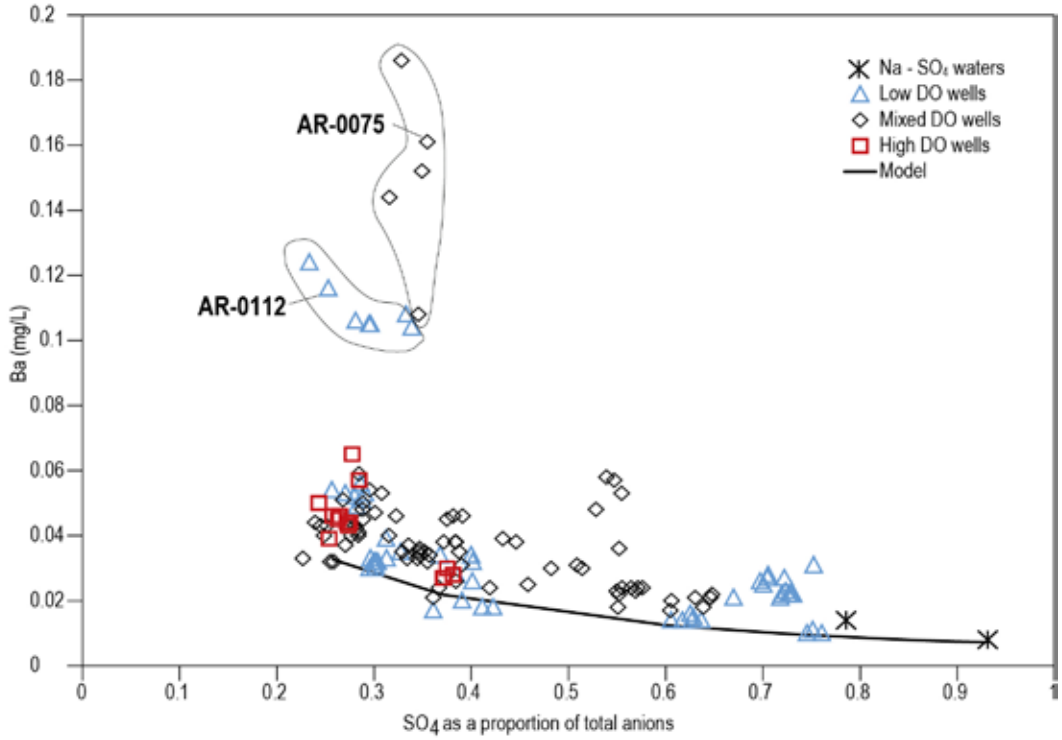

Figure 37. Barium plotted as a function of relative sulfate concentrations shows a general mixing trend but with elevated barium concentrations. Most groundwater ranges from saturated to super saturated with respect to barite.

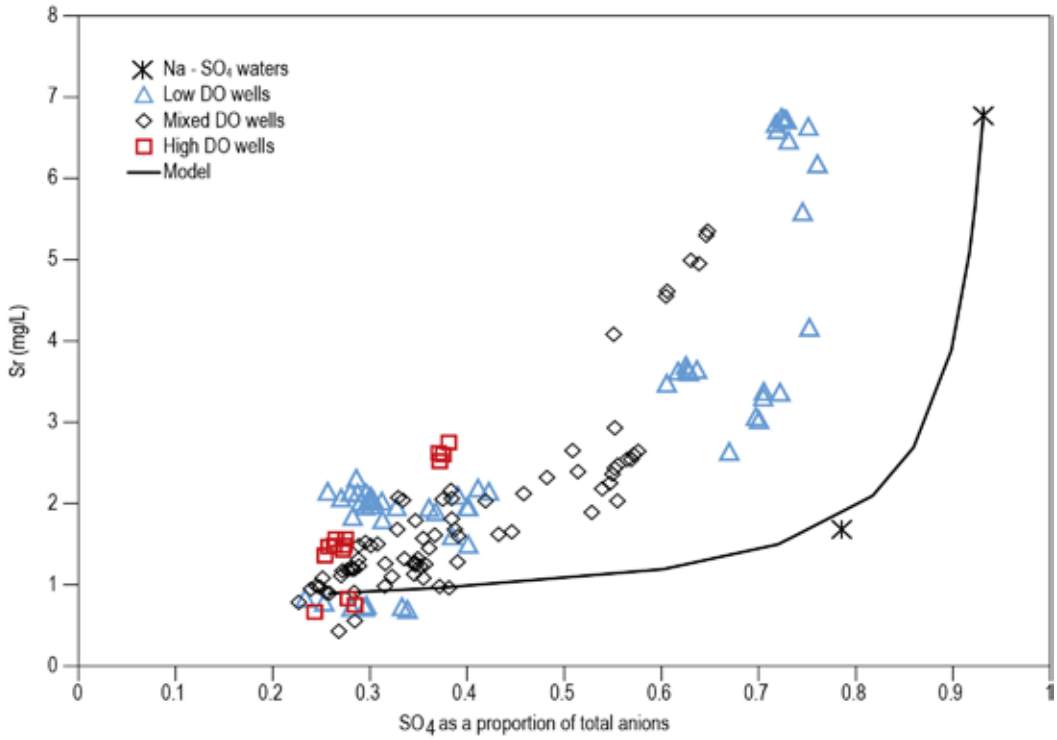

Figure 38. Strontium plotted as a function of relative sulfate concentrations shows a general mixing trend but with excess strontium observed for most groundwater samples.

one other endmember that is affecting the concentrations of minor constituents. It should be noted that AR-0075 exhibits much higher chloride and barium concentrations than is seen in other wells. AR-0112 also shows significantly higher chloride concentrations than most other wells. We speculate that there is a third mixing endmember that is characterized by high-total dissolved solids concentrations, with sodium and chloride as the major ions, which may be contributing relatively small amounts of water to the shallow aquifer system.

Trace metals and redox reactions

Redox conditions in an aquifer affect speciation and therefore the solubility of many metals. The dynamic nature of this shallow aquifer due to irrigation and groundwater/surface water interactions as demonstrated by the observed temporal dissolved oxygen concentrations in many wells, has implications for the mobilization of some metals of concern into the groundwater, possibly related to the Gold King Mine spill. We analyzed water samples for the following trace metals: silver (Ag), aluminum (Al), arsenic (As), boron (B), barium (Ba), beryllium (Be), cadmium (Cd), cobalt (Co), chromium (Cr), copper (Cu), iron (Fe), mercury (Hg), lithium (Li), manganese (Mn), molybdenum (Mo), nickel (Ni), lead (Pb), antimony (Sb), selenium (Se), tin (Sn), strontium (Sr), thorium (Th), titanium (Ti), uranium (U), vanadium (V), and zinc (Zn). Results for all these analyses can be seen in Appendix C. For most of these metals, analysis results were below the reporting limit for nearly all the samples.

The Gold King Mine spill of 2015 exhibited elevated levels iron, aluminum, manganese, lead, copper, arsenic, zinc, cadmium, and mercury (U.S. Environmental Protection Agency, 2016). During the course of the 2 years of sampling for this project after the spill, there does not appear to be any consistent increase to these constituents. This discussion focuses on iron, manganese, and aluminum, which observed in some water samples to be above SMCLs, as discussed above (Figure 24).

For iron, unlike most of the other cations, the total concentrations which include the dissolved constituent and solid or adsorbed phase, were often observed to be much higher than just the dissolved concentrations (Figure 40). We observe this trend more so at lower dissolved oxygen concentrations and to a slightly larger degree for the mixed dissolved oxygen wells. The temporal fluctuation of redox conditions due to changes in dissolved oxygen concentrations likely results in the dissolution and precipitation of iron hydroxides at lower and higher Eh values, respectively. Dissolved iron concentrations

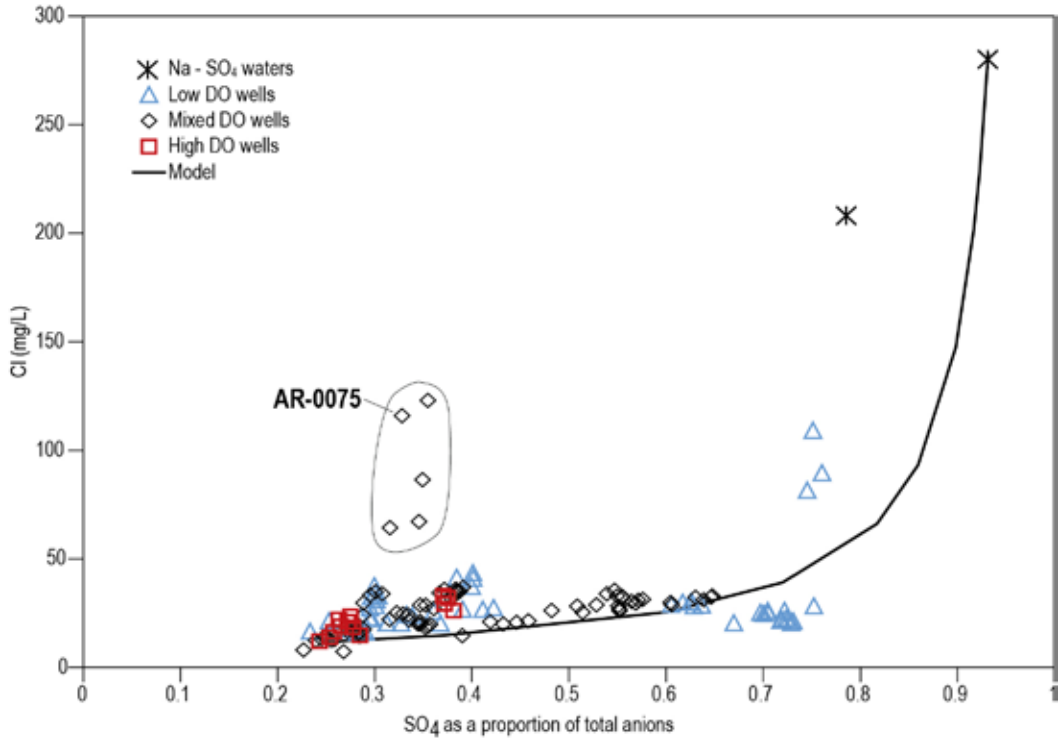

Figure 39. Chloride concentrations plotted as a function of relative sulfate concentrations largely plot close to mixing trend, but many wells exhibit higher chloride concentrations than can be explained by this two endmember mixing model alone.

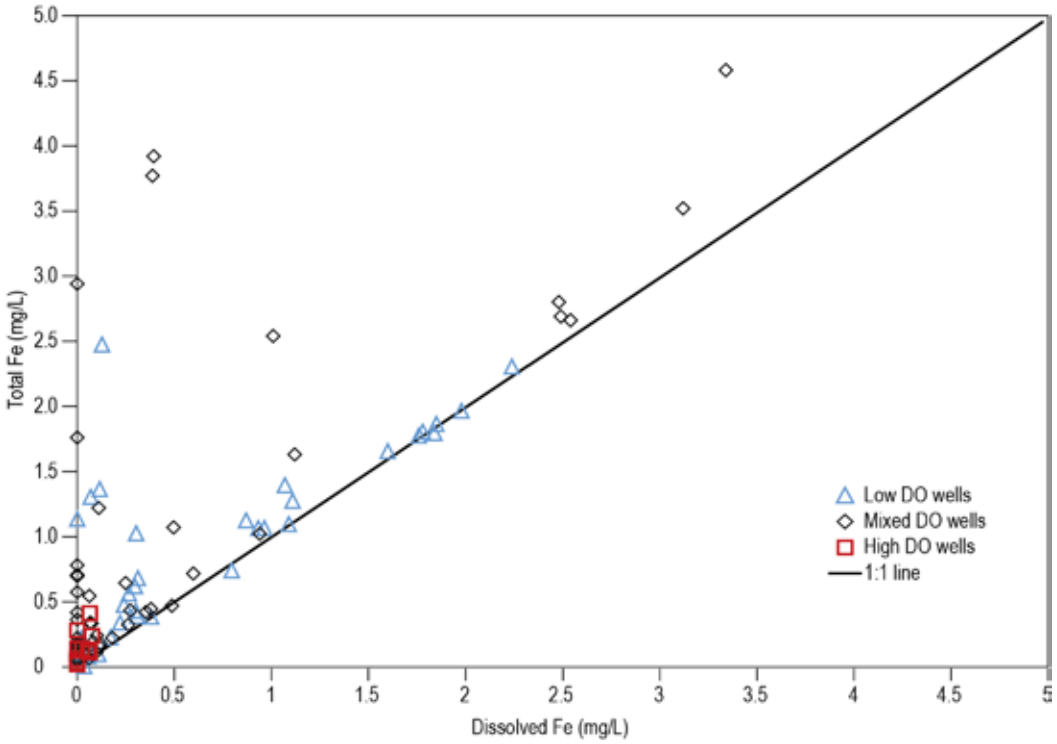

Figure 40. Total iron plotted as a function of dissolved iron (Fe). For points that plot on the 1:1 line, all of the iron present is in the dissolved phase. Deviation from the 1:1 line indicate the presence of iron in the solid state (iron (hydr)oxides).

are significantly higher in water with lower Eh values (Figure 41). For almost all of the water samples with iron concentrations exceeding the U.S. Environmental Protection Agency SMCLs, Eh values are less than 200 millivolts. Figure 42 shows an Eh-pH diagram for the Fe-O-H_2O system with ferrihydrite as the ferric oxide mineral along with groundwater data plotted on the diagram. This diagram may not accurately represent this groundwater system, which is likely more complex and includes interactions with sulfate and bicarbonate. However, it does suggest that for the observed range in Eh values, iron (hydr)oxides such as ferrihydrite are stable, but samples plotting at the lower end of the Eh range are very close to the boundary where dissolved iron (Fe^{2+}) and ferrihydrite are in equilibrium.

Unlike iron, most manganese in groundwater is in the dissolved state (Figure 43), which is predicted by the Eh-pH diagram for the Mn-O-H_2O system (Figure 44), showing almost all water samples plotting in the stability field for dissolved manganese (Mn^{2+}). However, we still observe that many of the waters with the highest manganese concentrations exhibit lower Eh values (Figure 45). The highest manganese concentrations shown in Figure 44, ranging from 2 to over 6.5 mg/L is from the well AR-0075, which stands out in many ways geochemically.

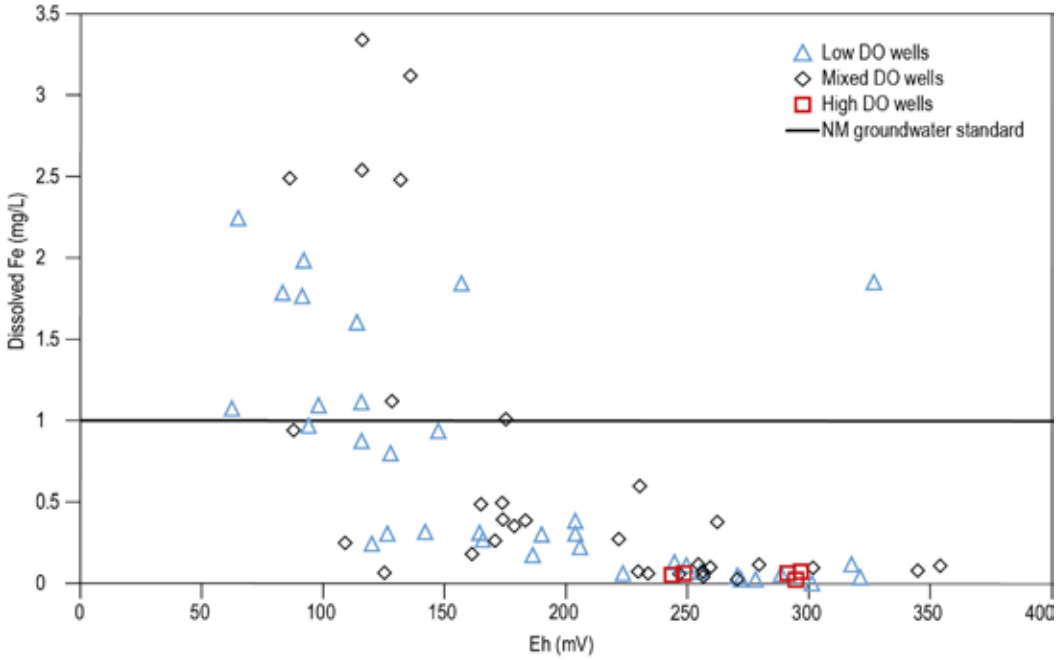

Figure 41. Dissolved iron (Fe) plotted as a function of Eh. Waters with lower Eh values (in millivolts, mV) exhibit higher dissolved iron content.

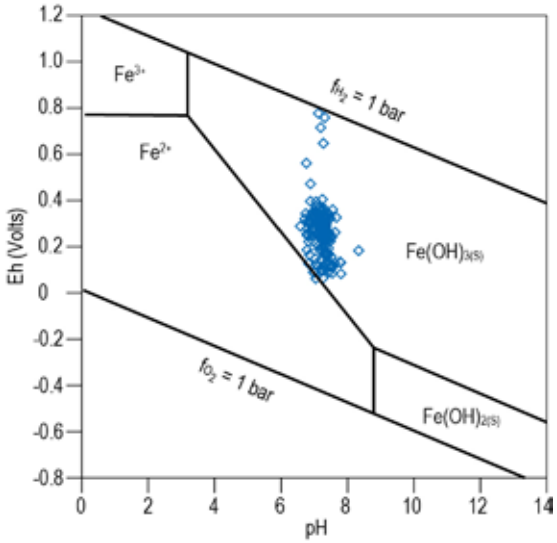

Figure 42. Eh-pH diagram for Fe-O-H_2O system with data plotted on the diagram.

It is apparent that groundwater with the highest iron and manganese concentrations is associated with Eh values of less than 200 millivolts, which accounts for about 25% of the water samples collected for this study. The spatial variability for redox conditions in the study area is likely related to: 1) the spatial distribution of organic matter and other potential reductants in the aquifer, 2) the spatial distribution of potential redox buffers such as MnO_2 and $Fe(OH)_3$, and 3) the circulation rate of groundwater (Drever, 1982). These characteristics and their implications for the presence of high manganese and iron concentrations, including the possible relationship to legacy acid mine drainage and/or the Gold King Mine Spill is discussed more below.

Dissolved aluminum was measured in only one sample, which was collected from AR-0214. As

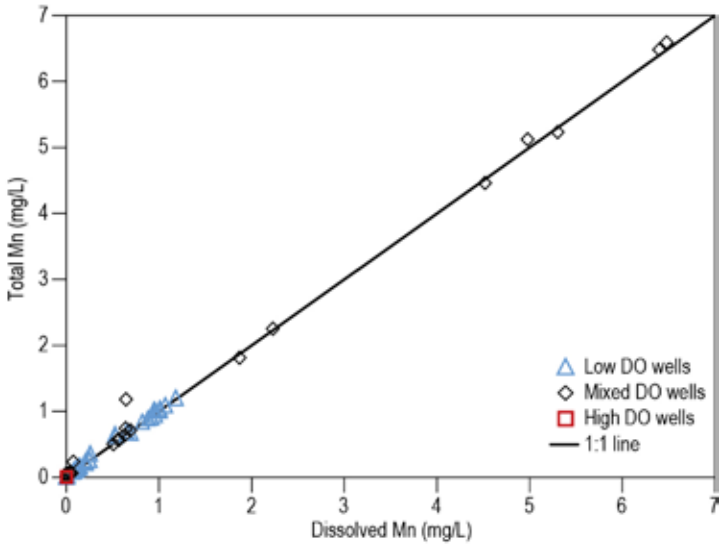

Figure 43. Total manganese (Mn) as a function of dissolved manganese shows that most manganese in groundwater is in the dissolved phase.

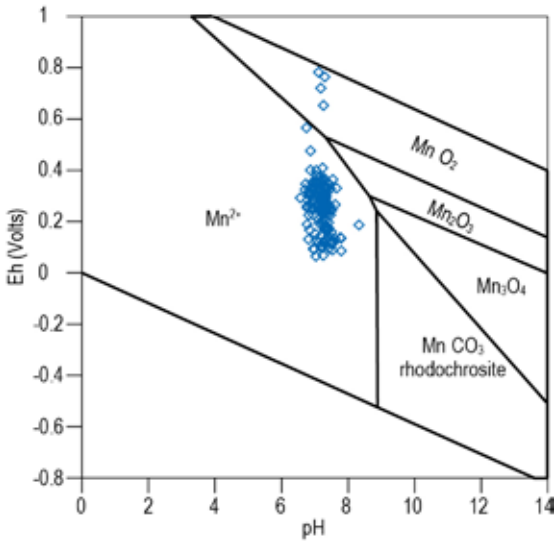

Figure 44. Eh-pH diagram for Mn-O-H_2O system along with data shows that most water samples plot in the stability field for dissolved manganese (Mn^{2+}).

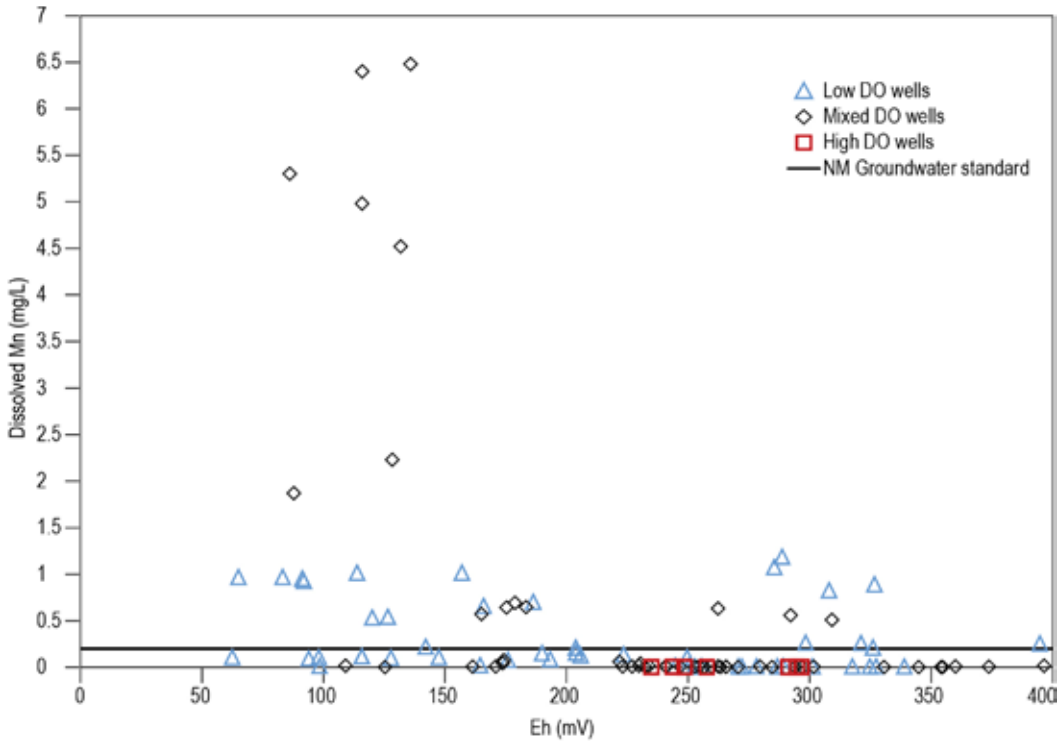

Figure 45. Dissolved manganese as a function of Eh shows that water with the highest manganese (Mn) concentrations exhibit the lowest Eh values.

mentioned above, AR-0213 and AR-0214 are completed in bedrock (likely the Nacimiento Formation) and produce water that is high in total dissolved solids and is characterized by a sodium-sulfate water type, which is distinct from all water samples collected in the alluvial aquifer. The observed dissolved aluminum may be due to the dissolution of aluminosilicate minerals in the San Jose or Nacimiento Formations, suggesting this deeper water that is mixing with the shallow groundwater is a source of aluminum. However, it should be pointed out that dissolved aluminum in AR-0213 was below the reporting limit. It is not surprising that dissolved aluminum was not detected in any of the other groundwater samples, as aluminum minerals are relatively insoluble at near neutral pHs. The measurable total aluminum in several samples indicates a source of aluminum. While aluminosilicates in the aquifer may be the source, it is

also possible that water associated with legacy acid mine drainage pollution in the Animas river and/or the Gold King Mine spill could be the source of this particulate or colloidal aluminum. Aluminum and iron were the dominant metals in the Gold King Mine plume (Sullivan et al., 2017).

Stable Isotopes of Hydrogen and Oxygen

The stable isotopes of oxygen and hydrogen are useful tools for tracing the hydrologic cycle. The isotopic composition of a water sample refers to the ratio of the heavier isotopes to the lighter isotopes (R) for the hydrogen and oxygen that make up the water molecules. Because these stable isotopes are part of the water molecule, small variations in these ratios act as labels that allow tracking of waters with different stable isotopic signatures. All isotopic compositions in this report are presented as relative concentrations, or the per mil deviation of R of a sample from R of a standard (VSMOW) shown in the equation below:

$$\delta = \frac{R_{sample} - R_{standard}}{R_{standard}} *1000‰$$

It is useful to plot stable isotope data on a δD vs $\delta^{18}O$ graph, as shown in Figure 46. In general, most precipitation plots on or near the global meteoric water line (GMWL) with a slope of 8 and a deuterium excess (y-intercept) of 10 as demonstrated by Craig (1961). However, the linear trend that characterizes local precipitation in a specific area may deviate from the GMWL with a similar slope but a different deuterium excess. Isotopic characterization of local precipitation is often very useful for identifying groundwater recharge sources and mechanisms. We found no local meteoric water lines (LMWL) that had been identified for this specific region. We sampled the Animas River at three locations within the study area during the March, June, and October 2016, and January 2017 sampling events (Figure 46). We collected samples from the river for stable isotopic analysis at many more locations (Figure 16) during the March and June 2017 sampling events. The stable isotopic compositions of river samples collected in June 2017, which include sample locations in Colorado, exhibit an evaporation line that shows the isotopic evolution of spring runoff water as it evaporates, with the lightest values at the headwaters near Silverton, and the heaviest values near Farmington. Assuming the water collected near the headwaters represents non-evaporated snowmelt, an assumed LMWL for the winter precipitation in the San Juan Mountains was estimated with a slope of 8

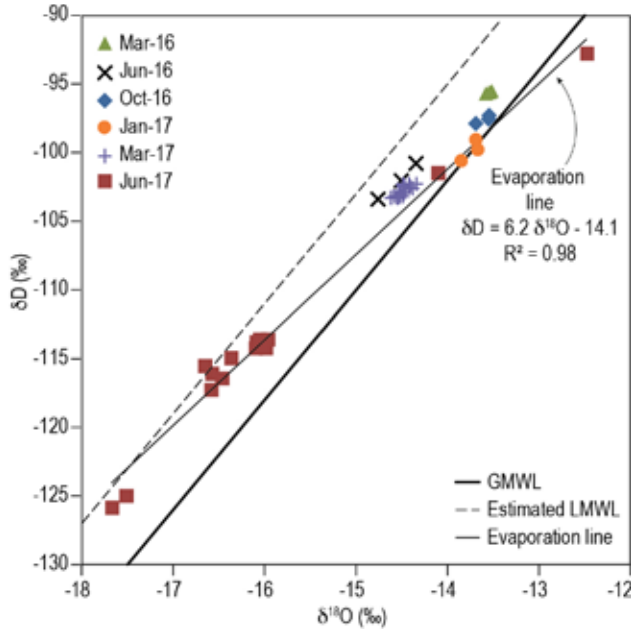

Figure 46. Stable isotopic compositions of river samples collected at different seasons.

that intersected the isotopically lightest river samples. The resulting deuterium excess is 17, which is similar to that of the LMWL identified in the Sacramento Mountains in southern New Mexico by Newton et al. (2012). For the purpose of this study, this is a reasonable estimation of the LMWL, but for future work, it would be worth the effort to construct a LMWL for the high San Juan Mountains near Silverton using stable isotope data for precipitation.

Other river samples collected at different times also plot on or near the evaporation line. Deviation from the observed evaporation line likely represents evaporation under slightly different conditions, such as temperature and relative humidity. Therefore, the isotopic composition of all river samples is likely due to evaporation of winter precipitation in the San Juan Mountains. During the March and January 2016 and March 2017 sampling events, the river was probably at baseflow conditions where river water is primarily derived from groundwater discharge upstream of the study area. Therefore, the stable isotopic composition of groundwater to the north is similar to that of river water. The evaporative signature of groundwater to the north is due to irrigation on the Animas valley floodplain all along the river. Robson and Wright (1995) concluded that in the Florida Mesa area just south of Durango, the primary recharge source to the shallow alluvial aquifer was irrigation water. Water level fluctuations in the study area discussed above, where water levels increase during irrigation season and decrease during the winter indicate that irrigation

is an important recharge source for the shallow alluvial aquifer in New Mexico also.

Average stable isotopic data for almost all groundwater samples plot on or near the evaporation line (Figure 47). As was seen with the water chemistry, AR-0213 and AR-0214 also exhibit distinct stable isotopic compositions with much lighter or more negative values. These are old waters from the Nacimiento/Ojo Alamo aquifer which are described by Phillips et al. (1986). The anomalously light isotopic signature is indicative of a cooler wetter climate during the Pleistocene. As with the chemistry data, there is also some isotopic evidence of mixing of this regional groundwater and the shallow irrigation recharge (Figure 48). The trend is subtle due to the fact that an evaporation trend, which increases the isotopic ratio, dominantly controls the isotopic composition of the shallow groundwater. With the exception on one well (AR-0031), water with a relative sulfate concentrations greater than 0.6 (which is greater than 5% mixing of Na-SO_4 water) (Figure 36), exhibit δD values less than -100‰ and as low as -104‰. For relative sulfate concentrations less than 0.6, while δD values exhibit a large range of values many samples have values greater than -100‰. Well AR-0031 shows the highest degree of enrichment due to evaporation.

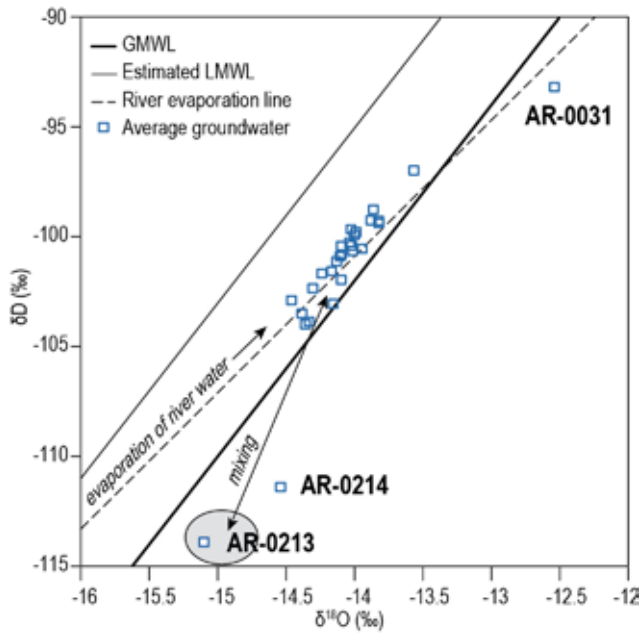

Figure 47. The average stable isotopic compositions of most groundwater plots along or near the river evaporation line. There may be mixing of evaporated river water and regional water from the Nacimiento Formation (AR-0213, AR-0214).

Groundwater age

We collected nine water samples for tritium and carbon-14 analysis during the March 2017 sampling event. In addition to the 4 regional wells (Table 4), five other wells in the shallow alluvial aquifer were chosen mainly to get a fairly uniform coverage across the study area. Tritium and carbon-14 data is shown in Table 9 and Figure 49.

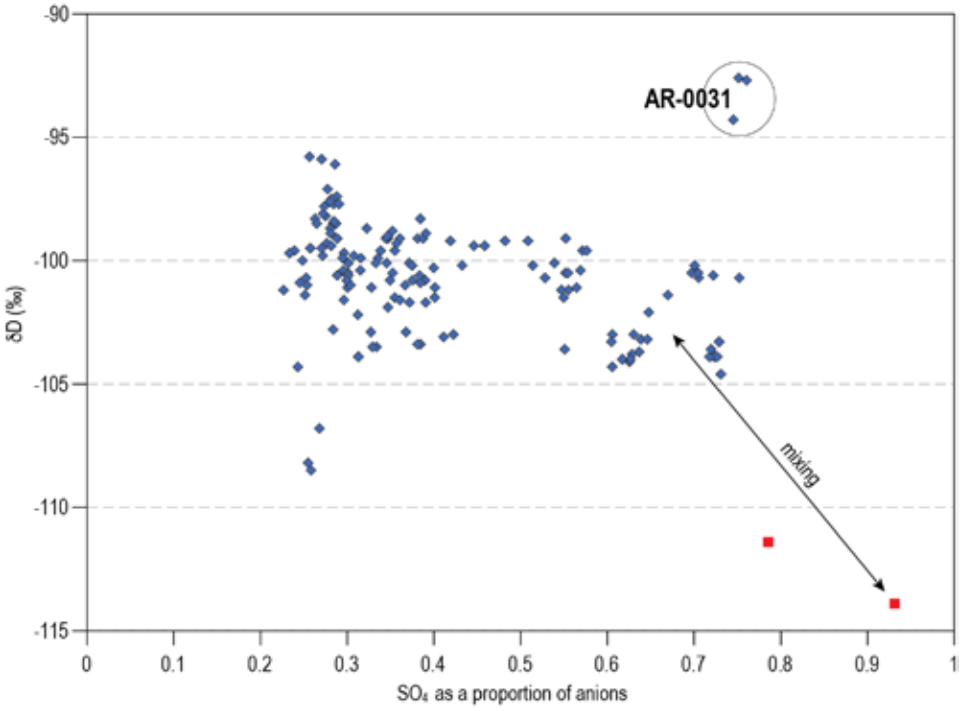

Figure 48. Stable isotope δD values for groundwater as a function of relative sulfate concentration. Lighter δD values for water with higher relative sulfate concentrations indicates mixing of fresh water Ca-HCO_3 waters and high-TDS Na-SO_4 waters from the Nacimiento Formation aquifer.

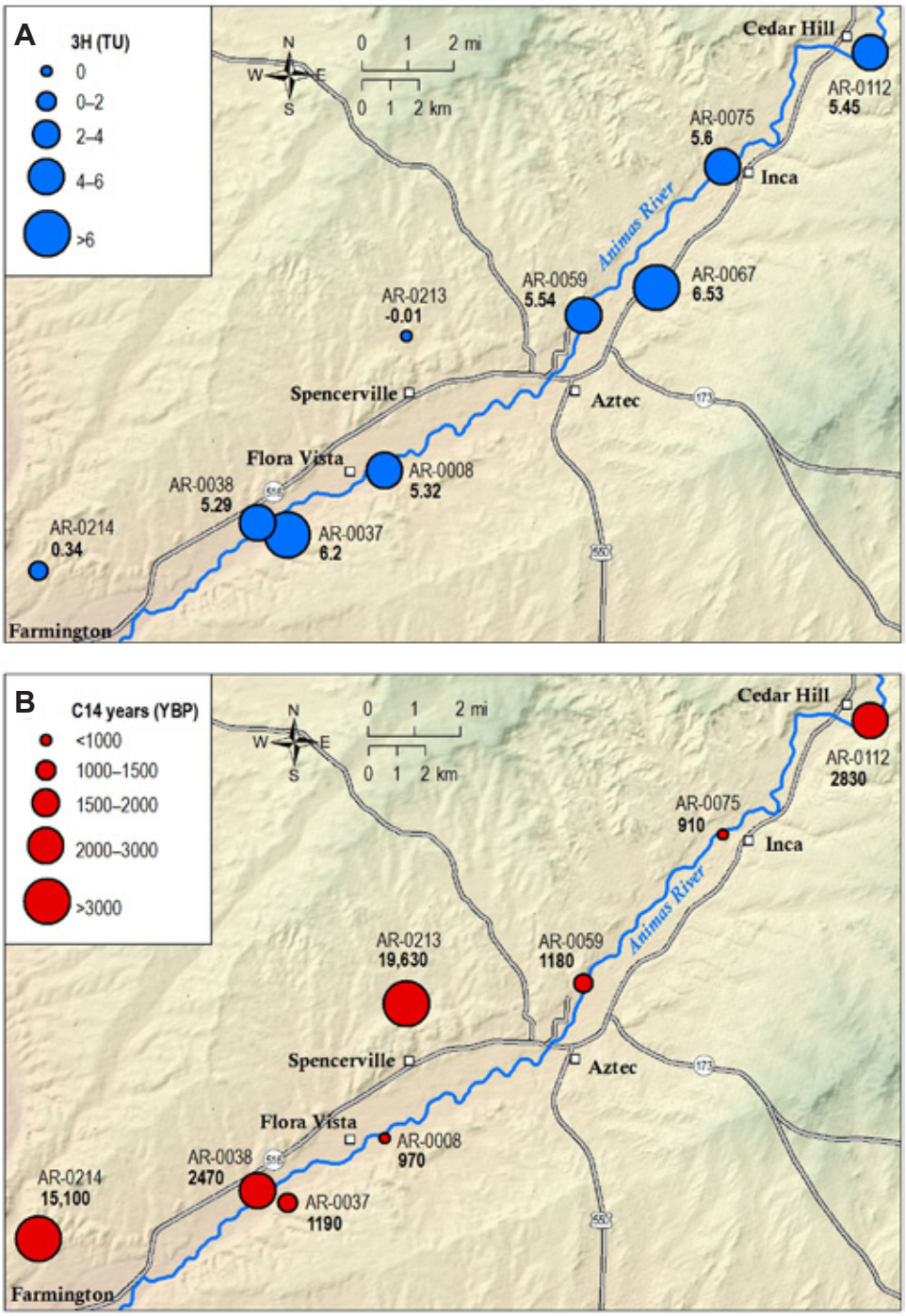

Figure 49. Groundwater age (environmental tracers) maps. **A**—Tritium (^3H) data for regional groundwater (AR-0013 and AR-0014) shows little or no tritium, indicating that the groundwater produced by those wells is older than 50 years old. All other wells produce water containing between 5 and 6.2 TU (Tritium units), indicating that most shallow groundwater is modern water that is less than 10 years old. **B**—Apparent carbon-14 (C14) ages show that AR-0213 and AR-0214 are much older than the other groundwater samples. All other samples, which exhibit tritium concentrations of modern water, show apparent carbon-14 ages ranging from 910 to 2,470 years before present (YBP).

Table 9. Tritium and carbon-14 results. Tritium units (TU) and years before present (YBP) are described in text.

Site ID	**Tritium** (TU)	**Carbon-14** (YBP)
AR-0008	5.32	970
AR-0037	6.2	1190
AR-0038	5.29	2470
AR-0059	5.54	1180
AR-0067	6.53	1860
AR-0075	5.6	910
AR-0112	5.45	2830
AR-0213	-0.01	19,630
AR-0214	0.34	15,100

Tritium (^3H), a radioactive isotope of hydrogen with a half-life of 12.4 years, is produced naturally in the atmosphere by cosmic radiation and enters the hydrologic cycle via precipitation as part of water molecule. Tritium concentration is measured in Tritium Units (TU), where one TU indicates a tritium-hydrogen atomic ratio of 10^{-18}. The tritium content of precipitation varies spatially and temporally, with average values in the Southwestern U.S. and Mexico ranging from 2 to 10 TU (Eastoe et al., 2012). Between 1991 and 2005, the tritium content of precipitation in Albuquerque, NM ranged from 4.5 to 19.1 TU, with an average of 8.8 TU (IAEA/WMO, 2017). Newton et al. (2012) observed tritium concentrations in precipitation in the Sacramento Mountains in southern New Mexico to range from 3 to 10 TU. Assuming initial tritium concentrations in snow melt in the San Juan Mountains are similar to those discussed above, tritium in groundwater can be used to estimate a qualitative age with the general interpretation that groundwater with tritium concentrations between 5 and 10 TU is modern water that is less than 10 years old. All water samples except AR-0213 and AR-0214 have tritium concentrations between 5 and 7 TU, indicative of modern water. AR-0213 and AR-0214 show tritium values of zero and 0.34 TU respectively, indicating that that water is older than 50 years.

Carbon-14 ages shown in Figure 49B are apparent ages. We did not attempt to correct for hydrogeologic processes such as carbonate dissolution that usually results in apparent ages that are older than the actual age of the water. For the purpose of this study, apparent carbon-14 ages are sufficient to confirm the two mixing endmembers as identified by the major ion distribution and tritium ages. Wells AR-0213 and AR-0214 show apparent carbon-14 ages of 19,630 and 15,100 years before present (YBP), respectively. The older water collected from the Nacimiento/Ojo Alamo aquifer with anomalously light isotopic signatures by Phillips et al. (1989) exhibited corrected carbon-14 ages ranging from 7,000 to 35,000 YBP. Therefore, while the corrected ages for AR-0213 and AR-0214 may be significantly younger than apparent ages, they are obviously still much older than all other water samples, which have apparent carbon-14 ranging from 910 to 2,830 YBP. With the observed high tritium content and apparent carbon-14 dates for all shallow groundwater samples analyzed for carbon-14, mixing of modern fresh water with a small amount of high total dissolved solids older water appears to be a very common process in this aquifer.

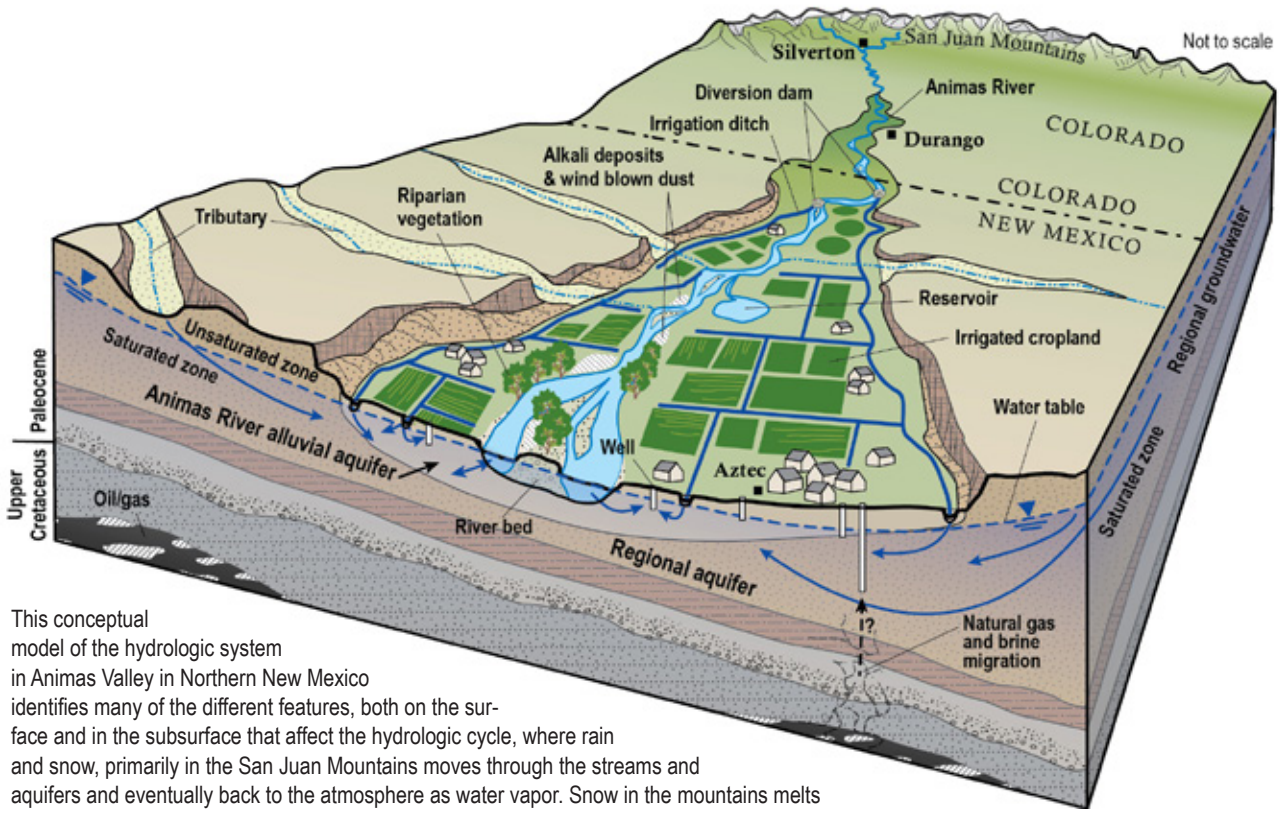

This conceptual model of the hydrologic system in Animas Valley in Northern New Mexico identifies many of the different features, both on the surface and in the subsurface that affect the hydrologic cycle, where rain and snow, primarily in the San Juan Mountains moves through the streams and aquifers and eventually back to the atmosphere as water vapor. Snow in the mountains melts in the late spring, filling the mountains streams with fresh water that feeds the Animas River in Colorado and flows through northeastern New Mexico. Water in the river is used as drinking water for local communities for local industry, and farmers use it to irrigate their crops. Irrigation water that is not used by vegetation infiltrates into the subsurface to recharge the shallow aquifer that is made up of gravel, sand, silt, and clay sediments. Some snow and rain from the San Juan Mountains that is thousands of years old also contributes to the shallow groundwater by flowing upwards from the bedrock aquifer that lies below the alluvium. Other recharge sources to the shallow groundwater include local precipitation and water in ephemeral streams and tributaries to the Animas River, and in some areas, water from the Animas infiltrates into the aquifer directly from the river. Groundwater in the shallow aquifer flows southwest (down stream) and toward the river and ultimately discharges into the river. Along its flow path, groundwater is intercepted by wells that produce water for irrigation and domestic use and by riparian vegetation. Water in the Animas feeds the San Juan River near Farmington, New Mexico, which flows into Lake Powell in Utah.

IV. DISCUSSION

Hydrogeologic Conceptual Model

Recharge

Groundwater recharge is the process by which water moves from the surface into an aquifer. The two primary recharge sources to the shallow alluvial aquifer adjacent to the Animas River in New Mexico are: 1) river water via irrigation, and 2) regional groundwater recharge from the surrounding upland bedrock geology, and ultimately the San Juan Mountains to the north. Evidence for these two recharge sources is presented below.

Irrigation water—There several lines of evidence that irrigation to agricultural fields is the primary source of groundwater recharge. Irrigation season typically begins in March and ends in October. During this time period, river water is diverted to a canal system that transports water to agricultural fields throughout the valley. Water levels in over 50% of the wells that were measured show a clear correlation with irrigation season, where water levels increase beginning in March or April and continue to increase throughout most of the summer and then begin to decrease in October or November when the irrigation diversions are discontinued (Figure 14).

Continuous measurements of water levels and specific conductance in some wells (Figure 20) not only show an increase in the water level at the beginning of irrigation season, but a decrease in specific conductance, which indicates the input of river water which generally exhibits significantly lower specific conductance values than that of groundwater. As discussed above, observed increases in dissolved oxygen with coincident decreases in total dissolved solids indicate the input of river water in many wells. While there may be some river water moving directly from the river into the groundwater system, irrigation return flow is the dominant process by which river water recharges the shallow aquifer.

Water chemistry supports the identification of the fresh water mixing endmember as ultimately being river water. Water chemistry for river water sampled by the U.S. Geological Survey in 2016 (Blake et al., 2017) is shown on a Piper diagram and the sulfate mixing curve in Figure 50 and Figure 51, respectively. On the anion ternary diagram, river water plots along the linear trend observed for groundwater towards the fresh calcium-bicarbonate endmember but does not exhibit the highest relative bicarbonate concentrations. Likewise, in Figure 51, river samples plot near the mixing line close to the fresh water endmember but some groundwater shows smaller relative sulfate concentrations. The general chemistry for river water likely shows significant variability seasonably and from year to year due to variations in the relative proportions of groundwater discharge, annual snowmelt, or monsoon rains that may contribute to the total river discharge.

Irrigation practices all along the Animas River from Durango to Farmington likely account for most groundwater recharge to the shallow alluvial aquifer. Robson and Wright (1995) concluded that irrigation water is the largest source of recharge in La Plata County, Colorado, along the Animas and Florida Rivers, just south of Durango. As will be discussed

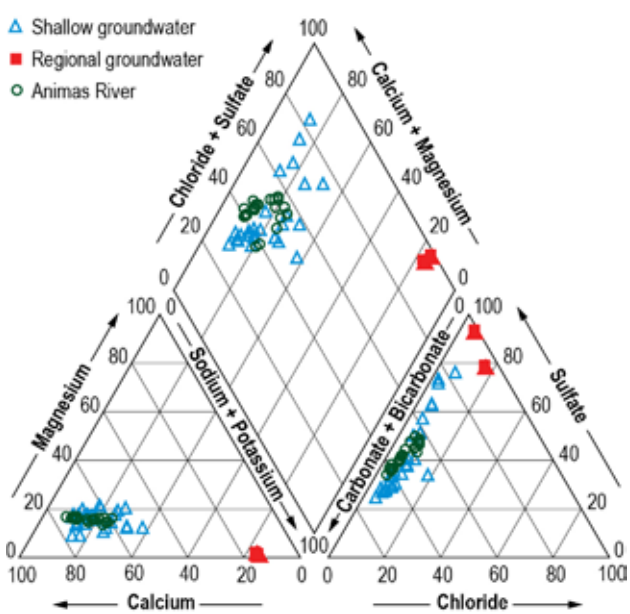

Figure 50. Piper diagram shows chemistry data for average groundwater compositions along with Animas River samples collected by the U.S. Geological Survey in 2016 (Blake et al., 2017).

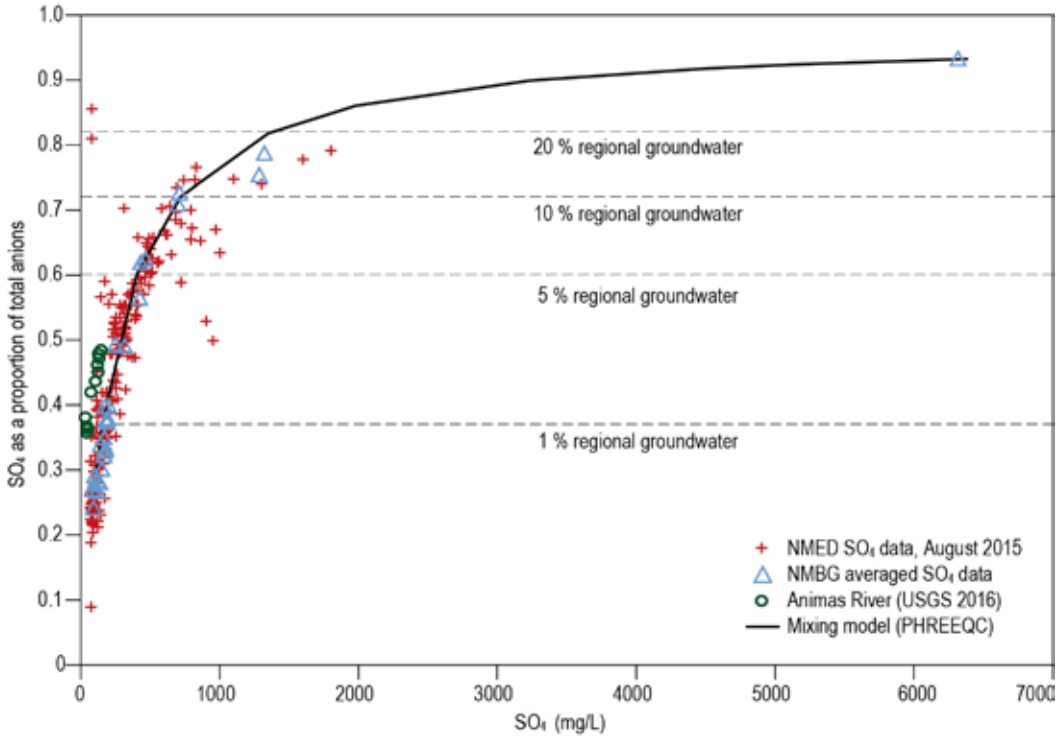

Figure 51. Shallow groundwater samples collected by the U.S. Environmental Protection Agency and New Mexico Environment Department in August 2015 and Animas River samples collected by the U.S. Geological Survey in 2016 plot of modeled mixing curve.

below, groundwater in the shallow aquifer flows mostly from northeast to southwest and toward the river. Groundwater that discharges to the river all along the Animas is a mixture of river water from the current or previous irrigation season and river water from past irrigation seasons. At any given time, river water therefore contains some proportion of irrigation return flow that includes irrigation water from past irrigation seasons. River water exhibits the freshest water with the smallest proportion of irrigation return flow during the spring runoff when the river stage is high due to snowmelt from the high San Juan Mountains making its way to the Animas River via mountain streams. This trend can be seen in the specific conductance measurements for river water shown in Table 5.

Groundwater recharge of irrigation water likely occurs along many of the irrigation canals and ditches and in agricultural fields, where this water is applied to water crops. Irrigation water infiltrates through the soil and reaches the water table fairly quickly, increasing groundwater almost immediately after irrigation season begins.

Regional groundwater recharge—The mixing curve shown in Figure 51 includes data for over 100 groundwater samples collected by the U.S. Environmental Protection Agency and New Mexico Environment Department during August 2015 immediately after the Gold King Mine spill. This mixing model fits the data remarkably well and can explain the major ion distribution for almost all shallow groundwater in the entire study area. An increase in the relative sulfate concentration indicates an increase in the mixing proportion of older regional groundwater from the Nacimiento/Ojo Alamo aquifer. Recharge to the Nacimiento/San Jose/Animas Formation aquifers primarily occurs at the edge of the San Juan Basin near Durango, CO (Figure 52). It takes groundwater thousands of years to flow along deep flow paths from this recharge area to where it was sampled near Farmington. Spatial trends observed for several constituents, including sulfate and total dissolved solids (Figure 25), suggest that the relative contribution of this regional groundwater increases to the southwest (downstream). Figure 52 shows that average relative sulfate concentrations are fairly constant between the state border and Aztec. South of Aztec, where we see most sulfate concentrations increase significantly is coincident with the beginning of the gradual thinning of the Nacimiento and Ojo Alamo Formations due to the structure of the San Juan Basin. These sandstones are underlain by the Kirtland Shale, which is an aquitard. Therefore as the Nacimiento/Ojo Alamo aquifer thins, water along these deep flow paths are forced up into the shallow groundwater system. Most shallow

groundwater sampled in the study area is comprised of less than 5% regional groundwater. Although some wells produced water with up to 20% regional groundwater (Figure 51).

Other recharge sources—Minor local recharge does occur, but its contribution is relatively small compared to the river water and regional components. Local recharge includes the infiltration of precipitation through unconsolidated sediments in the Animas Valley and focused recharge through the bottoms of arroyos and ephemeral tributaries to the Animas during flash floods.

Groundwater flow directions

The general groundwater flow direction, as shown by the water table contour map (Figure 10), is toward the river. Groundwater flows down gradient, perpendicular to water table contours. The overall shape of the water table contours in the valley form a 'V' pointing upstream. This indicates groundwater from the surrounding alluvial aquifer flows toward the river, resulting in what appears to be a typical gaining stream. However, by looking at the water levels in close proximity to the river, we found that the water table gradient is nearly flat in close proximity to the river. We observed that the water levels in some wells near the river during the winter and spring are below river elevation (wells highlighted in red in Figure 10). This suggests that the river could add water to the groundwater (a losing river). By examining a losing reach and refining the water table contours, we can better understand the groundwater flow direction and magnitude during periods of the year where the river is losing water to the alluvial aquifer by preforming Darcy flow calculations.

Darcy flow calculations—To estimate the distance from the river that wells may be impacted directly by water infiltrating from the river, we focused on a small portion of the water table map that appears to exhibit losing conditions. For this analysis we zoom in on AR-0059 and AR-0060, located 1.5 miles northeast of Aztec, on the west side of the river. From this analysis we can calculate radius of impact that

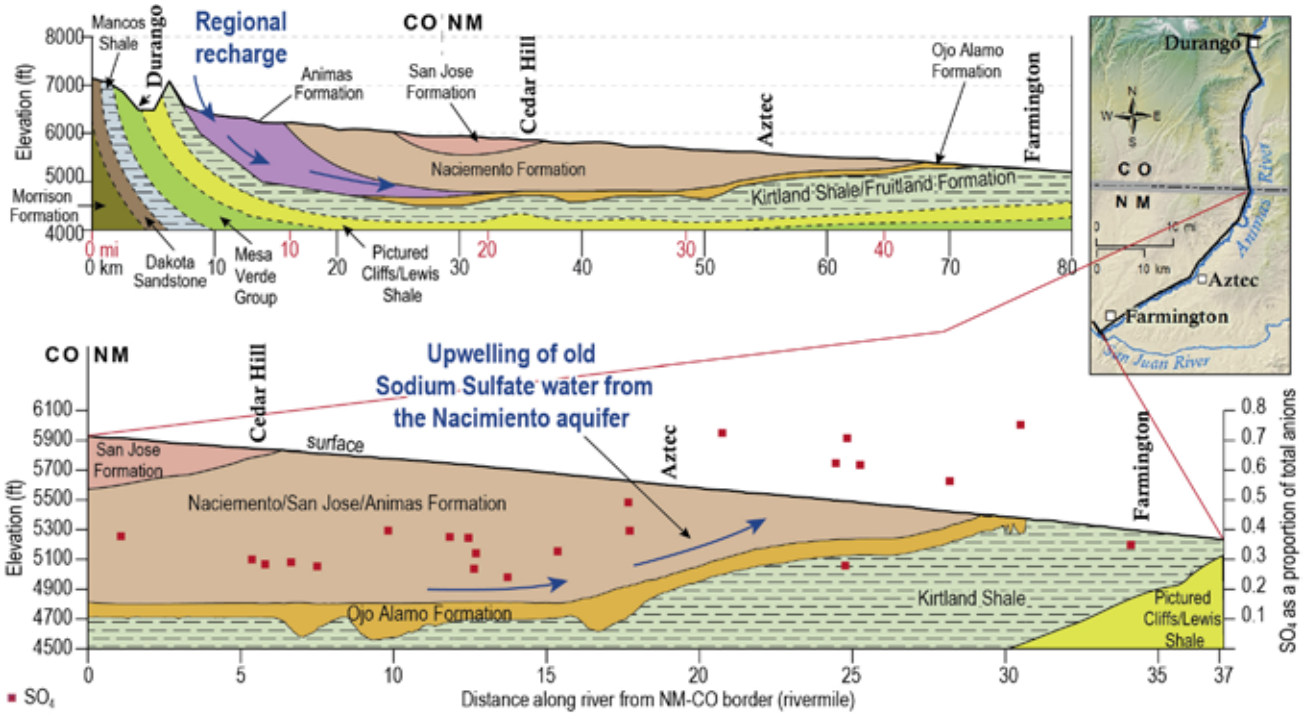

Figure 52. Schematic regional cross sections showing groundwater flowpaths in regional bedrock. Regional groundwater recharge to the Nacimiento/Ojo Alamo/San Jose aquifer occurs in the San Juan Mountains near Durango, at the northern edge of the San Juan Basin. Increased sulfate and total dissolved solids concentrations in shallow groundwater south of Aztec are due to the upwelling of old sodium-sulfate regional groundwater from the Nacimiento/Ojo Alamo aquifer as a result of the structure of the San Juan Basin. The thinning of this deeper aquifer forces regional groundwater into the shallow alluvial aquifer (which overlies the bedrock, but is not shown on this image). It should be noted that the horizontal distances shown on the NM cross-section (bottom) are river miles, resulting in a larger relative distance than is shown in the larger-scale cross-section (top). Red points refer to sulfate concentrations as a function, of the total anions, referring to the right axis on lower image.

seasonal fluctuations of the river and the water table can have on alluvial aquifer. Based on LiDAR modeling of the river stage, combined with U.S. Geological Survey gauging stations, we modeled the river stage in the Animas River during the groundwater level measurement periods. Using the modeled river stage and the measured groundwater level elevations we were able draw fine scale water table contours and calculate the water table gradient. With this a gradient and an estimate of hydraulic conductivity we can perform Darcy flow calculations to estimate to what extent surface water could infiltrate into the alluvial aquifer (Figure 53). Darcy flow (equation 1) is an equation used to estimate groundwater flow rates:

$$q = \frac{\Delta h}{\Delta s} \cdot k \qquad (1)$$

where q is specific discharge (volumetric flow rate per unit cross-sectional area, ft/day), $\frac{\Delta h}{\Delta s}$ is the hydraulic gradient (change in water level between the river and the well, Δh over the distance along the flow path, Δs), and k is the hydraulic conductivity. For this calculation, we assumed a hydraulic conductivity of 100 ft/day, which is a typical value for clean sand (Freeze and Cherry, 1979). We estimated that the specific discharge from the river in January was approximately 0.6 ft/day. To determine the velocity that water flows, the specific discharge (q) is divided by the porosity, which as assumed to be 0.3. In the given example, the groundwater velocity away from the river during the winter is roughly 2 feet per day. Water levels in wells near the river appear to be losing primarily during the non-irrigation season (~9 weeks). At most, the river water can flow roughly 130 feet along its flow path from the river before the gradient reverses, switching to a gaining river during the irrigation season, and groundwater begins to flow back toward the river. This is a rough approximation of the area around the river that may potentially be directly impacted by river water. Pumping from wells near the river during the winter has the potential to extend the zone of impact.

At the time of the GKM spill, gradients were reversed and the river was gaining, or neutral. During the winter, however, when the groundwater gradient from the river is negative, or losing, water from the river likely enters the aquifer system. As this water infiltrates into the aquifer it passes through the streambed, where mine waste was potentially deposited after the spill.

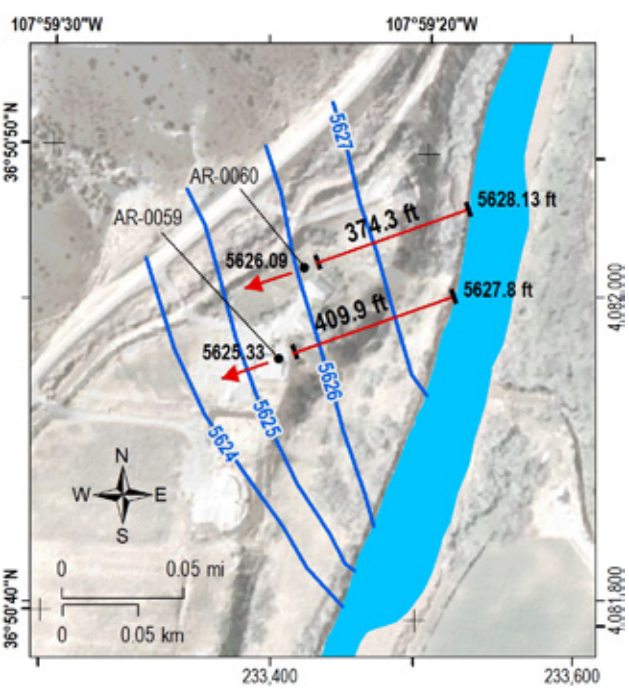

Figure 53. View of a losing reach in January 2016 located 1.5 miles northeast of Aztec. This map is used to determine the gradient and direction of groundwater flow for the calculation of the Darcy flow.

Analysis of U.S. Geological Survey stream discharge data—To estimate the degree to which the Animas River is a gaining river we used the U.S. Geological Survey flow gauges located in the study area to estimate the amount of water that diffusely discharges along the stream bed. There are three U.S. Geological Survey stream gauges along the Animas River in the study area. The Farmington gauge (09364500) is located roughly 1.5 miles upstream of the confluence with the San Juan River. The Aztec gauge (09364010) is located 1.8 miles downstream of the Highway 516 Bridge in Aztec, NM. The Cedar Hill gauge (09363500) is located in Colorado, 2.7 miles north of the state line. Using stream flow data recorded at these locations dating back over the past 27 years, we compared stream flow between the gauges.

To best understand the degree to which the river is gaining we looked at the difference in flow between the gauges during the winter, when the irrigation ditches were dry. Using the irrigation ditch flow records reported by the NM Office of the State Engineer (meas.ose.state.nm.us), we found that all of the ditches along this reach are shut off by the second week of November, and are not flowing again until early March. The daily average flow difference between each pair of gauges was found first. The average flow difference between gauges over the past 27 years was then averaged based on its given

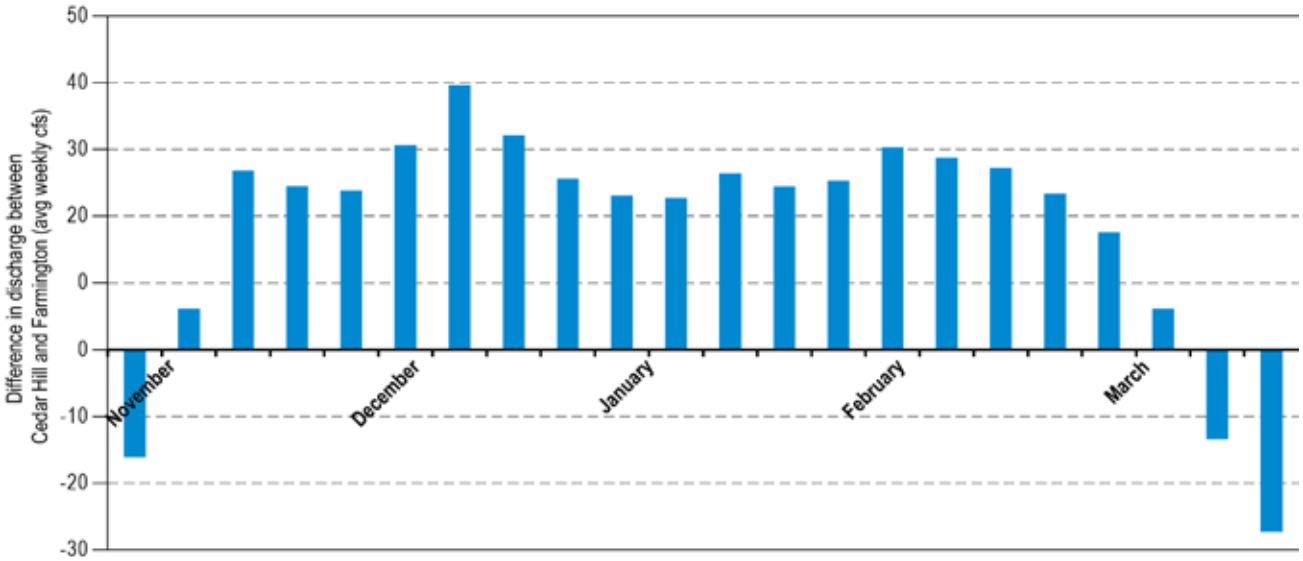

Figure 54. Difference in discharge (cfs) measured between Cedar Hill and Farmington during non-irrigation season. Positive values represent a gaining river, and negative values indicate losing conditions.

week (1–52) to understand the annual fluctuations (Figure 54). In the north, between the Cedar Hill and Aztec gauges (during the winter/non-irrigation period) the river was gaining on average 0.85 cubic feet per second per mile. In the south, between the Aztec and Farmington gauges the river was gaining 0.99 cubic feet per second per mile. This supports the water table maps and the assumption that the Animas River between the Colorado boarder and Farmington is a gaining reach. Additionally, the northern reach, between Cedar Hill and Aztec, where we identified zones that were more susceptible to losing conditions, showed slightly less gaining conditions than the southern reach. In total, during winter months, the Animas River gains, on average, 27 cfs as it flows through the study area. This represents a 10% increase in flow to the river supported by groundwater flow during winter months.

Groundwater/surface water interactions

While it is clear the majority of river water that recharges the shallow aquifer is irrigation water, there is evidence of river water infiltrating directly from the river to the aquifer. As discussed above, we have identified a few localized areas where hydraulic gradients between the water table and the river stage indicate losing conditions at some times (Figure 10 and Figure 11). Figure 19 shows continuous water level and specific conductance data for AR-0075, which is less than 10 feet from the river. This well exhibits a river-stage-controlled type hydrograph and shows a decrease in specific conductance that correlates with high river stages associated with spring runoff, beginning in March 2017. This indicates that this low specific conductance water is likely coming directly from the river.

Water level fluctuations in river-stage-controlled type wells as determined by hydrograph characteristics (Figure 13) are highly correlated with river stage. However, this correlation does not conclusively indicate the actual input of river water into the aquifer in these areas, which occur all along the Animas River. The water level fluctuations that correlate to river stage may be due to a pressure response where the groundwater levels increase or decrease to maintain a relatively constant hydraulic gradient with respect to the river.

We examined dissolved oxygen ranges for both river-stage-controlled and irrigation-controlled type wells to assess the mechanism that controlled groundwater level fluctuations (Figure 55). As discussed above, wells that exhibit a high range in dissolved oxygen concentrations over time represent a dynamic system and is the result of frequent events where oxygenated river water mixes with water in the aquifer in that area. For the river-stage-controlled type, and mixed dissolved oxygen wells, we observe a high dissolved oxygen range for wells within 300 feet of the river with the dissolved oxygen range decreasing with increased distance from the river. This trend suggests that for those wells, the observed water level increases were likely due to the actual input of river water and not a pressure response. For

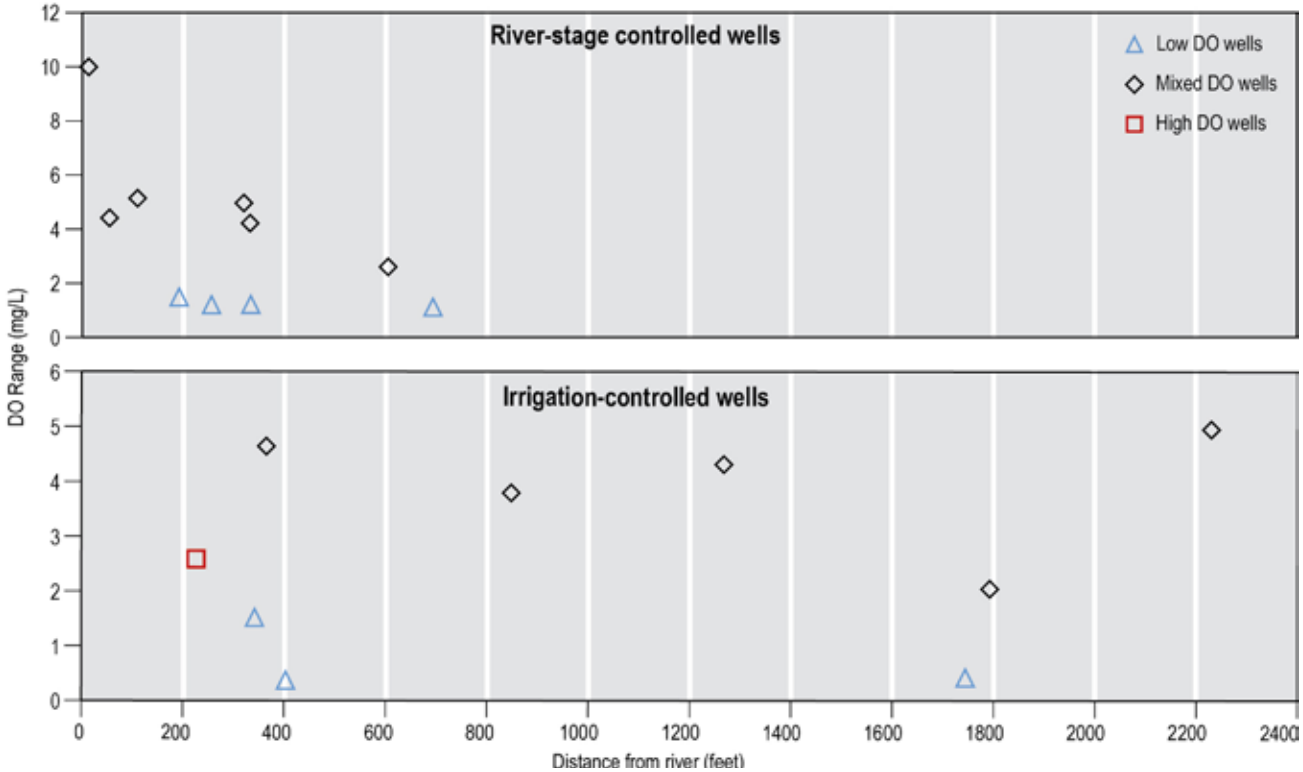

Figure 55. Observed range in dissolved oxygen concentrations as a function of distance from the river for river-stage-controlled and irrigation-controlled wells as determined by hydrograph characteristics.

the low dissolved oxygen wells, dissolved oxygen ranges were small and independent of their distance from the river, indicating that water level fluctuations in these wells are likely due to a pressure response rather than the input of river water. For irrigation controlled type wells, which are observed to be at much farther distances from the river than river-stage-controlled type wells, mixed dissolved oxygen wells show relatively high dissolved oxygen ranges with no correlation with distance from the river. This is expected because irrigation is the active application of water to ditches and fields, and the distance from the river is not a controlling factor in this process. For the river-stage-controlled type wells, the movement of water from the river to the aquifer depends on the hydraulic gradient, which is a function of distance from the river, and the hydraulic conductivity. These observations suggest that although groundwater levels are usually higher than river stage, river water does infiltrate directly into the aquifer in some areas at some times. According to the Darcy flow calculations discussed above and the data presented in Figure 55, wells in close proximity (< 300 feet) of the river are at risk of pumping water that has infiltrated into the aquifer directly from the river.

Potential Groundwater Contamination

Long before mining occurred in the headwaters of the Animas River, fractures and faults, caused by a collapsed caldera, served as conduits for warm mineral rich waters. Mining in the headwaters of the Animas River began in the 1860s when prospectors found rich ore deposits in the mountains surrounding Silverton, CO. Even before mining began, the springs emerging from the upper reaches of the Animas exhibited signs of acid drainage, as observed by 9,000 year old radiocarbon dates on ferricrete deposits in the Cement Creek drainage (Yager et al., 2016). Mining in the mountains served to greatly enhance the exposed surface area of the rocks in the mountains, allowing for more rapid oxidation and release of the minerals. The mine-waste rock piles that were deposited at the mouth of the mines consist of crushed rock that also serves as a source from which minerals are leached.

After mining in the area ended, steps were taken to reduce the concentrations of leachate that drains from the abandoned mines. Bulkheads were installed at the entrance to several of the larger mines and tunnels, leading the mines to fill with groundwater. By

flooding the mine works, the exposed rock surfaces of the mines are no longer able to oxidize as readily, reducing the acid concentration of the leachate.

The spill that occurred in August 2015 resulted from an earthen barrier in the Level 7 adit of the Gold King Mine being inadvertently breached. The water in the mine rapidly drained. The torrent of water that escaped as a result of the breach quickly eroded the waste rock pile outside of the mine. As result, roughly 490,000 kg (540 tons) of sediment was released during the Gold King Mine spill (U.S. Environmental Protection Agency, 2016). The sediment associated with the spill was differentiated from the existing background contamination by the elevated lead to aluminum ratio (Pb:Al). This signature is an indication of the spill, but not the Gold King Mine.

Downstream, in New Mexico, irrigation ditch operators reacted quickly and, to the extent possible, the irrigation network was closed during the spill, preventing the sediment and mine water from entering the ditches. As has been demonstrated, the irrigation network is responsible for a significant portion of the recharge that enters the alluvial aquifer. Following the initial plume from Gold King Mine, the irrigation ditches were reopened. During the initial spill, the U.S. Environmental Protection Agency estimates that only 10% of the sediment load was transported past Farmington, depositing roughly 432,000 kg (476 tons) of sediment in the Animas River (U.S. Environmental Protection Agency, 2016).

The U.S. Environmental Protection Agency reports that the sediment deposited during the spill did not remain stationary. The first major transport of sediment occurred during a fall storm that resulted in sufficient discharge to mobilize some of the sediments. The majority of the sediments, however, were transported the following year during the spring runoff floods due to the snow melting in the San Juan Mountains, which began in mid-May and continued through June (U.S. Environmental Protection Agency, 2016). As the irrigation ditches were open during both of these secondary transport events, it is possible that some Gold King Mine sediments were transported into the ditches.

While the Gold King Mine spill constituted a significant ecological disaster, it was by no means the largest mine spill in the Animas River (Church et al., 2007). In fact, it is estimated that the 48 historic mines/ mine–related sources in the headwaters of the Animas River discharge roughly 5.4 million gallons of acid mine drainage per day (U.S. Environmental Protection Agency, 2016).

Dissolved and colloidal metals—Manganese and iron are the only two dissolved metals in the shallow groundwater that we observed at concentrations that exceed U.S. Environmental Protection Agency secondary maximum contaminant levels. As discussed above, these high iron and manganese concentrations appear to be associated with low Eh values (Figure 41 and Figure 45). Although the primary recharge source, which is river water via irrigation, is well oxygenated, the measured Eh values and the presence of dissolved manganese in most wells indicates that the oxygen is consumed quickly, resulting in manganese oxides and iron hydroxides being the main redox buffers.

It is difficult to determine the source of the iron and manganese. Water in the Animas River has been observed with high iron and manganese total concentrations (most is likely adsorbed onto colloids and other particulates) (Blake et al., 2017), and these metals could originate from the headwaters and tributaries, such as Cement Creek and Mineral Creek (Church et al., 2007). However, they are also present in the aquifer sediments. The alluvial aquifer was derived from the erosion of Ojo Alamo and Nacimiento Formations that outcrop adjacent to the Animas Valley at higher elevations. These formations are made up of mostly fluvial sediments, and both iron and manganese are ubiquitous in these types of environments. Therefore, the spatial distribution of these high iron and manganese waters may be controlled by the location where these minerals were concentrated when deposited, both within the alluvial sediments and sediments deposited in the irrigation ditches and canals during irrigation season.

We must also consider the spatial distribution of reductants, such as organic matter, septic tank contamination, and quite possibly hydrocarbons, such as gas and oil. Of all wells sampled in the shallow aquifer, AR-0075 exhibits some of the lowest Eh values, ranging from 86 to 136 millivolts and contains the highest concentrations of iron and manganese by far, averaging 2.3 and 4.5 mg/L, respectively. Relatively high barium and chloride concentrations (Figure 37 and Figure 39) were also observed in the water produced by this well. These characteristics may suggest that the hypothesized third mixing endmember discussed above is a brine that may be associated with oil or gas in underlying geologic units.

The hypothesized third mixing endmember is likely characterized by high chloride and low sulfate concentrations so that small additions of this brine to the shallow aquifer will significantly increase chloride concentrations without affecting the sulfate

content, which is controlled by the addition high sulfate groundwater from the Nacimiento Formation. The mixing model described above predicts significantly lower barium and strontium concentrations than were observed, suggesting the third mixing component is relatively high in barium and strontium. Some brines associated with gas wells in Pennsylvania have been observed with high chloride, barium, and strontium and low sulfate concentrations (Dresel and Rose, 2010). Kelley et al. (2014) reviewed water chemistry data from the U.S. Geological Survey online produced waters database, and reported high total dissolved solids sodium-chloride type produced water in Cretaceous rocks such as the Pictured Cliffs and Cliff House Sandstones in the San Juan Basin.

Chafin (1994) found methane at concentrations that exceeded the reporting limit of 0.005 mg/L in 70 of 205 groundwater samples in the Animas River Valley in Colorado and New Mexico. Potential sources of dissolved methane included some biogenic gas from the Animas and Nacimiento Formations but mostly thermogenic gas from deep reservoirs such as the Dakota Sandstone and the Mesaverde Group. The upper Fruitland Formation and Kirtland Shale could also account for some of this observed methane in groundwater. Chafin (1994) concluded that natural leakage through fractures was possible, but manmade conduits probably account for most upward movement of gas to the shallow aquifer. It is likely that any hydrocarbons that may be leaking into the shallow system are accompanied by brines from the same geologic unit(s).

The biodegradation of petroleum hydrocarbons in groundwater often results in reducing conditions that can cause manganese and iron to dissolve from aquifer sediments (Klinchuch and Delfino (2000). Therefore, in areas with groundwater containing high manganese and iron content, the biodegradation of hydrocarbons from gas and oil sources in the area may be driving Eh values down resulting in the increased dissolution of manganese and iron. Well AR-0075 may be an extreme example of mechanisms that possibly play a role in controlling the spatial variability of redox conditions in the shallow aquifer and should be studied in more detail.

Dissolved aluminum was observed in several water samples. Excluding AR-0214, which had the highest concentration (0.161), aluminum concentrations ranged from 0.0005 to 0.0058 mg/L, and in 50% of water samples, concentrations were below the reporting limit of 0.0005 mg/L. Total dissolved aluminum was observed in most water samples, indicating the presence of aluminum that is adsorbed on colloids or other particulates in the water sample. A likely source for this colloidal aluminum is sediments and colloids from the Animas river, which may have originated from mines in the headwaters near Silverton, Colorado and possibly the Gold King Mine spill. Fortunately, aluminum is relatively insoluble in the alluvial aquifer due to pH values being near neutral. However, small changes in pH can result in higher dissolved aluminum concentrations in groundwater.

V. CONCLUSIONS

After the August 5, 2015 Gold King Mine released metal and sludge-laden water into Cement Creek and the Animas River, the New Mexico Bureau of Geology and Mineral Resources undertook a hydrologic assessment of the Animas River and its nearby alluvial aquifer in New Mexico, from the Colorado state line to Farmington, New Mexico. The purpose of this project was to evaluate possible effects from the mine release on the shallow groundwater near the Animas River in New Mexico. Analysis of water level and geochemical data collected between January 2016 and June 2017 have greatly improved our understanding of the hydrogeologic system in the Animas River Valley, including the identification of recharge sources, groundwater flow paths, groundwater/surface water interactions, and mechanisms by which potential contaminants may be mobilized in the shallow aquifer system.

The primary recharge source is river water via irrigation, where water infiltrates through the bottoms of irrigation ditches and canals and through soils in agricultural fields to the water table, which is usually less than 20 feet below the surface. This is an important consideration with regard to the Gold King Mine spill and possible impacts to groundwater quality. Contaminated sediment associated with the Gold King Mine spill that was possibly deposited in irrigation ditches and canals during or after the release, can possibly result in the contamination of the shallow aquifer. U.S. Environmental Protection Agency (2017) reported that much of the sediment deposited in the Animas River by the Gold King Mine spill was mobilized by large flow events that occurred after the spill, such as the spring snow melt flood in 2016. As irrigation water infiltrates through these sediments, metals such as iron, manganese and aluminum may be mobilized and transported to the shallow water table. So far, the groundwater quality does not appear to have been impacted through this recharge mechanism. However, continued monitoring of groundwater quality is recommended. Groundwater in the alluvial aquifer is estimated to be, on average, less than 10 years old and is a mixture of very young water derived from recent spring runoff in the San Juan Mountains and older irrigation recharge from past irrigation seasons. Therefore it may be several years before an impact to water quality in the shallow aquifer can be observed.

An important process that affects groundwater quality in the shallow aquifer is the input of regional groundwater that flows upward from the Nacimiento and Ojo Alamo Formations that underlie the alluvium. Most recharge to these deeper bedrock aquifers occurs at the edge of the San Juan Basin in the San Juan Mountains around Durango. This water was determined to be thousands of years old and is observed in small proportions in almost all of the groundwater that was sampled in the Animas River alluvial aquifer. Groundwater south of Aztec was observed to have a larger proportion of this regional component (up to 15% of the total water mixture) due to the thinning of the Nacimiento and Ojo Alamo Formations (Figure 52), which pinch out near Farmington due the structure of the San Juan Basin. This mixing process significantly affects the sulfate and total dissolved solids concentrations, which are observed to be higher south of Aztec (Figure 25).

While groundwater levels are usually above the river stage, wells that are in close proximity to the river (less than 300 feet) have a risk of pulling in river water into the aquifer, especially in areas where we occasionally observe a reversal of the hydraulic gradient between the groundwater and river. These gradient reversals were observed to occur north of Aztec around Cedar Hill and Inca, especially during the winter months. The implications related to the Gold King Mine spill, which occurred in August, is that these locations were likely still moving water toward the river, as gaining reaches, because the winter gradient reversal had not begun. To avoid possible future contamination to groundwater, we recommend that residents with wells within 300 feet of the river should avoid pumping during turbid surface water conditions such as monsoon storm events, or in the event of another spill similar to the Gold King Mine spill.

The input of irrigation water, which usually has high dissolved oxygen content, results in an observable increase in groundwater dissolved oxygen, which decreases fairly quickly due to mixing with groundwater that is depleted in dissolved oxygen and the

oxidation of organic matter by respiration. Manganese and iron, which are present at concentrations that exceed U.S. Environmental Protection Agency secondary maximum contaminant levels in some areas within the study area, appear to be the primary redox buffers that keep the Eh above zero millivolts. However, in areas where Eh drops below 200 millivolts, iron and manganese concentrations increase significantly. Dissolved iron and manganese in groundwater is from the dissolution of manganese oxides and iron (hydr) oxides that occurs naturally in the sediments of the aquifer. Iron and manganese may also come from river sediments that are deposited in irrigation ditches and canals from irrigation diversions from the river. Irrigation managers may want to consider limiting diversions during high river flows that are likely moving large amounts of sediments, such as storm events, and spring runoff floods.

VI. FUTURE WORK

Future work should include groundwater quality monitoring and sediment analysis in irrigation ditches. Continued monitoring of groundwater quality is necessary to assess possible impacts to groundwater quality from the Gold King Mine spill. Monitoring efforts should focus on shallow wells in close proximity and down gradient from irrigation ditches and canals and should include continuous measurements of water level, temperature, dissolved oxygen, and specific conductance and semi-annual sampling for general chemistry and trace metals. Results of this study provide information that can be used to help future monitoring efforts. For example, abrupt changes in continuous measurements of temperature, specific conductance, and water level associated with the commencement of flow in a nearby ditch would indicate that groundwater recharge is occurring near that location, likely as seepage through the bottom of the ditch. This information should be used to identify: 1) sampling wells that are most likely to provide pertinent information to help identify groundwater quality impacts from the Gold King Mine spill, and 2) specific ditches and canals that should be studied to assess the presence of contaminated sediment that may be associated with the Gold King Mine spill. Characterization of sediments associated with the Gold King Mine spill by U.S. Environmental Protection Agency (2017) should help to identify these sediments in irrigation waterways.

Water chemistry data from semi-annual sampling of wells should be used to better understand redox chemistry in the shallow aquifer by identifying and confirming specific dominant redox pairs and reactions, such as MnO_2/Mn^{2+} and $Fe(OH)_3/Fe^{2+}$. Future work should also focus on identifying manganese and iron sources in groundwater throughout the study area, with the specific goal of differentiating in-place sources in the aquifer sediments from sources originating from river sediments that were mobilized and deposited in irrigation ditches. It is also recommended to assess the spatial distribution of reductants such as organic matter, septic waste, and hydrocarbons. Groundwater analyses for dissolved organic carbon, carbon isotopes, methane and other hydrocarbons would be useful for these purposes.

Water is flowing out of the Red and Bonita Mine over orange stained waste rock piles. These waters contribute to Cement Creek, which flows into the Animas River near Silverton, Colorado.

ACKNOWLEDGMENTS

This project is successful only because of the generosity and gracious cooperation of well and land owners along the Animas Valley who allow us to access their wells to collect these essential data.

As the authors, we thank our colleagues and collaborators at the New Mexico Environment Department including Dennis McQuillan and Diane Agnew for feedback and support on this project. We would like to thank Dr. Patrick Longmire at the New Mexico Environment Department for taking time to meet with us and helping review the geochemistry data. We also kindly thank the USGS New Mexico Water Science Center staff contributions for assistance in water level measurements in August 2015, including Jesse Driscoll, Lauren Sherson, Nicole Thomas, and Amy Gallanter. During the August 2015 water level measurements, we had cooperation and assistance also from the New Mexico Office of the State Engineer's Office staff, particularly Doug Rappuhn, Rob Pine and Shawn Williams. We also thank Miriam Wamsley formerly with the New Mexico Department of Health for her help on water quality concerns related to private domestic wells.

We wish to acknowledge staff of the New Mexico Bureau of Geology and Mineral Resources who helped on this project including Scott Christenson (field data collection), Trevor Kludt (field data collection), Cathryn Pokorny (data management), Brigitte Felix (mapping and graphic support), Kylian Robinson (student, field data collection), Sara Chudnoff (field data collection), Mark Mansell (GIS work on geologic map), and Bonnie Frey and Dustin Baca (chemistry lab analysis).

Finally, we thank Dr. Geoffrey Rawling and Scott Christenson from the New Mexico Bureau of Geology and Mineral Resources for their reviews and constructive feedback that improved this report.

REFERENCES

Blake, J.M., Timmons, S.S., Bexfield, L. Brown, J., Newton, B.T., and Mamer, E., 2017 Surface-Water Groundwater Quality in Northwestern New Mexico after the Gold King Mine Release: Society for Mining, Metallurgy & Exploration Inc. Annual Conference and Expo, Denver, Colorado, February 20, 2017.

Craig, H., 1961, Isotopic variations in meteoric waters, Science, 133, 1702–1703.

International Atomic Energy Agency. 2010. WISER database. http://nds121.iaea.org/wiser/index.php (accessed August 16, 2010).

International Atomic Energy Agency. 2010. WISER database. http://nds121.iaea.org/wiser/index.php (accessed August 16, 2010).

Chafin, D.T., 1994, Sources and Migration Pathways of Natural Gas in Near-Surface Ground Water Beneath the Animas River Valley, Colorado and New Mexico.

Craigg, S.D., 2001, Geologic framework of the San Juan structural basin of New Mexico, Colorado, Arizona, and Utah, with emphasis on Triassic through Tertiary rocks: U.S. Geological Survey Professional Paper 1420, 70 pp.

Church, S.E., Kimball, B.A., Frey, D.L., Ferderer, D.A., Yager, T.J., and Vaughn, R.B, 1997, Source, transport, and partitioning of metals between water, colloids, and bed sediments of the Animas River, Colorado: U.S. Geological Survey, Open-File Report 97-0151, http://pubs.usgs.gov/of/1997/ofr-97-0151/index.shtml

Church, S.E., von Guerard, Paul, and Finger, S.E., eds., 2007, Integrated investigations of environmental effects of historical mining in the Animas River watershed, San Juan County, Colorado: U.S. Geological Survey Professional Paper 1651, 1,096 p. plus CD-ROM. [In two volumes.]

Church, S.E., Owen, J.R., von Guerard, P., Verplanck, P.L., Kimball, B.A., and Yager, D.B., 2007, The effects of acidic mine drainage from historical mines in the Animas River watershed, San Juan County, Colorado—What is being done and what can be done to improve water quality?; *in* DeGraff, J.V., ed., Understanding and Responding to Hazardous Substances at Mine Sites in the Western United States: Geological Society of America Reviews in Engineering Geology, v. XVII, p. 47–83, doi: 10.1130/2007.4017(04)

Cunningham, W.L., and Schalk, C.W., 2011, Groundwater technical procedures of the U.S. Geological Survey: U.S. Geological Survey Techniques and Methods 1–A1, 151 p.

Drever, J.I., 1982, The Geochemistry of Natural Waters: Prentice Hall, New Jersey, 436 p.

Dresel, P.E., and Rose, A.W., 2010, Chemistry and Origin of Oil and Gas Well Brines in Western Pennsylvania: Pennsylvania.

Eastoe, C.J., Watts, C.J., Ploughe, M., and Wright, W.E., 2011, Future Use of Tritium in Mapping Pre-Bomb Groundwater Volumes: Groundwater, v. 50, no. 1, p. 870–093.

Freeze, R.A., and Cherry, J.A., 1979, Groundwater: Prentice Hall, Inc., New Jersey, 604 p.

IAEA/WMO, 2017. Global Network of Isotopes in Precipitation, The GNIP Database, Accessible at: http://www.iaea.org/water

Kelley, S., Engler, T., Cather, M., Pokorny, C., Yang, C, Mamer, E., Hoffman, G., Wilch, J., Johnson, P., and Zeigler, K., 2014, Hydrologic Assessment of Oil and Gas Resources Development of the Mnacos Sale in the San Juan Basin, New Mexico: NM Bureau of Geology and Mineral Resources Open-File Report 566, 64 p., https://geoinfo.nmt.edu/publications/openfile/details.cfml?Volume=566

Kenney, T.A., 2010, Levels at gaging stations: U.S. Geological Survey Techniques and Methods 3-A19, 60 p.

Klinchuch, L.A., and Delfino, T.A., 2000, Reductive Dissolution and Precipitaiton of Manganese Associated with Biodegradation of Petroleum Hydrocarbons: Environmental Geosciences, v. 7, no. 2, p. 69–79. Langmuir, D., 1997, Aquaeous Environmental Geochemistry: New Jersey, Prentice-Hall, Inc., 600p.

Langmuir, D., 1997, Aqueous Environmental Geochemistry: Prentice Hall, New Jersey, 600 p.

Newton, B.T., Rawling, G.C., Timmons, S.S., Land, L.L., Johnson, P.S., Kludt, T.J., and Timmons, J.M., 2012, Sacramento Mountains Hydrogeology Study: NM Bureau of Geology and Mineral Resources Open-File Report 543, 77p., https://geoinfo.nmt.edu/publications/openfile/details.cfml?Volume=543

Phillips, F.M., Peeters, L.A., and Tansey, M.K., 1986, Paleoclimatic Inferences from an Isotopic Investigation of Groundwater in the Central San Juan Basin, New Mexico: Quaternary Research, no. 26, p.179–193.

Phillips, F.M., Tansey, M.K., and Peeters, L.A., 1989, An Isotopic Investigation of Groundwater in the Central San Juan Basin, New Mexico: Carbon 14 Dating as a Basis for Numerical Flow Modeling, Water Resources Research, v. 25, no. 10, p. 2259–2273.

Robson, S.G., Wright, W.G., Ground-Water Resources of the Florida Mesa Area, La Plata County, Colorado: U.S. Geological Survey Water-Resources Investigations Report 95–4190, 30 p.

Stumm, W., Morgan, J.J., 1996, Aquatic Chemistry, Chemical Equilibrium and Rates in Natural Waters, 3rd edition: John Wiley & Sons, Inc., New York, 1022 p.

Timmons, S., Mamer, E., and Pokorny, C., 2016, Groundwater monitoring along the Animas River, New Mexico: Summary of groundwater hydraulics and chemistry from August 2015 to June 2016, NM Bureau of Geology and Mineral Resources, Final Technical Report, 44 p. https://geoinfo.nmt.edu/resources/water/amp/brochures/FTR_Animas_River_Sept_2016_LR.pdf

Timmons, S.S., Land, L.L., Newton, B.T., and Grey, B., 2013, Aquifer Mapping program technical document: Water sampling procedures, analysis and systematics: NM Bureau of Geology and Mineral Resources Open-File Report 558, 14p., https://geoinfo.nmt.edu/publications/openfile/details.cfml?Volume=558

U.S. Environmental Protection Agency, 2017, Analysis of the Transport and Fate of Metals Released from the Gold King Mine in the Animas and San Juan Rivers (Final Report). U.S. Environmental Protection Agency, Washington, DC, EPA/600/R-16/296, 2017.

Parkhurst, D.L. and Appelo, C.A.J., 1999, User's guide to PHREEQC (Version 2)—A computer program for speciation, batch-reaction, one-dimensional transport, and inverse geochemical calculations: U.S. Geological Survey Water-Resources Investigations Report 99-4259, 310 p.

WHO, 2003, Iron in Drinking-water: Background document for development of WHO Guidelines for Drinking-water Quality, World Health Organization, WHO/SDE/WSH/03.04/08. http://www.who.int/water_sanitation_health/dwq/chemicals/iron.pdf

WHO, 2010, Aluminum in Drinking-water: Background document for development of WHO Guidelines for Drinking-water Quality, World Health Organization, WHO/HSE/WSH/10.01/13. http://www.who.int/water_sanitation_health/water-quality/guidelines/chemicals/aluminium.pdf?ua=1

WHO, 2011, Manganese in Drinking-water: Background document for development of WHO Guidelines for Drinking-water Quality, World Health Organization, WHO/SDE/WSH/03.04/104/REV/1. http://www.who.int/water_sanitation_health/dwq/chemicals/manganese.pdf

Yager, D.B., Fey, D.L., Chapin, T.P., and Johnson, R.H., 2016, New perspectives on a 140-year legacy of mining and abandoned mine cleanup in the San Juan Mountains, Colorado, in Keller, S.M., and Morgan, M.L., eds., Unfolding the Geology of the West: Geological Society of America Field Guide 44, p. 377–419, doi:10.1130/2016.0044(16).

New Mexico Bureau of Geology and Mineral Resources

A division of New Mexico Institute of Mining and Technology

Socorro, NM 87801
(575) 835 5490
Fax (575) 835 6333
www.geoinfo.nmt.edu